

AUTOMATED OPTIMIZATION STRATEGIES FOR HORIZONTAL WELLBORE  
AND HYDRAULIC FRACTURE STAGES PLACEMENT IN UNCONVENTIONAL  
GAS RESERVOIRS

A Dissertation

by

TATYANA PLAKSINA

Submitted to the Office of Graduate and Professional Studies of  
Texas A&M University  
in partial fulfillment of the requirements for the degree of

DOCTOR OF PHILOSOPHY

Chair of Committee,	Eduardo Gildin
Committee Members,	Akhil Datta-Gupta
	Michael King
	Yuefeng Sun
Head of Department,	A. Daniel Hill

May 2015

Major Subject: Petroleum Engineering

Copyright 2015 Tatyana Plaksina

## ABSTRACT

In the last decades rapid advances in horizontal drilling and hydraulic fracturing technologies ensure production of commercial quantities of natural gas from many unconventional reservoirs. Reservoir management and development strategies for shale and tight gas plays have evolved from ad hoc approaches to more rigorous strategies that involve numerical optimization in presence of multiple economic and production objectives and constraints. Application of an automated integrated optimization framework for placement of horizontal wellbores and transverse hydraulic fracture stages along them has potential of increasing shale gas reserves and projects' revenue even further.

This dissertation introduces a novel integrated evolutionary-based optimization framework for placement of horizontal wellbores and hydraulic fracture stages that allows enhancing production from shale gas formations and provides a solid foundation for future field-scale application once better understanding of shale petrophysics and geomechanics is developed. The proposed optimization workflow is developed and tested in stages. First, we summarize what has been done in the subject field previously by scholars and identify what is missing. Second, we present assumptions for the shale gas simulation model that make our framework and the simulation model applicable. Third, we pre-screen several economic and petrophysical parameters in order to identify the most significant for the subsequent sensitivities analysis. Forth, we develop evolutionary-based optimization strategy for placement of hydraulic fracture stages

along a single horizontal wellbore. We investigate how sensitive the optimization results to changes in the key parameters pre-selected during pre-screening. Fifth, we enhance the framework to handle multiple horizontal producers, discuss the conditions when such approach is applicable, and extensively test this integrated workflow on a suite of simulation runs. Finally, we implement and apply multi-objective optimization approach (the improved non-dominated sorting genetic algorithm) to the problem of optimal HF stage placement in shale gas reservoirs and analyze the efficiency of our evolutionary-based optimization scheme in presence of multiple conflicting or non-conflicting objectives.

Based on our extensive testing and rigorous formulation of the optimization problem, we find that the chosen evolutionary framework is effective in calculating the optimal number of horizontal wells, the number of HF stages, their specific locations along the wells as well as their half-length. We also conclude that further computational efficiency can be achieved if minimum stage spacing and same chromosome elimination procedure are used. The multi-objective approach has been tested on conflicting and non-conflicting objectives and proved to compute the Pareto optimal front of solutions (or production scenarios) in computationally efficient manner.

## DEDICATION

To my beloved family for their love, patience, and kindness

## ACKNOWLEDGEMENTS

I would like to express my sincere gratitude to all people who have given me their support and attention during my stay at Texas A&M and preparation of this dissertation. First and foremost, I would like to thank my academic advisor, Dr. Eduardo Gildin, for his guidance, support, faith, and cooperation. His continuous encouragement and interest in this research gave me strength and inspiration to complete this work. I also would like to thank my committee members, Dr. Datta-Gupta, Dr. King, Dr. Sun, and Dr. Hascakir for sharing with me their expertise and providing me with stimulating comments and feedback. If not for their valuable input and far-reaching knowledge, this dissertation could not exist in its current shape and depth.

I express my gratitude to all my colleagues in our research group and classmates. I also want to give special thanks and deep appreciation to my teammate, Dr. Xiaodan Ma, who started working on this sponsored project as a part of her dissertation and prepared the road that made my journey much smoother and more fulfilling. I thank Xiaodan for all Crisman and conference presentations as well as valuable help with code and the model. I would like to acknowledge the Crisman Institute of the Texas A&M University for the financial support and the Harold Vance Department of Petroleum Engineering for computational resources.

Finally, I cordially thank my dear family for their patience, endless support, and love.

## NOMENCLATURE

$b$	Discount rate, %/100/year
$C_p$	Well penetration cost per grid block, \$
$C_w$	Base cost for drilling a horizontal well, \$
$C_f$	Hydraulic fracturing cost per stage, \$
$C_{fb}$	Hydraulic fracturing base cost per stage, \$
$C_{fl}$	Hydraulic fracturing cost per unit of length, \$/ft
$C_p$	Penetration cost of per drilled grid block
$N_{HF}$	Number of hydraulic fracture stages
$K$	Total number of steps in simulation
$k$	Time index
$L_w$	Length of the horizontal portion of the producer in grid blocks
$Q_g^k$	Gas production rate, mscf/day
$Q_w^k$	Water production rate, stb/day
$O$	Operating cost of the producing well, \$/day
$r_g$	Gas price, \$/mscf
$t^k$	Year period, days
$N_{prod}$	Production well index
$u$	Control variable vector
$u^*$	Optimal control variable vector

$\tilde{u}$	Portion of a chromosome that encodes half-length of hydraulic fracture stage
$\hat{u}$	Portion of a chromosome that encodes number of horizontal wellbores
$hl_{max}$	Maximum feasible half-length, ft
$hl_{min}$	Minimum feasible half-length, ft
$nl_{max}$	Maximum feasible number of wells
$nl_{min}$	Minimum feasible number of wells
$x_{length}$	Length of hydraulic fracture stage, ft
$\Delta t_k$	Time step for NPV calculation

## TABLE OF CONTENTS

	Page
ABSTRACT .....	ii
DEDICATION .....	iv
ACKNOWLEDGEMENTS .....	v
NOMENCLATURE .....	vi
TABLE OF CONTENTS .....	viii
LIST OF FIGURES .....	x
LIST OF TABLES .....	xv
CHAPTER I INTRODUCTION .....	1
1.1 Background .....	1
1.2 Research Scope .....	5
1.3 Literature Review .....	7
1.3.1 Wellbore Placement .....	7
1.3.2 HF Stage Design and Placement .....	11
1.3.3 Numerical Optimization Methods .....	14
1.3.4 Multi-objective Optimization .....	16
1.4 Dissertation Outline .....	17
CHAPTER II SHALE GAS MODELING AND UNCERTAINTY ASSESSMENT .....	19
2.1 Introduction .....	19
2.2 Shale Gas Modeling .....	20
2.2.1 Shale Fabric and Impact on HF Geometry .....	20
2.2.2 Stress-Related HF Geometry in Shale Gas Simulation Model .....	23
2.3 Shale Gas Models and Assessment of Uncertain Parameters .....	25
2.3.1 Design of Experiments for Uncertainty Assessment .....	26
2.3.2 Shale Gas Model Description and NPV Response Function .....	28
2.3.3 Full Factorial DoE for Anisotropic Shale Model .....	31
2.3.4 Full Factorial DoE for Isotropic Shale Model .....	33
2.4 Results, Observations and Conclusions .....	33
CHAPTER III HF STAGE PLACEMENT OPTIMIZATION .....	39

3.1 Introduction .....	39
3.2 Evolutionary-Based Stochastic Optimization .....	39
3.2.1 Genetic Algorithm with Strong Elitism.....	40
3.2.2 Shale Gas Model and Single-Objective Function .....	44
3.3 Optimization with GA.....	48
3.3.1 HF Stages Placement Optimization with Fixed Half-Length.....	50
3.3.2 HF Stage Placement and Half-Length Optimization.....	57
3.4 HF Stage Placement Optimization in Presence of Uncertainty.....	65
3.5 Conclusions .....	74
<b>CHAPTER IV INTEGRATED EVOLUTIONARY-BASED OPTIMIZATION FRAMEWORK FOR HORIZONTAL WELL AND HF STAGE PLACEMENT.....</b>	<b>75</b>
4.1 Introduction .....	75
4.2 Framework Assumptions.....	75
4.3 Novel Framework Structure and Implementation.....	78
4.4 Integrated Framework Testing .....	81
4.5 Results and Discussion.....	85
4.6 Conclusions .....	91
<b>CHAPTER V MULTI-OBJECTIVE EVOLUTIONARY OPTIMIZATION FOR HF STAGE PLACEMENT .....</b>	<b>93</b>
5.1 Introduction .....	93
5.2 Approaches to MOO .....	93
5.3 Application of NSGA-II to HF Placement Problem .....	97
5.4 NSGA-II Testing and Results .....	101
5.5 Conclusions and Observations .....	105
<b>CHAPTER VI CONCLUSIONS AND RECOMMENDATIONS .....</b>	<b>107</b>
6.1 Conclusions .....	107
6.2 Future Research Directions .....	111
<b>REFERENCES.....</b>	<b>114</b>
<b>APPENDIX A .....</b>	<b>122</b>
<b>APPENDIX B .....</b>	<b>124</b>

## LIST OF FIGURES

	Page
Figure 1.1. The U.S. natural gas production (in TCF) by the source, 1990-2040 (adopted from <a href="http://www.eia.gov">http://www.eia.gov</a> ). .....	2
Figure 1.2. Typical horizontal well placement, length, and spacing in a shale gas reservoir (e.g. the Bakken field), and stimulated reservoir volumes for each hydraulically fractured well.....	4
Figure 2.1. Aerial view of a portion of a shale reservoir with high stress anisotropy due to presence of clay.....	22
Figure 2.2. Aerial view of a portion of a shale reservoir with low stress anisotropy (isotropic stress distribution) due to high silica (sand or silt) volume.....	22
Figure 2.3. Aerial view of a shale reservoir model with high stress anisotropy. One horizontal well has six transverse HF stages.....	24
Figure 2.4. Aerial view of a shale reservoir model with isotropic stress. One horizontal well has six transverse HF stages. SRV and the main HF have the same permeability.....	25
Figure 2.5. UA workflow for initial screening of economic and petrophysical parameters.....	27
Figure 2.6. Pressure depletion visualization after (a) 0 years, (b) 1 year, and (c) 5 years for DoE run 1 for the anisotropic shale model. ....	32
Figure 2.7 Chart showing change in NPV response (after 1 year of production) resulting from high and low values of each parameter considered in anisotropic scenario. ....	35
Figure 2.8 Chart showing change in NPV response (after 5 years of production) resulting from high and low values of each parameter considered in anisotropic scenario. ....	36
Figure 2.9 Chart showing change in NPV response (after 1 year of production) resulting from high and low values of each parameter considered in isotropic scenario. ....	37

Figure 2.10 Chart showing change in NPV response (after 5 years of production) resulting from high and low values of each parameter considered in isotropic scenario. ....	38
Figure 3.1. Evolutionary search strategy of GA illustrated for a function of two variables and one global maximum. ....	41
Figure 3.2. Generalized structure of GA involves genetic operators: crossover, mutation, and elitism.....	42
Figure 3.3. GA uniform crossover mask applied to elite and current chromosome to obtain next generation chromosome.....	43
Figure 3.4. GA mutation operator changes random number of random genes in all chromosomes except the elite to ensure diversity. ....	44
Figure 3.5. 3D rendering of the shale gas simulation geomodel (DX property) with maximum half-length of HF stages. ....	45
Figure 3.6. Close-up 3D rendering of LGR for the shale gas simulation geomodel (DX property) with maximum half-length of HF stages. ....	45
Figure 3.7. 3D rendering of HF stages along a single horizontal wellbore at the beginning of production.....	46
Figure 3.8. Detailed workflow for HF stages placement and half-length optimization problem with GA integrating MATLAB code and Eclipse simulation results. ....	50
Figure 3.9. Interpretation of GA’s chromosomes and generations for optimization of number of HF stages, their locations, and spacing given specific HF half-length.....	51
Figure 3.10. Stochastic optimization of HF stages placement with GA over 10 generations with 30 chromosomes in each generation. ....	52
Figure 3.11. Results of four test runs of GA over 10 generations with 30 chromosomes in each generation juxtaposed with one GA test run over 30 generations with 60 chromosomes. Optimal number of stages and HF locations. ....	53
Figure 3.12. Cross-plot of the highest discounted NPV values for four test runs versus running time (GA over 10 generations with 30 chromosomes in each generation).....	54

Figure 3.13. GA for optimization of number and locations of HFs. Evolution of chromosomes through 30 generations exhibits convergence by crossover and diversity by mutation. ....	55
Figure 3.14. Highest NPV values after 20 years across 30 generations with 60 chromosomes in GA test run. ....	56
Figure 3.15. Interpretation of GA's chromosomes and generations for HF stage placement and half-length optimization problem. ....	58
Figure 3.16. Stochastic optimization of HF stage placement and half-length with GA over 10 generations with 30 chromosomes in each generation. ....	59
Figure 3.17. Optimal number and HF locations for GA over 10 generations with 30 chromosomes in each generation. ....	61
Figure 3.18. Cross-plot of the highest discounted NPV values for four test runs versus running time (GA over 10 generations with 30 chromosomes in each generation).....	62
Figure 3.19. Evolution of chromosomes through 30 generations exhibits convergence by crossover and diversity by mutation. ....	63
Figure 3.20. Highest NPV values across 30 generations in GA test run.....	64
Figure 3.21. Optimal HF stages placement after 30 generations in GA test run. ....	65
Figure 3.22. Juxtaposition of optimal HF stage locations for an ensemble of 5 geological realizations (each realization has varying matrix permeability +/-20% and +/- 50% from the base geomodel). ....	67
Figure 3.23. Juxtaposition of optimal HF stage locations for an ensemble of 5 geological realizations (well location is unchanged from model to model). ....	68
Figure 3.24. Effect of uncertainty in shale matrix permeability on optimal discounted NPV values.....	69
Figure 3.25. Effect of uncertainty in shale matrix permeability: percent change in discounted NPV values from the optimized base value. ....	69

Figure 3.26. Juxtaposition of optimal HF stage locations for uncertain gas price varying from -50% to +50% from the base value (well location is unchanged from model to model).....	72
Figure 3.27. Effect of uncertainty in gas price on optimal discounted NPV values. ....	73
Figure 3.28. Effect of uncertainty in gas price: percent change in discounted NPV values from the optimized base value.....	73
Figure 4.1. Aerial view of homogeneous matrix permeability field with three horizontal wellbores with symmetrical transverse HF stages.....	77
Figure 4.2. Flowchart of the GA-based integrated framework for optimal placement of multiple horizontal wells and HF stages. ....	78
Figure 4.3. GA chromosome encoding the number and length of horizontal wells as well as the number, spacing, and half-length of HF stages. ....	79
Figure 4.4. Graphical interpretation of one iteration of the integrated optimization framework.....	82
Figure 4.5. Variability of HF half-lengths within the last generation. ....	83
Figure 4.6. Variability of well numbers within the last generation.....	83
Figure 4.7. Evolution and convergence of HF half-length over 30 generation.....	84
Figure 4.8. MATLAB output of monotonically increasing 5-year discounted NPVs over 30 generations with 60 chromosomes each.....	85
Figure 4.9. Summary plot of discounted NPVs from four test runs with varying minimal interval between HF stages.....	88
Figure 4.10. Summary plot of HF half-lengths from four test runs with varying minimal interval between HF stages.....	89
Figure 4.11. Cross-plot of running time, discounted NPVs, and simulator calls from four test runs with varying minimal interval between HF stages. ....	90
Figure 5.1. The Pareto Front of non-dominated Pareto optimal solutions for a generic MOO problem. ....	95
Figure 5.2. Scatter plot showing short- and long-term discounted NVPs generated by the simulation model.....	98

Figure 5.3. Scatter plot showing long-term discounted NVPs vs water production generated by the simulation model. ....	99
Figure 5.4. NSGA-II improved scheme for producing new generations without an increase in evaluations of the objective function. ....	100
Figure 5.5. The Pareto front after the first generation of NSGA-II for non-conflicting objectives. ....	101
Figure 5.6. The Pareto front after 30 generations of NSGA-II for non-conflicting objectives. ....	102
Figure 5.7. NSGA-II results with optimal locations of HF stages and their half-length after 30 generations of NSGA-II for non-conflicting objectives. ....	103
Figure 5.8. The Pareto front (in red) after 20 generations of NSGA-II for conflicting objectives (long-term NPV and cumulative water production). ....	104
Figure 5.9. NSGA-II results with optimal locations of HF stages and their half-length after 20 generations of NSGA-II for conflicting objectives. ....	105

## LIST OF TABLES

	Page
Table 2.1 Shale gas reservoir properties used in the DoE simulation model.....	29
Table 2.2 Economic parameters used in the DoE response model. ....	30
Table 2.3 Parameter screening using stepwise regression statistical analysis (short-term discounted NPV for anisotropic model). ....	34
Table 2.4 Parameter screening using stepwise regression statistical analysis (long- term discounted NPV for anisotropic model). ....	36
Table 3.1 Parameters for shale gas model and the NPV function (Ma, 2013).....	47
Table 3.2 Rock matrix permeability values for ensemble of geologic realizations. ....	66
Table 3.3 Gas price values for optimization under uncertainty. ....	70
Table 4.1 Summary of integrated placement runs with varying minimum HF spacing. ....	86
Table 4.2 Reservoir and economic parameters used for the test model. ....	87
Table 5.1 Pseudo-code of NSGA-II (Deb, 2002).....	96
Table A.1 Two-level full factorial DoE for anisotropic horizontal stress model.....	122
Table A.2 Two-level full factorial DoE for isotropic horizontal stress model. ....	123

# CHAPTER I

## INTRODUCTION

### 1.1 Background

In recent years natural gas from unconventional reservoirs such as shale and tight sand has become a significant portion of the US domestic energy supply (**Fig. 1.1**). From the 1970s, increasing gas prices and improvements in reservoir characterization and stimulation techniques attracted many operating companies to the plays that were previously considered sub-commercial due to their extremely low matrix permeability and fast decline rates. Further advances in drilling technology (including directional and horizontal wells), in manufacturing and design of hydraulic fracturing materials (including proppants and software for adequate modeling of hydraulic fractures), as well as in understanding of geomechanical rock properties and flow patterns have expanded the circle of natural gas producers on the market (Holditch, 2007). Nowadays, the industry experiences a need to merge rigorous shale reservoir characterization, completion results, and expert knowledge with fast and efficient numerical optimization techniques that can enhance unconventional natural gas reserves and increase the net present value (NPV) of the shale and tight gas projects.

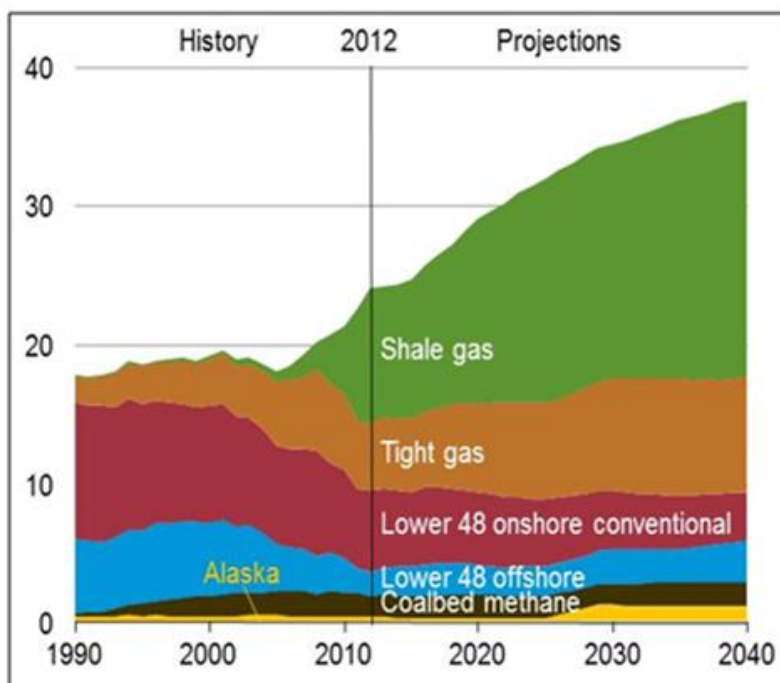


**Figure 1.1. The U.S. natural gas production (in TCF) by the source, 1990-2040 (EIA, 2013).**

To achieve the short- and long-term goals of commercial gas production in a particular unconventional gas reservoir, in general it is necessary to find solutions to two main problems: how many horizontal producing wells to drill and how many hydraulic fracture (HF) stages to place. Then, these two inter-dependent problems can be further subdivided and specified: where the horizontal wells should be placed and where and how long HF stages along these wells should be. Optimal placement of multiple HF stages with non-even spacing in heterogeneous permeability field is a challenging problem by itself in terms of its numerical complexity, especially when automatic stochastic optimization algorithms are used. This optimization task attempts to achieve maximum revenue and/or production rate while minimizing operating costs and capital

investments that are subject to geological, design, and economic constraints. In addition to this, even for one horizontal well the number of parameters to be optimized can be so large that the search space becomes intractable with the most popular gradient-based optimization algorithms. Thus, without a good understanding of the parameter search space and uncertainties as well as a solid optimization approach, knowledge of experienced engineers and large suites of simulations will yield suboptimal and inefficient results.

Another optimization task that is equally important to address for the best economic results is the placement of horizontal wells. A number of automatic optimization algorithms have been devised and applied to similar problems in conventional reservoir engineering and management. These algorithms have been developed to place vertical producers and injectors, horizontal and directional wells as well as multilateral wells. Well placement in a conventional reservoir, though similar in technical execution, is slightly different in unconventional plays. More specifically, because shale and tight sand reservoirs have extra low matrix permeability, we do not expect to see early boundary dominated flow and to produce effectively from the regions beyond stimulated reservoir volume (SRV). Therefore, it is essential to space the wells in the way that they produce the reservoir fairly uniformly, economically, and without significant interference with each other (**Fig. 1.2**). The best industry practices suggest that parallel arrangement of the stimulated producers is the preferred well placement strategy. This field observation helps reduce complexity of the optimization problem, because now it can be solved as a two-dimensional problem with well-defined

geometrical constraints. However, the presence of HF stages with variable half-length makes the problem of optimal placement of parallel horizontal wells a non-trivial numerical undertaking.

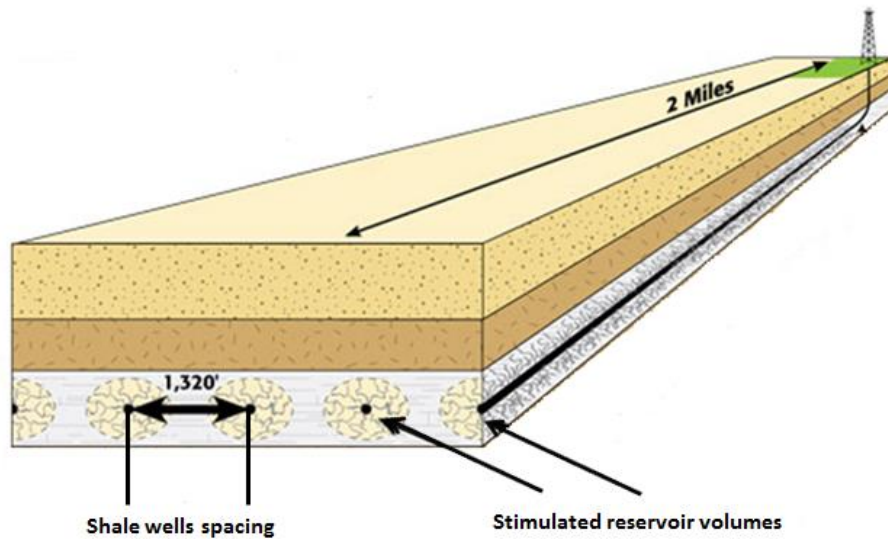


**Figure 1.2. Typical horizontal well placement, length, and spacing in a shale gas reservoir (e.g. the Bakken field), and stimulated reservoir volumes for each hydraulically fractured well.**

The major objectives of this dissertation are to explore conceptually, mathematically, and numerically the problem of optimal placement of horizontal wells and HF stages along them, to assess uncertainty of the key parameters and address such uncertainties and their effects with appropriate mathematical tools, and to develop an integrated optimization framework that can effectively handle multiple objectives for homogeneous matrix permeability maps. In order to assess profitability of a project and

the overall performance of the optimization workflow, we utilize the economic function NPV that is modified and adjusted for variable half-length of HF stages, number of the wells, and multiple short- and long-term objectives. We particularly focus on application of a genetic algorithm (GA) with strong elitism and its modifications to the optimization problem stated above. This research investigates the limits of GA's applicability, computational efficiency, and the level of details (including those pertaining to economics, geology, production, reservoir management, numerical simulation, stimulation design) that the automated framework allows to handle. We introduce more complexity to the objective function as well as the statement of our optimization problem as we explore overall performance of the workflow.

## 1.2 Research Scope

Placement of multiple HF stages along horizontal wells in shale reservoirs has proved to be an effective strategy for production of commercial quantities of natural gas (Holditch, 2007). However, depending on reservoir properties, optimal spacing, half-length, and number of HF stages may vary significantly and yield quite different economic results for different design configurations. In addition to this, non-optimal placement of several parallel wells might cause them to interfere with each other and lead to sub-commercial production rates. Thus, simultaneous optimization of HF stage parameters (such number, spacing, and half-length) and spacing and number of horizontal wellbores is essential for better project economics.

Currently, there exists no integrated optimization framework that allows to place wells and HF stages along them in a systematic way using the discounted NPV function as the major comparative basis for the production configurations. This dissertation pursues construction and implementation of such computationally efficient integrated optimization workflow as the main objective. Among specific objectives of the dissertations are:

- i. Discuss assumptions and applicability of the shale simulation model depending on actual shale reservoir properties and geomechanics;
- ii. Study sensitivities of the key shale model parameters and illustrate the impact of uncertainty in them on optimization results;
- iii. Formulate, implement, and test the optimization framework that effective for placement of HF stages along a single well and then extend it to fully integrated workflow that places traditional zipper-fracs along multiple wellbores;
- iv. Develop the strategy to optimize the HF parameters in presence of multiple conflicting or non-conflicting objectives (economic or production).

The deliverables of this research include full description of the assumptions that render our optimization strategies applicable, full disclosure of all algorithms used and implemented within the topic of this dissertation, and extensive test results with the source code.

### 1.3 Literature Review

Simultaneous optimal placement of horizontal wells with HF stages along them in unconventional gas reservoirs is a unique problem that has not been addressed as an integral process. Nonetheless, the components of this complex problem has been addressed my academic and industry scholarship. This section provides a succinct overview of up-to-date research contributions in wellbore placement optimization (vertical and directional), HF stage design and placement in shale gas reservoirs, numerical optimization algorithms, and multi-objective optimization strategies.

#### 1.3.1 Wellbore Placement

Wellbore placement, which is the key component of our novel optimization framework, has been extensively researched and successfully applied in industry. Most articles and papers on the subject deal with optimization of vertical infill producer wells and water injectors for waterflooding projects in conventional oil reservoirs. Though not directly related to horizontal well placement in unconventional gas reservoirs, this research can provide some valuable insight on suitable optimization methodology. In addition to this, recent trend in directional and horizontal drilling has launched a massive research wave in optimization of horizontal well placement.

Bittencourt and Horne (1997) are among the first researchers to apply rigorous computer-aided optimization approaches to the problem of field development. In their work the authors elaborate on advantages and limitations of GA, polytope, and Tabu methods in the context of petroleum engineering and well placement for large projects.

The detailed analysis and test runs on field model demonstrate good performance of their hybrid GA in terms of improved NPV of the project and computational time.

Guyaguler and Horne (2001) develop systematic way of placing vertical wells in conventional reservoirs with a hybrid genetic algorithm and utility theory approach under geologic uncertainty and risk attitude of the decision-making. Their key finding highlights the power of the GA framework that is capable to achieve satisfactory optimal solutions within reasonable computational time.

Montes et al. (2001) investigate performance of genetic algorithms in vertical well placement optimization and outline their advantages and possible limitations. The authors perform sensitivity study of total oil production by varying key features of GA: population size, number of generations, seed, and specifics of genetic operators. The study affirms that GAs can be used for complex field cases; however, convergence and stability might be potential issues.

Forouzanfar et al. (2010) depart from stochastic gradient-free methods and apply adjoint gradient algorithm to optimization of vertical well placement. The author propose two-stage approach: on the initial stage their method determines total injection and production rates for the reservoir lifetime and on the second stage it optimizes number, types, locations, and rates of wells. For practical purposes bottom hole pressure of each well is constrained nonlinearly and values of the NPV function and its gradient are used for the well elimination routine.

Nakajima and Schiozer (2003) tackle the problem of horizontal well placement in conventional oil reservoirs with three methods: simulation, analytical, and fuzzy logic.

Their numerical simulation method is essentially a well elimination process that achieves highest NPV with the smallest number of wells at given spacing. Analytical method takes advantage of Babu and Odeh model of horizontal well performance. Fuzzy logic operates a set of rules and parameters in order to build a quality map of the reservoir without running excessive number of simulator runs.

Yeten (2003) presents an optimization framework based on combination of a genetic algorithm, a hill climber, and an artificial neural network that allows to place horizontal wells with possible laterals in conventional oil reservoirs. His method assembles chromosomes for GA optimization out of the key well parameters: heel and toe locations, length, and inclination angles. To measure the efficiency of the optimization process, the author uses the NPV function that is sensitive to changes in well types, location, trajectories, and well control strategies.

Similarly to the previous author, Ding (2008) considers the problem of complex horizontal well placement in highly heterogeneous conventional oil reservoirs. The study compares performance of two optimization strategies (GA and CMA-ES) for a number of objective functions. After sensitivity study the author concludes that evolutionary strategies are most suitable for non-linear problems such as well placement optimization and depending on chosen population size CMA-ES might yield more accurate solution.

Emerick et al. (2009) take the idea of optimal horizontal well placement in conventional reservoirs to a new level by introducing Genocop III method (a variation of GA). The authors implement and describe the software tool capable of finding optimal number of wells by adjusting their trajectories, types (injector or producer), and lengths. They test

their framework on several field and synthetic cases and observe significant improvement of NPV in comparison to heuristic well placement approach.

Following up on Yeten's research, Abukhamsin (2009) investigates performance of continuous and binary versions of GA for multilateral well placement. He conducts sensitivities study on major GA parameters and concludes that continuous GA produces slightly higher values of the objective function. The author also focuses on geologic uncertainties associated with his real field example and impact of these uncertainties on the optimization results.

Bouzarkauna et al. (2010) compare Emerick's implementation of GA with Genocop III with CMA-ES for horizontal well placement problem. The authors investigate the effects of adaptive penalties with rejection on the method's convergence within the feasible region. Computation efficiency of the method is then enhanced application of local meta-models that allow to substitute the objective function with a locally weighted regression. As a result of these improvements, the authors observe comparable NPV results for both CMA-ES implementations, but local meta-models help reduce the number of simulator call by up to 25%.

Morales et al. (2010) apply GA and GA variation (Minimal Variation or MiniVar) to optimization of horizontal well placement in condensate reservoirs. The authors test both conventional implementation of GA and the MiniVar modification on a field model and find that for their formulation of the NPV objective function GA with MiniVar process gives higher cumulative condensate and gas production as well as

revenue. The authors also observe that intuitive placement of wells in such complex systems as gas condensate fields is a priori suboptimal and sometimes impossible.

Lyons and Nasrabadi (2013) couple vertical well placement optimization with history matching in order to increase certainty of optimal well locations. They perform well placement with GA and history matching with EnKF and by alternating these two processes improve values of the objective function and reduce the CPU time. The authors compare their results for the PUNQ-S3 field with those by other researchers and conclude the validity of their simultaneous optimization and uncertainty reduction method.

Now that the well placement literature is reviewed and the main contributions are identified, we turn to the subject of optimization of HF stage placement.

### 1.3.2 HF Stage Design and Placement

The problem of HF placement has become a prolific field of research in the last decade. Most of the scholarly effort concentrates on optimization of HF characteristics from the geomechanical point of view. Though geomechanical aspects of HF placement are very important to understand to unlock the full potential of a shale reservoir, there is a need for an efficient framework that can calculate locations, half-length, and number of HF stages in presence of necessary information. The following sub-section reviews research concerning optimization techniques in HF placement.

Cipolla et al. (2010) lay the groundwork and discuss the most recent developments in reservoir modeling that help represent HF networks more realistically.

In their study the authors analyze how observed micro-seismic information from HF jobs can be transferred to a reservoir simulator in order to model production for an extended period of time. They also discuss that such details as gas desorption might not be always as significant as previously thought and others like Young's modulus of overlooked might have a dramatic impact on ultimate gas recovery. The study proposes to model presence of HFs with single porosity and dual permeability model with LGR around HFs.

Mayerhofer et al. (2010) elaborate on efficiency of multi-stage hydraulic fracturing process in shale gas reservoirs and discuss the concept of SRV. The key findings of their micro-seismic observation and numerical simulation are as follows. Natural fracture network, shale thickness, and stress field have significant impact on SRV and, thus, on HFs and horizontal well spacing. While these features are impossible to control while performing hydraulic fracturing jobs, they are important to include into an optimization method. The authors also observe maximum well performance with large SRVs and closely spaced HFs. However, economic feasibility of such design they leave as a subject for another study.

In his thesis Holt (2011) investigates applicability of finite difference, SPSA (Simultaneous Perturbation Stochastic Approximation), and EnOpt algorithms to placement of HF stages in a shale reservoir with homogeneous permeability field. The author focuses on a number of optimization techniques that include optimization of fractures locations only as well as HF stages number and locations. In addition to this,

Holt conducts tests of a well placement technique with EnOpt and concludes that this algorithm is the most applicable to both well and HF stages placement problems.

Wilson and Durlofsky (2012) address the problem of computational efficiency in HF stages placement and well placement by investigating surrogate models and general pattern search. The authors reduce simulation time by tuning surrogate reservoir models that incorporate fewer physical effects such as desorption and dual-porosity dual-permeability concept. They substitute these detailed models with a single porosity equivalent that is “history matched” to reproduce the results of the full-physics models. Because the surrogates are faster, it is possible to apply a generalized search algorithm to obtain the optimal lengths, locations, and numbers of HF stages for a given number of wells. The researchers demonstrate the validity of the surrogate models by sensitivity study focused on possible fluctuations of gas prices.

Gao et al. (2012) develop and test on a field case of a tight gas reservoir a completely automated framework for optimal design of non-uniformly spaced HF's along a horizontal well. The authors take GA as a basis for their optimization and consider a number of effects such as stress shadowing and non-Darcy flow in order to maximize their definition of NPV. In addition to spacing, the study takes into consideration the effect of half-length variation when HF's are outer or inner (closer to heel and toe or toward the middle of the well).

Yu and Sepehrnoori (2013) investigate optimal placement of uniformly spaced HF's along two horizontal wellbores by response surface method (RSM). They use NPV as an objective function in their optimization scheme and incorporate in their evaluation

uncertainty in the key parameters: reservoir permeability, porosity, fracture spacing, fracture conductivity, gas desorption, and fracture half-length. The authors propose this approach in order to estimate optimal drainage area and guide engineers to avoid interference when placing additional wells and designing HF treatment plans.

### 1.3.3 Numerical Optimization Methods

At the basis of our integrated optimization framework, we place the optimization engine that is supposed to be computationally efficient and suitable for the discrete problem of interest. In this dissertation we focus on a gradient-free evolutionary stochastic algorithm (GA) that has all necessary properties: robustness, efficiency, and accuracy. In other words, this method obtains reasonable global optimal values for a number of similar problems in reasonable computational time. This subsection presents a variety of optimization algorithms based on their classification and properties. From this summary, the choice of GA as the primary optimization engine becomes clear.

A “good” optimization algorithm (whether it is deterministic or stochastic) must be able to find the solution with necessary precision without being too sensitive to the quality of the input data (Nocedal and Wright, 2006). Deterministic algorithms converge to the same optimal point (whether it is global or local) if they start from the same initial point. To verify that the obtained optimal solution is the best approximation of the global optimum, it is essential to run deterministic methods from a number of different initial points. Stochastic algorithms, on the other hand, have a certain probability (even if it is very small) of selecting any point in the search domain. Therefore, such algorithm will

eventually encounter the global maximum (Reed and Marks II, 1999). For practical purposes though we select termination criteria in order to approximate the global maximum with a stochastic method in a finite number of iterations.

In addition to deterministic and stochastic categories, optimization algorithms can be divided into gradient-based and gradient-free groups. Gradient-based methods require computation of a gradient of the objective function in each iteration to estimate the best direction of search and approximate the next step solution. Among the most popular gradient-based algorithms we can mention first-order optimization method called steepest ascent (or descent), conjugate gradient method, Broyden-Fletcher-Goldfarb-Shanno (BFGS) algorithm, and the most fundamental Newton's method. All these methods require either the first or second order derivatives of the objective function. Gradient-free algorithms, on the other hand, do not require calculation of the gradient or Hessian which might be of advantage in optimization of complex non-convex non-linear objective functions. This group of optimization methods is represented by genetic algorithms (GAs), covariance matrix adaptation – evolutionary strategy (CMA-ES), particle swarm optimization (PSO), etc.

Stochastic evolutionary-based gradient-free algorithms such as genetic algorithms (Holland, 1975) are particularly appealing to solve the problems that have control vectors with a large number of dimensions. Evolutionary strategies are also effective for the problems for which input that can be easily formulated as binary values. GAs are flexible and can be easily modified to meet the needs of a specific problem as long as the control vector can be represented as 0's and 1's. GAs are global

maximization methods. Specifics of the stochastic GA that lies in the engine of our novel optimization framework are discussed in the upcoming chapters of this dissertation.

#### 1.3.4 Multi-objective Optimization

Multi-objective optimization (MOO) is the next frontier of many engineering problems. It encompasses numerical optimization strategies that allow to evaluate solutions in presence of multiple objectives that can be conflicting or not. On many occasions engineers attempt to maximize performance or reliability while minimizing costs. In problems like these, it is instrumental to have algorithms that handle multiple objectives efficiently and economically.

Deb et al. (2002) offer the improved version of non-dominated sorting GA (NSGA-II) that manages two competing (or non-conflicting) objectives and has lower computational complexity in comparison to regular NSGA. The authors demonstrate high performance of the improved algorithm on a number of test functions and juxtapose the test results it with those from the regular NSGA.

Konak et al. (2006) compare and contrast several MOO algorithms based on GA and discuss their advantages and shortcomings as well as possibility of making these algorithms parallel. The authors provide detailed pseudo-codes for all algorithms that become particularly handy in the last chapters in this dissertation.

Following up on the development of Deb et al. (2002), Han et al. (2013) apply Pareto-based MOO algorithms to history matching problems in petroleum reservoir engineering. They set up problems with conflicting objectives and observe performance

of the MOO methods on synthetic test functions as well as a realistic field example. Success in application of NSGA-II for a number of functions including those pertinent to reservoir management gives us confidence in its application for optimal placement of HF stages in unconventional gas reservoirs in the upcoming chapters.

#### 1.4 Dissertation Outline

This dissertation is structured in the way that takes the reader from the survey of the current scholarship regarding modeling of shale gas reservoirs and applications of numerical optimization framework for horizontal well and HFs placement to solutions of specific optimization problems. In Chapter II, we discuss strategies for numerical modelling of shale gas reservoirs that take into consideration rock fabric features. We consider how stress anisotropy can be represented in shale gas simulation models by means of stimulated reservoir volume and local grid refinement. In the same chapter we perform sensitivities analysis of the key petrophysical and economic parameters.

In Chapter III, we state mathematically the problem of HS stage placement, define the objective function, and address implementation and testing of the specific optimization algorithm, GA. This chapter features multiple test runs that demonstrate GA's performance on small and large domains. In addition to that, we fully develop the framework for optimization of HF locations, number, and half-length.

In Chapter IV, we present complete and integrated framework for optimal placement of horizontal wells and HF stages along them. We also discuss all necessary assumptions that enable the reader to use this framework effectively. The chapter

contains wealth of detailed information about the inner structure of the framework as well as extensive test cases and results including those with varying minimal spacing between HF stages.

In Chapter V, we shift our attention to MOO problems and present our implementation of NSGA-II for optimization of HF stage placement in presence of two objectives. We investigate two cases: one with non-conflicting objectives (short- and long-term discounted NPVs) and one with conflicting objectives (long-term discounted NPV and water production). At the end of the chapter we demonstrate Pareto fronts of optimal solutions for both MOO cases.

Finally, in Chapter VI, we discuss major achievements of this dissertation, its impact, and propose some future venues that current research has opened.

## CHAPTER II

### SHALE GAS MODELING AND UNCERTAINTY ASSESSMENT

#### 2.1 Introduction

In this chapter, we discuss applicability of a numerical simulation model of a shale gas reservoir for experimental design, evaluation of the objective function, and ultimately calculation of optimal values for all variables in the control vector. Because of limited access to the field and lab data and proprietary nature of geomodels built in industry, we developed and tested a simulation shale gas model and history matched it against the Barnett field production data (Ma, 2013). This shale gas reservoir model designed with Schlumberger ECLIPSE™ 300 (E300) reservoir simulator, can be easily customized and suited for uncertainty assessment and subsequent optimization of placement of horizontal wellbores and transverse HF stages (version 2012.2). In this study, we take further steps and assess uncertainty in additional key parameters that were not previously addressed. The design of experiments that uses the shale gas simulation model to obtain the response of the natural system to changes of input parameters, allows to identify the “heavy hitters” among the parameters. Later the parameters that have the greatest impact on the model response are used to generate several realizations of the shale gas model and assess the performance of the optimization framework under uncertainty.

## 2.2 Shale Gas Modeling

Development of a fit-for-purpose numerical simulation model of a shale gas reservoir that can be effectively used in production optimization is not a trivial problem due to geological, geochemical, and geomechanical complexities of shale formations. The following sections present to the reader current challenges in shale reservoir modeling and their possible solutions.

### 2.2.1 Shale Fabric and Impact on HF Geometry

One of the biggest challenges in characterization of shale formations is their compositional and geo-spatial variability. Geochemical composition of shales varies not only from one play to another, but also within one geological unit (King, 2010). This fact has a great impact on stimulation techniques as well as numerical modeling of fluid flow in a shale medium (Vishkai et al., 2014). Because it is possible to observe a change from mostly siliceous matrix composition to calcareous and argillaceous matrix composition even within one shale play, we have to make assumptions about shale composition for numerical simulation purposes that are both general and not completely detached from what can be observed in nature.

For shales with predominantly siliceous matrix composition with high clay content (e.g. the Barnett shale formation), petrophysics experts observe high horizontal stress anisotropy (one principal horizontal stress direction is significantly larger than another). Stress anisotropy is related to closure stress which is determined by presence of significant amount of certain clays (Waters et al., 2011). Schematic **Fig. 2.1** illustrates

this scenario. Here the horizontal stress perpendicular to the horizontal wellbore  $\sigma_{Hmax}$  is much larger than  $\sigma_{Hmin}$  and, thus, we expect to see a long HF oriented perpendicular to the minimum horizontal stress direction. Although the main HF has high (or infinite) conductivity, adjacent to it SRV is not going to have significant aerial extent and conductivity. Savitski et al. (2013) became aware of the problem of varying HF geometry due to horizontal stress anisotropy and rock fabric composition, and proposed to model HFs explicitly when it is critical for economic decisions.

For shale formations with predominantly siliceous matrix composition with low clay content, the log interpretation usually shows low horizontal stress anisotropy and, thus, lower closure stress. In this scenario both horizontal principal stresses ( $\sigma_{Hmax}$  and  $\sigma_{Hmin}$ ) are comparable and we expect to see a wide and diverse network of fractures caused by either breaking of the shale fabric or re-activation of pre-existing natural fractures. Cipolla et al. (2009) discussed this and above-mentioned situations and proposed that they should be distinguished into different cases and treated separately. Schematic **Fig. 2.2** shows this scenario. Two horizontal principal stresses are similar; and as a result, we observed aerially extensive SRV with relatively high conductivity without pronounced main HF.

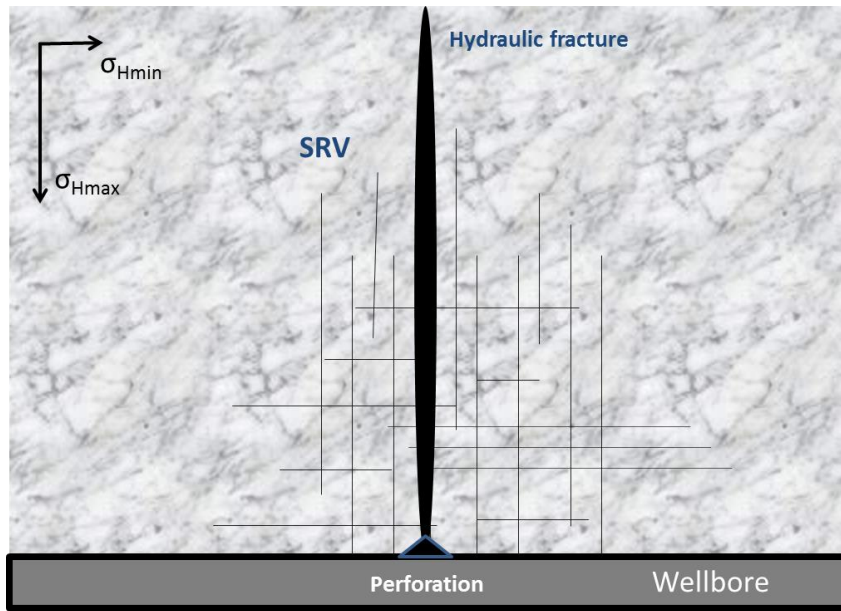


Figure 2.1. Aerial view of a portion of a shale reservoir with high stress anisotropy due to presence of clay.

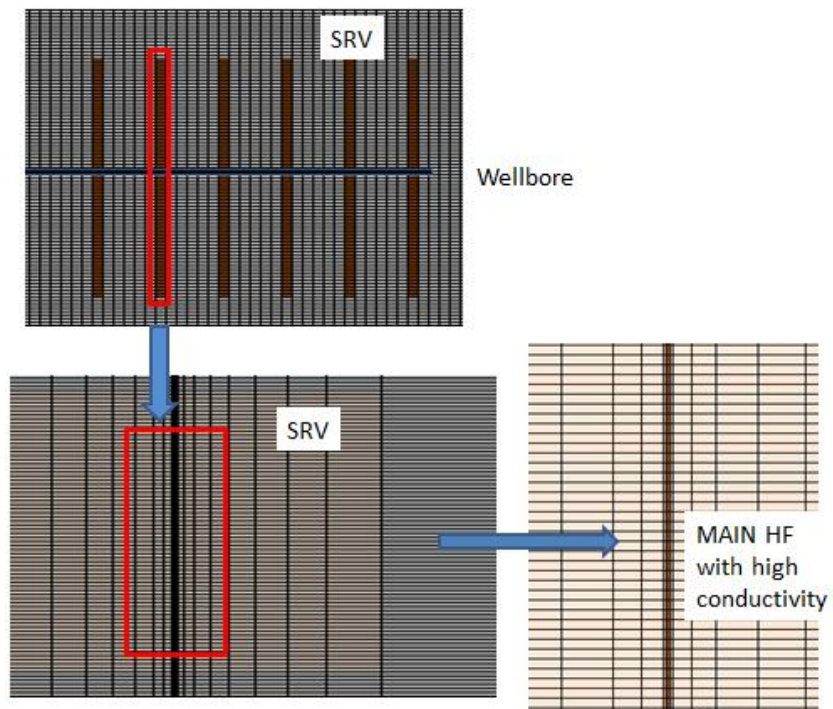


Figure 2.2. Aerial view of a portion of a shale reservoir with low stress anisotropy (isotropic stress distribution) due to high silica (sand or silt) volume.

Of course, mineralogy of shales is not confined to silica-dominated. Shales with significant content of carbonates may also exhibit high or low closure stresses. For the purposes of this dissertation, we only consider silica-based shale fabric with two distinct features: high and low stress anisotropy. Now that we have established that rock fabric composition has a great impact on the geometry of HFs, let us discuss the implications of these two stress-related scenarios on shale gas simulation models.

### 2.2.2 Stress-Related HF Geometry in Shale Gas Simulation Model

Awareness of stress-related anisotropy that affects propagation and geometry of HF changes the way we represent HF stage and SRV for simulation purposes. More specifically, for the scenario of high horizontal stress anisotropy HF stages are modelled as illustrated on **Fig. 2.3**. Successive magnification of the grid reveals explicit modelling of HF stages with SRV grid blocks and logarithmic LGR. Because the horizontal stress anisotropy is significant and it is difficult to re-activate sealed natural fractures in the direction of the minimal horizontal stress, we represent the HF stage as a high (or infinitely) conductive main HF created by LGR with 0.4 feet wide central block and low permeability SRV. This is an idealized and yet representative model of the high stress anisotropy scenario (Ma, 2013).



**Figure 2.3. Aerial view of a shale reservoir model with high stress anisotropy. One horizontal well has six transverse HF stages.**

A simulation model that approximates behavior of the system as shown in **Fig. 2.2**, should account for re-activation of multitude of natural fractures and creation of a diverse highly-permeable network of fractures. **Fig. 2.4** demonstrates the successive magnification of a grid for isotropic horizontal stress model. Here high permeability SRV is used to represent a large fracture network while keeping LGR. Note that in this case, there is no explicit high (or infinite) conductivity central portion of HF stage.

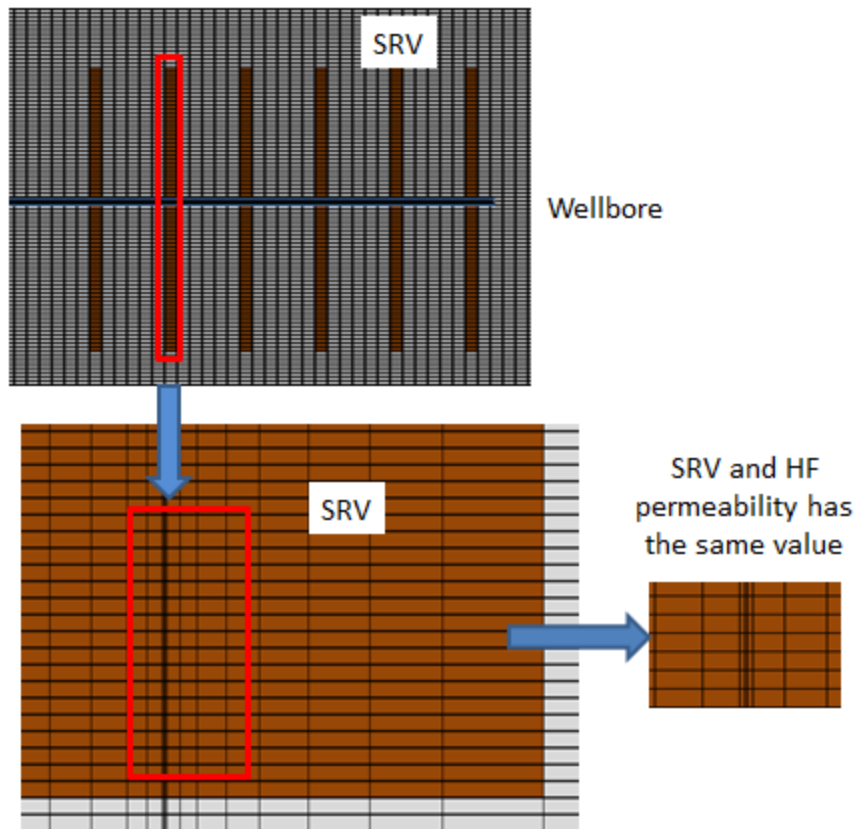


**Figure 2.4. Aerial view of a shale reservoir model with isotropic stress. One horizontal well has six transverse HF stages. SRV and the main HF have the same permeability.**

### 2.3 Shale Gas Models and Assessment of Uncertain Parameters

Before we explore automated optimization strategies for placement of HF stages, it is essential to assess uncertainty in some key parameters used in both types of shale gas models. This uncertainty analysis helps identify those that significantly influence the response (or the value of the objective function) of the system. Ideally, the uncertainty assessment should be done as an outer loop of the overall optimization framework, so that optimal locations of HF stages and wellbores are considered in the context of uncertain geological and economic parameters. This approach, however, requires

prohibitively large computational capacities currently unavailable in the academic environment. Therefore, uncertainty assessment (at least its parameter screening part) is decoupled from the optimization framework and executed on a fixed production design (in other words, we use a simulation model with one horizontal wellbore with predefined number of HF stages with specified half-length and locations).

The following sub-sections present the overview of a popular UA technique, design of experiment (DoE), with a specific application to modeling fluid flow in a shale gas reservoir. First, we discuss the shale gas model and the key parameters analyzed in UA. Then, we present full factorial design for anisotropic and isotropic models of a shale reservoir. Finally, we statistically analyze the results of both DoE's and make recommendations for generating ensembles of realizations for further optimization.

### 2.3.1 Design of Experiments for Uncertainty Assessment

Though reasonable ranges of values for the key petrophysical and economic parameters (such as gas prices, cost of hydraulic fracturing jobs, rock matrix permeability, SRV permeability, etc.) are known with certain confidence and documented in literature, it is difficult to define them precisely for a particular shale model. This happens because economic parameters tend to change due to improvement in technology or availability of materials (e.g. reduction or increase in cost of horizontal drilling or hydraulic fracturing, availability of certain proppants and their cost). Gas prices can also be affected by attractiveness of other sources of energy or production techniques (e.g. situations when hydraulic fracturing might not be acceptable stimulation strategy in some sensitive

geographical areas or when influx of cheaper gas from conventional gas reservoirs makes shale gas less attractive and, thus, more expensive resource). Though historical shale gas prices and operating costs are known, any projections of these trends into the future are inherently uncertain. Shale petrophysical properties and HF stage design parameters can also be uncertain. Rock matrix permeability, HF conductivity, and SVR permeability often fall into laboratory measured ranges; however, the precise values are rarely if ever known. To assess the impact of uncertainty in the key economic and petrophysical parameters on the response of the simulated shale gas system, we propose the initial screening of the parameters set with full factorial 2-level DoE. Schematic **Fig. 2.5** shows the UA screening workflow for both anisotropic and isotropic horizontal stress scenarios.

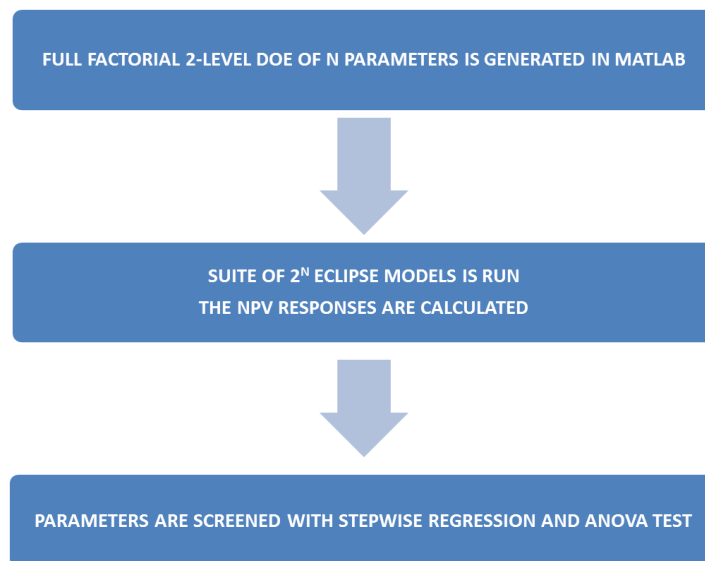


**Figure 2.5. UA workflow for initial screening of economic and petrophysical parameters.**

To screen a set of parameters for significance and choose descriptive models of complex system behavior, scientists usually devise an experimental design with a number of cases or test runs that provide system responses. These responses can then be used to analyze how changes in the key parameters influence the responses. One of the most systematic and thorough ways to assess uncertainty is full factorial DoE. Each parameter takes two, three, or more values from a certain reasonable range (usually measured in labs or surveyed from literature) and depending on how many values each parameter takes, DoE can be two-level (high and low values), three-level (high, medium, and low values), or mixed-level (combination of parameters with different levels). For our study, we select two-level full factorial DoE and obtain NPV responses for each arrangement of the parameters.

### 2.3.2 Shale Gas Model Description and NPV Response Function

In order to screen the uncertain model parameters and identify the most significant ones, for both isotropic and anisotropic scenarios we use a shale gas simulation model with the core parameters as defined in the **Table 2.1** (Ma et al., 2013).

**Table 2.1 Shale gas reservoir properties used in the DoE simulation model (Ma et al., 2013).**

<i>Parameters</i>	<i>Values</i>	<i>Unit</i>
Model width	1420	ft
Model length	2000	ft
Model thickness	200	ft
Initial reservoir pressure	3000	psi
Reservoir temperature	150	°F
Rock density	161	lbs/ft <sup>3</sup>
Producing bottom hole pressure	500	psi
Wellbore length	1400	ft
Production period duration	5	years
Matrix porosity	6	%
Total gas content	70	%
Langmuir pressure	650	psi
Langmuir volume	0.096	mscf/ton
Hydraulic fracture height	200	ft
Hydraulic fracture half-length	260	ft
Number of hydraulic fractures	16	stages

Production design is kept the same for all runs: one horizontal wellbore with sixteen (16) transverse HF stages. The HF stages are spaced uniformly. In addition to the model parameters, we use several fixed economic parameters to obtain the NPV function responses for each run. These parameters are summarized in **Table 2.2** (Schweitzer, 2009; Bruner, 2011).

**Table 2.2 Economic parameters used in the DoE response model (Schweitzer, 2009; Bruner, 2011).**

<i>Parameters</i>	<i>Values</i>	<i>Unit</i>
Discount rate	12.5	%
Drilling base cost per well (vertical part)	2,000,000	\$
Drilling cost per grid block (horizontal part)	6,000	\$
Daily operating expenses per well	60	\$

To perform a statistical study and screen out the least significant parameters from the set that was chosen for the UA, we define the response function (NPV) that combines economic, petrophysical, and HF design parameters. The NPV function defined for one horizontal producer with fixed number of transverse HF stages in **Eq.2.1** (Holt, 2011) provides necessary response values:

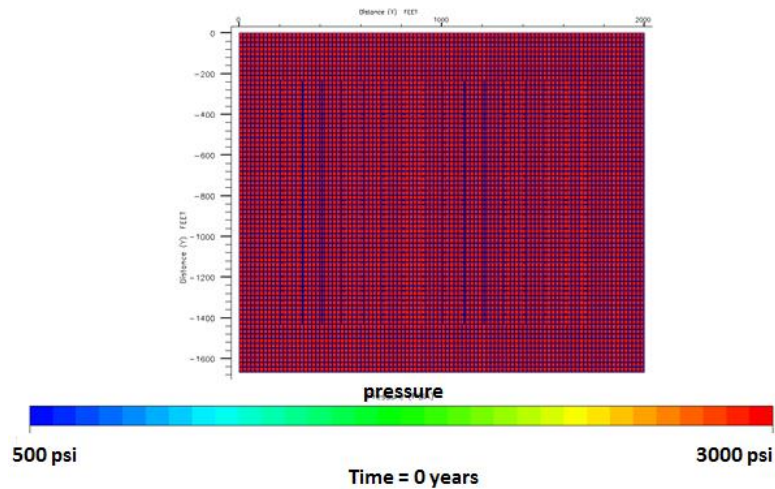
$$NPV = \sum_{k=1}^K \frac{(Q_g^k \cdot r_g - Q_w^k \cdot r_w - O) \cdot \Delta t^k}{(1 + b)^{tk/365}} - (C_w + N_{HF}C_f + L_w C_p). \quad (2.1)$$

In this expression,  $k$  is time index,  $K$  is the total number of time periods simulated [days],  $Q_g^k$  is gas production rate during time period  $k$  [mscf/day],  $r_g$  is gas price [\$/mscf],  $Q_w^k$  is water production rate during time period  $k$  [bbl/day],  $r_w$  is cost of water disposal [\$/bbl],  $O$  is operational cost of the well per day [\$/day],  $\Delta t^k$  is duration of the  $k$ th time period [days],  $b$  is a discount rate [%/100/year],  $C_w$  is base cost of drilling the vertical part of the producer well [\$],  $N_{HF}$  is the number of HF stages,  $C_f$  is hydraulic fracturing cost per stage [\$],  $L_w$  is the length of the horizontal portion of the producer in grid blocks, and  $C_p$  is well penetration cost per grid block [\$].

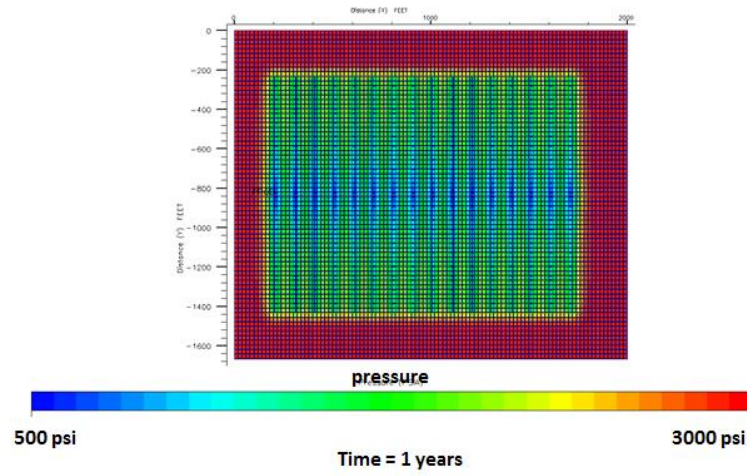
### 2.3.3 Full Factorial DoE for Anisotropic Shale Model

This section provides the reader with comprehensive setup of the two-level full factorial DoE for the scenario when the shale reservoir has high horizontal stress anisotropy (which is the most prevalent way to model shale reservoirs and will be the focus for the rest of this dissertation). Here, we are interested in investigating effects of high and low values of HF stage permeability, SRV permeability, shale rock matrix permeability, gas price, and cost of hydraulic fracturing. Two-level full factorial DoE for five (5) parameters yields 32 test runs that are listed in the **Table A.1** (Appendix A).

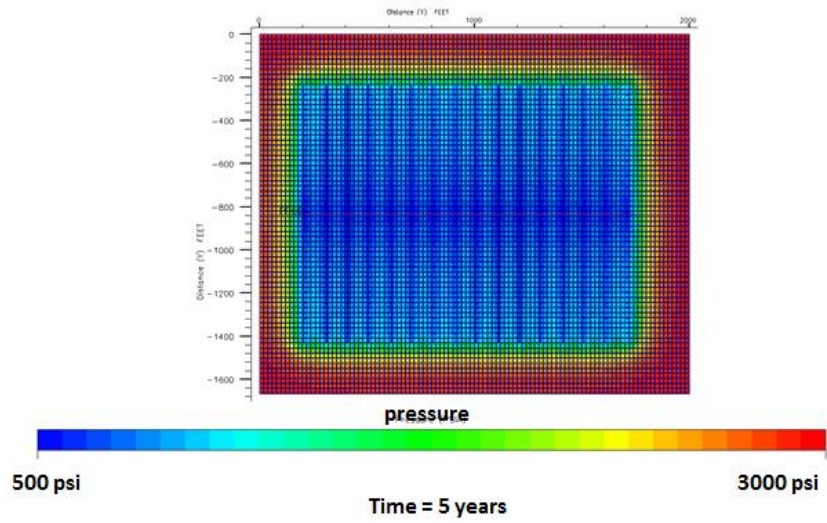
For fluid flow visualization purposes, we provide a series of pressure maps for one DoE run (**Fig. 2.6**). At the onset of production (**Fig. 2.6(a)**), only HF stages are flowing gas and water into the wellbore. As production time progresses (**Fig. 2.6(b-c)**), the reservoir pressure is quickly depleted due to relatively low SRV permeability (caused by stress anisotropy) and extra-tight rock fabric permeability.



(a)



(b)



(c)

Figure 2.6. Pressure depletion visualization after (a) 0 years, (b) 1 year, and (c) 5 years for DoE run 1 for the anisotropic shale model.

### 2.3.4 Full Factorial DoE for Isotropic Shale Model

For isotropic scenario, we eliminate the variable for HF permeability because now it is modelled with higher SRV permeability (while LGR is still preserved, it does not have the central grid block with infinite conductivity, but rather that of SRV). **Table A.2** (Appendix A) gives specific values for assessed parameters and all cases for the DoE.

### 2.4 Results, Observations and Conclusions

In this section, we analyze the results obtained from suites of simulation run for both anisotropic and isotropic models using tornado charts in addition to rigorous statistical tools available in the software R (2013). Let us now look at the results from anisotropic model runs and screen the most significant explanatory variables (or parameters).

Appendix B provides detailed R code and the dataset that produced the linear regression model in **Table 2.3**. This model combines four of the explanatory variables and it was selected from a set of possible models using stepwise regression and Akaike information criterion (see Appendix B for details). The chosen model has the highest adjusted  $R^2$  and AIC from all models analyzed (Akaike, 1974). From the **Table 2.3** we observe that HF permeability has been eliminated as it is the least important variable. Meanwhile, matrix permeability ( $km$ ), price of gas ( $pg$ ), and hydraulic fracturing cost ( $hcost$ ) have the highest significance codes. Simply put, the asterisks notation means that more of them explanatory variable has, the more unlikely that the NPV has no relationship with this variable and, thus, the more it is significant in explaining NPV responses.

**Table 2.3 Parameter screening using stepwise regression statistical analysis (short-term discounted NPV for anisotropic model).**

```

Call:
lm(formula = y1npv ~ ksrv + km + pg + hcost, data = ani)

Residuals:
    Min       1Q   Median       3Q      Max
-942821 -501230  109958   586573  743052

Coefficients:
            Estimate Std. Error t value Pr(>|t|)
(Intercept) -4.392e+06  4.935e+05  -8.899 1.63e-09 ***
ksrv         8.707e+08  2.697e+08   3.228 0.00326 **
km           3.606e+09  2.452e+08  14.707 2.07e-14 ***
pg           8.367e+05  8.091e+04  10.341 6.88e-11 ***
hcost       -1.200e+01  1.214e+00  -9.888 1.81e-10 ***
---
Signif. codes:  0 '***' 0.001 '**' 0.01 '*' 0.05 '.' 0.1 ' ' 1

Residual standard error: 686500 on 27 degrees of freedom
Multiple R-squared:  0.9411,    Adjusted R-squared:  0.9324
F-statistic: 107.9 on 4 and 27 DF,  p-value: 3.414e-16

```

Calculation of percent change in NPV values due change in explanatory variable resented on semi-tornado chart in **Fig. 2.7** corroborates the findings of the statistical analysis. Here as well, in short-term production (after 1 year) gas price and matrix permeability are the most significant parameters. Permeability of HFs, which are usually treated as infinite conductive small grid blocks, for simulation purposes is also demonstrated insignificant.

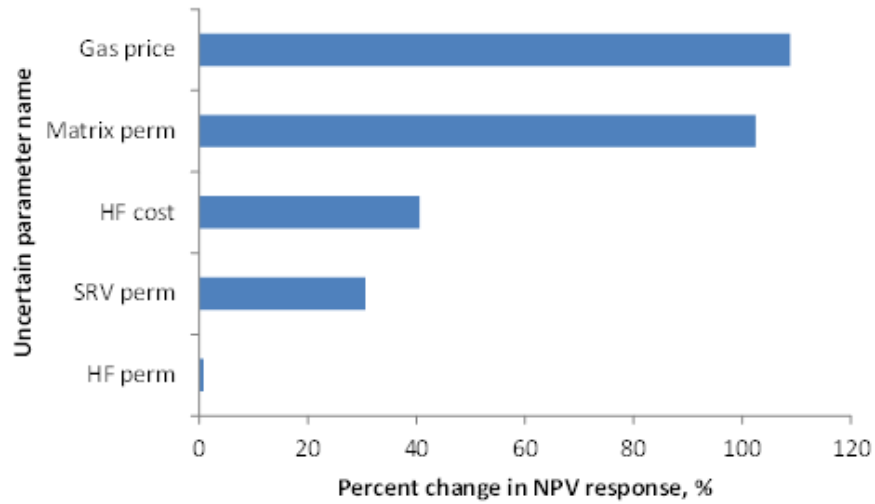


**Figure 2.7** Chart showing change in NPV response (after 1 year of production) resulting from high and low values of each parameter considered in anisotropic scenario.

If we consider long-term production (5 years) in anisotropic model, we observe that the same explanatory variables are significant (**Table 2.4**). The visual representation of percent change in NPV response due to change in the parameters (**Fig. 2.8**) also illustrate the significance of matrix permeability, price of gas, and cost of hydraulic fracturing. Permeability of SRV is slightly less significant than the three parameters mentioned above. These observations are important for the upcoming study of optimization of HF stage placement under uncertainty in Chapter III. More specifically, we are going to focus on assessment of robustness of optimization results (HF stage locations and number) as matrix permeability and gas price range within +50% and -50% from the base values.

**Table 2.4 Parameter screening using stepwise regression statistical analysis (long-term discounted NPV for anisotropic model).**

```

Call:
lm(formula = npv ~ ksrv + km + pg + hcost, data = ani)

Residuals:
    Min       1Q   Median       3Q      Max
-1527420  -657759   171839   832788  1192361

Coefficients:
            Estimate Std. Error t value Pr(>|t|)
(Intercept) -5.531e+06  7.464e+05  -7.411  5.69e-08 ***
ksrv         1.231e+09  4.079e+08   3.018  0.0055 **
km           5.194e+09  3.708e+08  14.006  6.68e-14 ***
pg           1.574e+06  1.224e+05  12.862  5.00e-13 ***
hcost       -1.200e+01  1.836e+00  -6.538  5.20e-07 ***
---
Signif. codes:  0 '***' 0.001 '**' 0.01 '*' 0.05 '.' 0.1 ' ' 1

Residual standard error: 1038000 on 27 degrees of freedom
Multiple R-squared:  0.9387,    Adjusted R-squared:  0.9296
F-statistic: 103.4 on 4 and 27 DF,  p-value: 5.844e-16
    
```

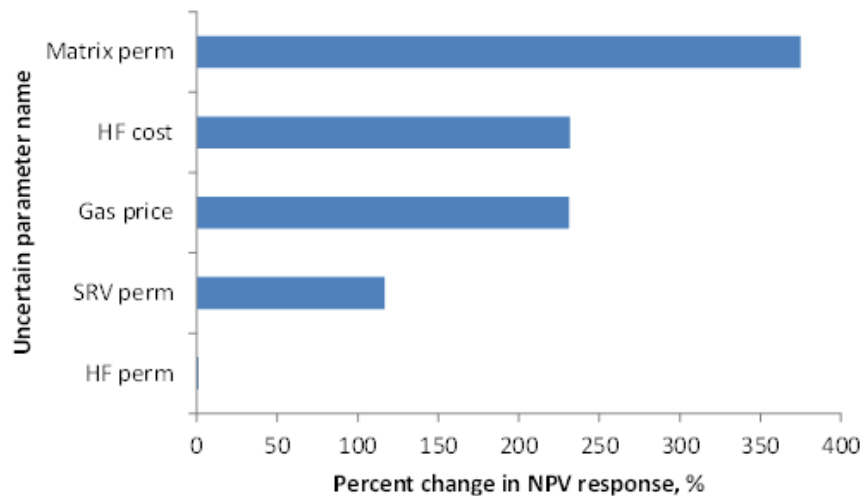


**Figure 2.8 Chart showing change in NPV response (after 5 years of production) resulting from high and low values of each parameter considered in anisotropic scenario.**

Appendix B provides R code and statistical summaries for models fitted for NPV responses after one (1) and five (5) years of production in isotropic models. Similarly to anisotropic runs, we observe that the same three explanatory variables (matrix permeability, cost of hydraulic fracturing, and gas price) are the most significant parameters that influence NPV responses. **Figs. 2.9 and 2.10** are the visual aid to see the relative impact of change in the uncertain parameters on the percent changes in the response values.

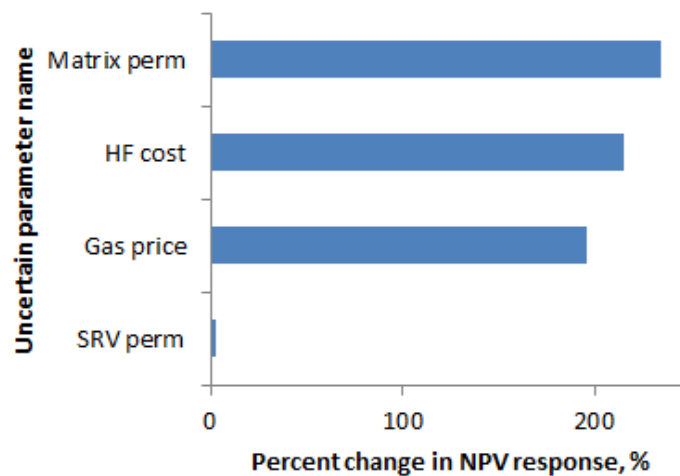


**Figure 2.9 Chart showing change in NPV response (after 1 year of production) resulting from high and low values of each parameter considered in isotropic scenario.**

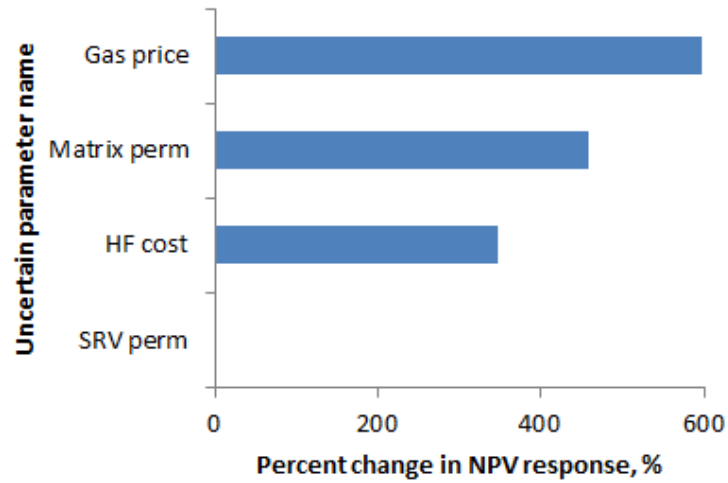


**Figure 2.10 Chart showing change in NPV response (after 5 years of production) resulting from high and low values of each parameter considered in isotropic scenario.**

In conclusion of the chapter, we emphasize that even though there are conceptual differences between simulation models corresponding to anisotropic and isotropic shale gas systems, they are fairly similar in their response to change in the key parameters. We observed that both anisotropic and isotropic simulation models were significantly affected by uncertainty in matrix permeability values, changing cost of hydraulic fracturing, and fluctuations of gas prices. Therefore, in the subsequent chapters for the purposes of optimization and UA we will focus exclusively on anisotropic models and investigate the effects of uncertainty in matrix permeability and gas prices on optimal placement of HF stages.

## CHAPTER III

### HF STAGE PLACEMENT OPTIMIZATION

#### 3.1 Introduction

In this chapter, we discuss implementation and application of the evolutionary-based stochastic optimization algorithm to the problem of optimal placement of HF stages. First, we introduce the derivative-free evolutionary algorithm (GA) with strong elitism and discuss its relevance and efficiency in solving discrete optimization problems. We also observe how the objective function changes as the set of optimization parameters changes (as we develop the workflow to optimize fixed HF half-length to variable half-length). Second, we apply the algorithm to HF stage placement and test it extensively on a shale gas simulation model. In this chapter, we particularly interested in implementation of single-objective long-term NPV optimization workflow (in comparison to multi-objective optimization framework in the subsequent Chapter V). Last, we test the robustness of the optimization results in presence of uncertainty in the key petrophysical and economic parameters: rock matrix permeability and gas price.

#### 3.2 Evolutionary-Based Stochastic Optimization

Nowadays, reservoir simulation and production optimization experts rely primarily on heuristic methods when it comes to optimization of the number of HF stages and their spacing. Often the problem is excessively constrained due to difficulty with assessment of too many parameters that are optimized in non-systematic manner. To address these challenges and assist the engineers in making the decisions, we propose a framework

that helps search the parameters domain in systematic fashion and customize the search criteria based on the economic and/or production objectives. This goal is impossible to achieve without a reliable optimization algorithm that can be used efficiently as the engine in the heart of the optimization workflow. Below we elaborate on relevance of stochastic gradient-free evolutionary optimization algorithms for the discrete problems of finding most profitable HF stage spacing, number, and half-length.

### 3.2.1 Genetic Algorithm with Strong Elitism

Genetic Algorithm (GA) is one of the most popular stochastic derivative-free optimization methods that mimics natural selection and evolution (Holland, 1975). GA constructs the initial generation of chromosomes randomly or by some probabilistic rule and then evolves these chromosomes based on the information obtained from the previous generation. Each chromosome is used as an input vector to evaluate the objective (or fitness) function. GA has many advantages in comparison to other gradient-free and gradient-based algorithms that make it attractive for our optimization framework. GA makes no assumptions about convexity, linearity, or continuity of the objective function. This property of GA is extremely valuable in the case of the complex objective function that might include both discrete and continuous input parameters. GA is perfectly suited for integer programming and continuous problems because the control vector can be represented as an array of 0's and 1's and easily manipulated even for a very large number of dimensions. Although the algorithm does not guarantee convergence to the global maximum in finite time, each next solution is expected to be

as good as or better than one in the previous step (if the best chromosome or elite is passed to the next generation consistently, thus, GA with strong elitism). Finally, as the dimensions of the problem increase (the size of the control vector), GA's ability to randomly sample a wide portion of the domain becomes particularly critical (**Fig 3.1**).

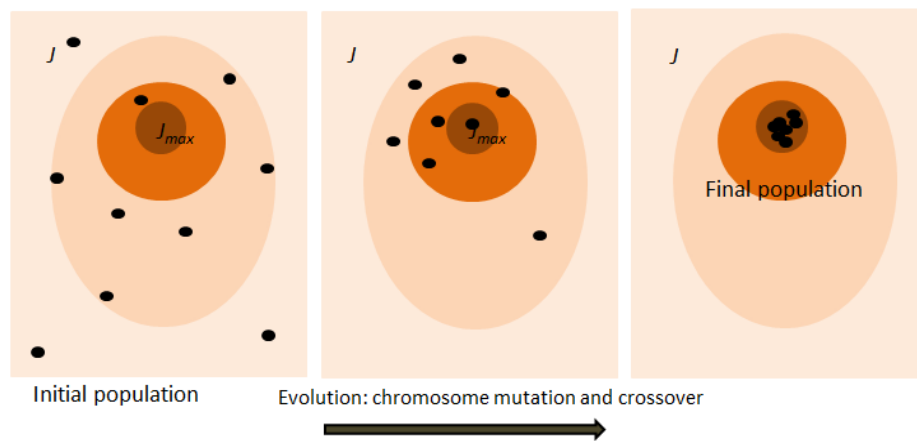


**Figure 3.1. Evolutionary search strategy of GA illustrated for a function of two variables and one global maximum.**

Although GA has many modifications and formulations depending on the nature of the problem of interest, most GA implementations use crossover, mutation, and elitism as genetic operators to evolve chromosome from generation to generation. **Fig. 3.2** demonstrates the most generalized structure of GA that might use the maximum number of generations or variance inside one generation as the termination criteria.

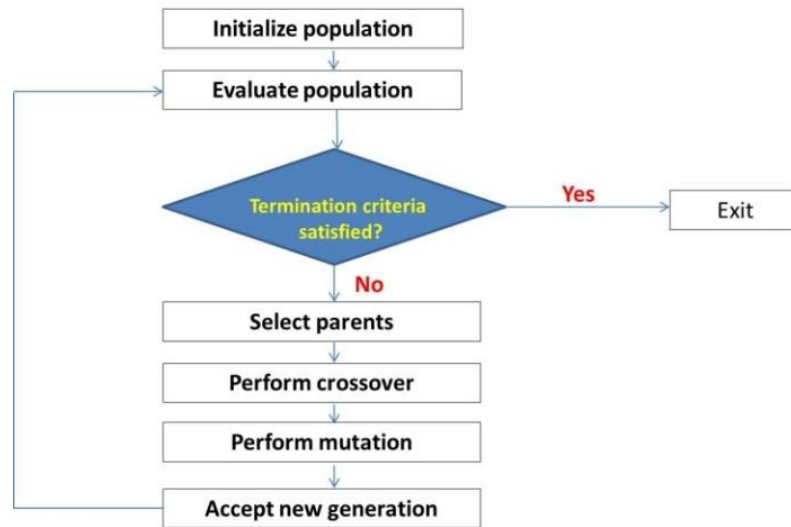


**Figure 3.2. Generalized structure of GA involves genetic operators: crossover, mutation, and elitism.**

Genetic operators are essential parts of the algorithm that determine how fast it will converge and how thoroughly it will search the input vector domain. Crossover operator can be implemented with one point, two points, multiple points, or a uniform mask. First three types choose one, two, or several points to cut and then splice two parental chromosomes in order to obtain the new one. The last type is similar to multiple-point crossover with the exception that the precise locations of crossover points are unknown in advance and generated from the uniform distribution. Uniform mask crossover is illustrated in **Fig. 3.3**.

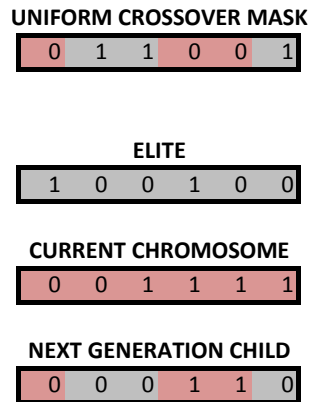


**Figure 3.3. GA uniform crossover mask applied to elite and current chromosome to obtain next generation chromosome.**

Another important genetic operator is mutation (**Fig. 3.4**). Unlike crossover that ensures convergence toward the current improved solution, mutation introduces random gene perturbations to the main search trend to keep diversity within current generation and keep exploring the domain. **Fig. 3.4** illustrates another feature of GA with strong elitism that does not allow the optimal solution to degenerate from generation to generation. Passing the elite chromosome to the next generation without mutation guarantees that the next generation will improve the optimal solution or at least remain as good as the previous one.

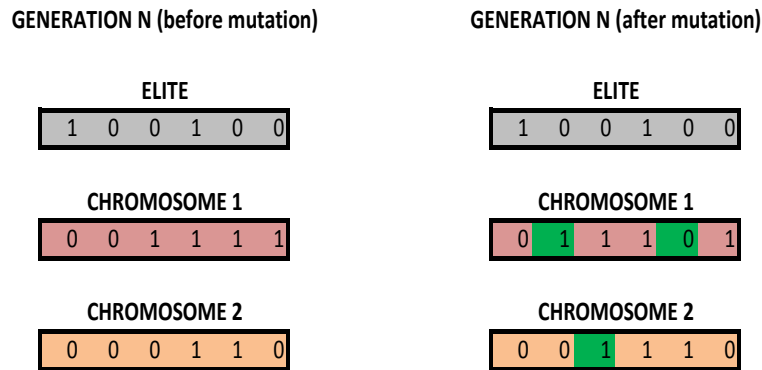


**Figure 3.4. GA mutation operator changes random number of random genes in all chromosomes except the elite to ensure diversity.**

Values of the objective function serve as quantitative measure of chromosomal performance within generation. Chromosomes and the fitness function acquire meaning depending on the problem. For example, in our application chromosomes refer to arrangements of HF stages, their spacing along the horizontal wellbore as well as half-length of the HF stages and the fitness function is the long-term discounted NPV.

### 3.2.2 Shale Gas Model and Single-Objective Function

To test the performance of GA, we use the anisotropic shale gas simulation model with some fixed averaged values for the key economic and reservoir parameters surveyed from literature (**Table 3.1**). **Figs. 3.5-3.7** give the reader visual aid in geometry and possible spacing of HF stages. They also illustrate specific implementation of LGR to accommodate fluid flow into HFs.

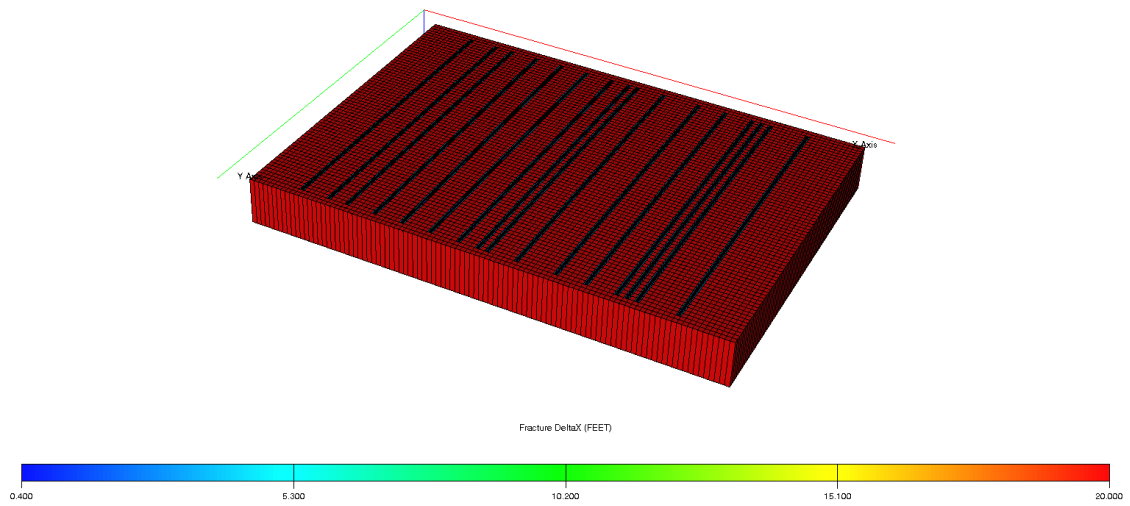


**Figure 3.5. 3D rendering of the shale gas simulation geomodel (DX property) with maximum half-length of HF stages.**

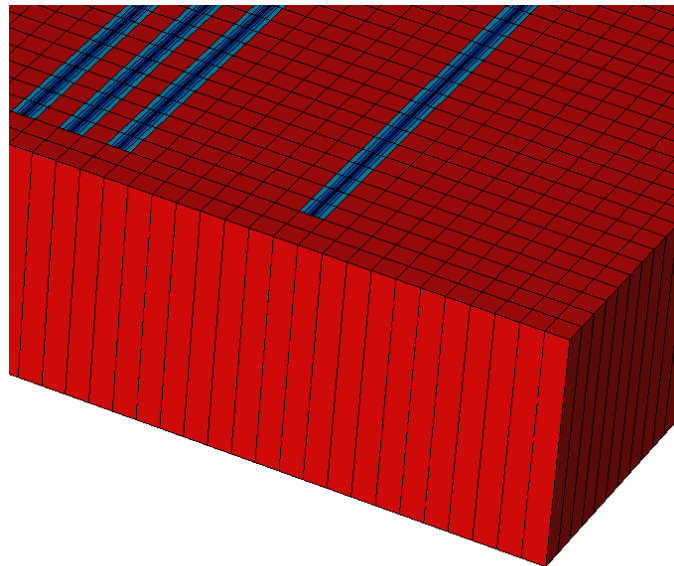


**Figure 3.6. Close-up 3D rendering of LGR for the shale gas simulation geomodel (DX property) with maximum half-length of HF stages.**

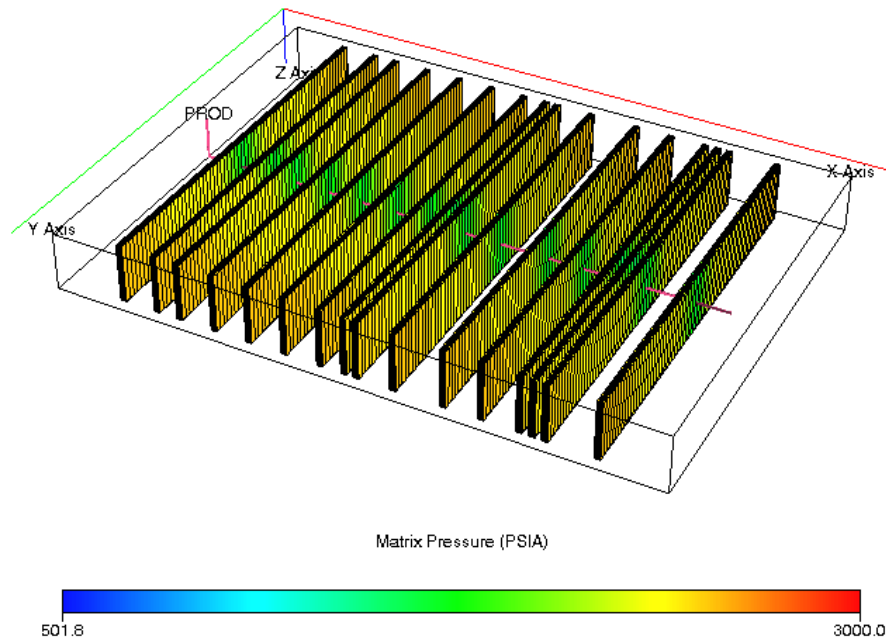


**Figure 3.7. 3D rendering of HF stages along a single horizontal wellbore at the beginning of production.**

**Table 3.1 Parameters for shale gas model and the NPV function (Ma, 2013).**

<b>Parameters</b>	<b>Values</b>	<b>Unit</b>
Model width	1420	ft
Model length	2000	ft
Model thickness	200	ft
Initial reservoir pressure	3000	psi
Reservoir temperature	150	°F
Rock density	161	lbs/ft <sup>3</sup>
Producing bottom hole pressure	500	psi
Wellbore length	1400	ft
Production period duration	5	years
Matrix porosity	6	%
Total gas content	70	%
Langmuir pressure	650	psi
Langmuir volume	0.096	mscf/ton
Hydraulic fracture height	200	ft
Hydraulic fracture half-length	260 or variable	ft
SRV permeability	0.08	md
Drilling base cost per well (vertical part)	2,000,000	\$
Drilling cost per grid block (horizontal part)	6,000	\$
Daily operating expenses per well	60	\$
Gas price	3.2	\$/mscf
Base cost per HF stage	75,000	\$
Cost per length of HF stage	2,000	\$/ft
Discount rate	12.5	%

Though the discounted NPV objective function is defined similarly to that in **Eq. 2.1**, the expression is customized to account for increasing cost of HF stage with increasing half-length. Thus, the final form of the objective function which is optimized by GA for a single horizontal wellbore follows:

$$NPV = \sum_{k=1}^K \frac{(Q_g^k \cdot r_g - Q_w^k \cdot r_w - O) \cdot \Delta t^k}{(1 + b)^{t^k/365}} - (C_w + N_{HF}(C_{fb} + C_{fl}x_{length}) + L_w C_p). \quad (3.1)$$

Here,  $k$  is time index,  $K$  is the total number of time periods simulated [days],  $Q_g^k$  is gas production rate during time period  $k$  [mscf/day],  $r_g$  is gas price [\$/mscf],  $Q_w^k$  is water production rate during time period  $k$  [bbl/day],  $r_w$  is cost of water disposal [\$/bbl],  $O$  is operational cost of the well per day [\$/day],  $\Delta t^k$  is duration of the  $k$ th time period [days],  $b$  is a discount rate [%/100/year],  $C_w$  is base cost of drilling the vertical part of the producer well [\$],  $N_{HF}$  is the number of HF stages,  $C_{fb}$  is hydraulic fracturing base cost per stage [\$],  $C_{fl}$  is the cost of HF stages per unit of length [\$/ft],  $x_{length}$  is length of HF stage [feet],  $L_w$  is horizontal portion of the producer in grid blocks, and  $C_p$  is well penetration cost per grid block [\$].

### 3.3 Optimization with GA

As we mentioned above, GA comes in variety of implementations and modifications depending on the problem. For the discrete problem of placing HF stages along a single horizontal wellbore and optimizing their half-length, binary GA is a suitable option.

Thus, the optimization problem that GA solves can be described mathematically as follows:

$$u^* = \underset{u \in U}{\operatorname{arg\,max}} \operatorname{NPV}(u), \quad (3.2)$$

In **Eq. 3.2**,  $u^*$  is the vector containing optimal or nearly optimal locations of HF stages as well as their half-length. We make an assumption that all HF stages have the same half-length for the homogeneous matrix permeability map which is consistent with current understanding and simulation practices.

For the purposes of testing GA and its running time, we also do not impose excessive constraints on the optimization problem. For example, in this chapter we do not always use specification of the minimal interval between HF stages. Though it is common in industry to space HF stages no closer than 50-150 feet between each other, in this chapter, we deliberately allow the algorithm to space HF stages according to changes in the NPV objective function and each gridblock penetrated by the well can be a potential place for a HF stage (King, 2010). In this way, we can observe if the algorithm spaces the HF stages fairly uniformly which is an expected outcome for homogeneous matrix permeability. For HF placement optimization under parameter uncertainty at the end of this chapter, however, we will use minimal spacing between stages of at least 40 feet in order to speed up the computation.

Schematic **Fig 3.8** presents detailed optimization workflow with the GA engine. The framework connects in seamless fashion ECLIPSE™ 300 simulator with (version 2012.2) with optimization code written in MATLAB.

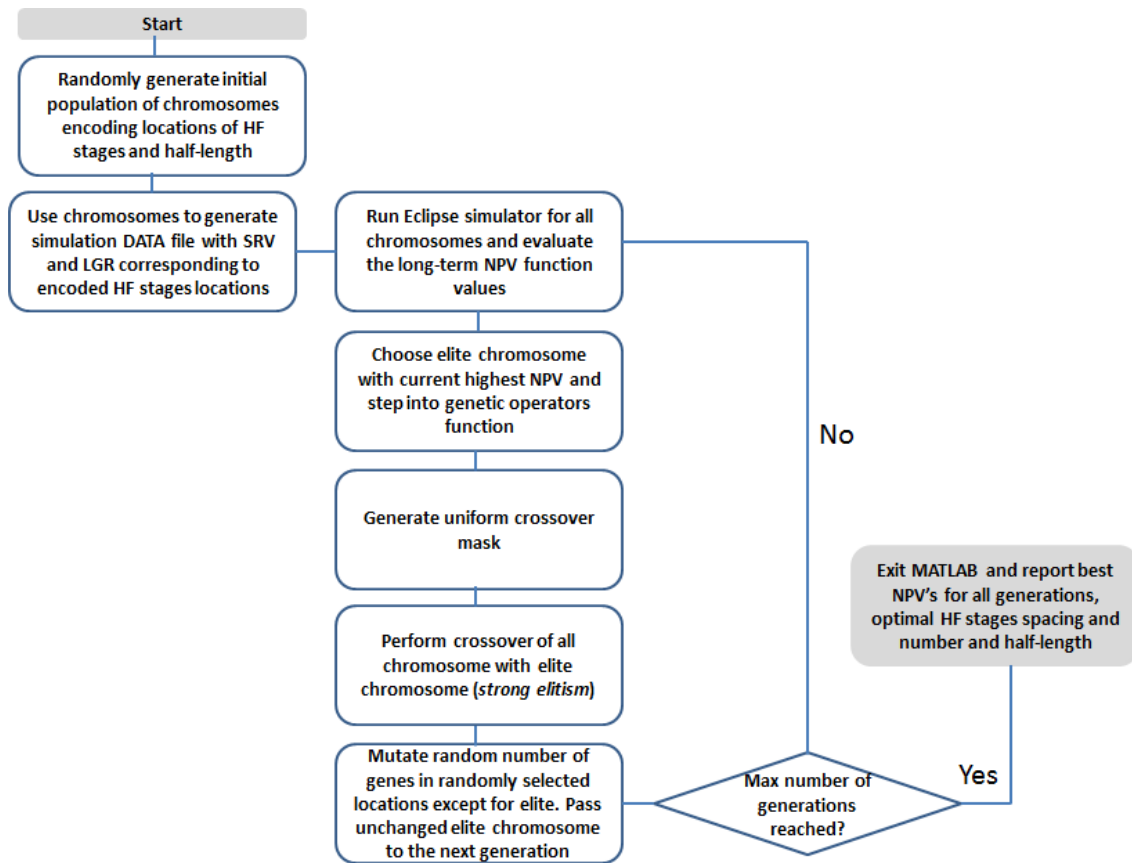


**Figure 3.8. Detailed workflow for HF stages placement and half-length optimization problem with GA integrating MATLAB code and Eclipse simulation results.**

### 3.3.1 HF Stages Placement Optimization with Fixed Half-Length

This section provides test cases for HF number and spacing optimization with fixed half-length. In addition to analyzing the optimal results, we are interested in efficient computational performance, thus, number of simulator calls and running time are provided for later comparison with coupled half-length optimization test cases for the same shale gas model.

**Fig. 3.9** gives graphical aid to understand how GA encodes HF locations, number, and spacing. Each column corresponds to one possible arrangement of HF stages along a horizontal wellbore. For the test cases in this chapter, we do not introduce minimal interval between stages and, therefore, each grid block penetrated by the well is a potential location for HF stage. The number of columns refers to the number of individual chromosomes within generation. Color code provides visual interpretation of spacing and intensity of HF placement.

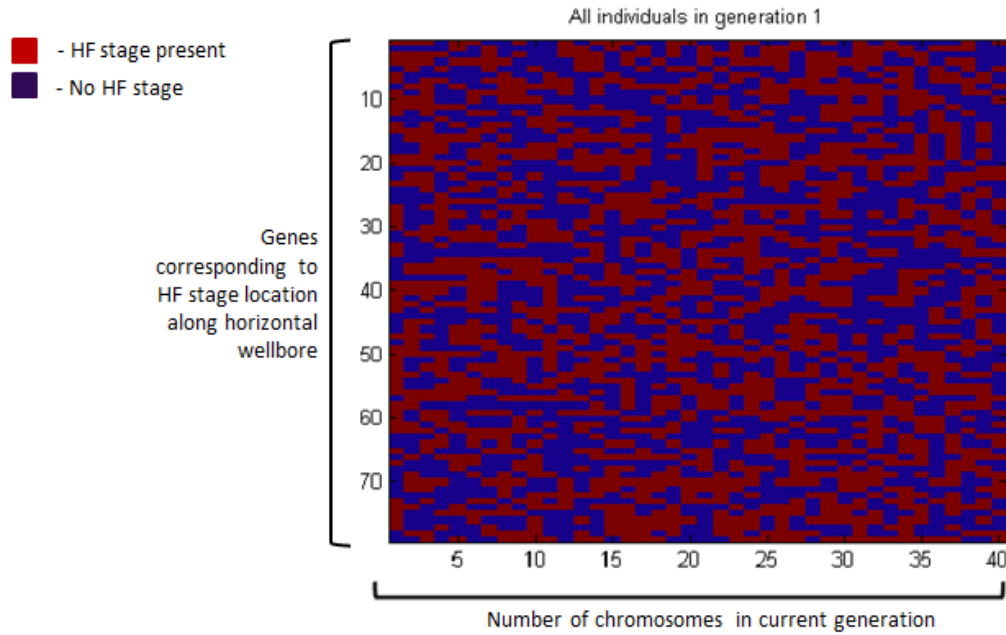


**Figure 3.9. Interpretation of GA’s chromosomes and generations for optimization of number of HF stages, their locations, and spacing given specific HF half-length.**

Because GA test runs with large number of generations and chromosomes within generation are computationally demanding, below we provide smaller GA test runs that

optimize number and locations of HF stages for a given fixed HF half-length (e.g. 13 grid blocks or 260 feet). The line plot in **Fig. 3.10** presents the results of the four runs. We observe that due to stochastic nature of selection of the initial population as well as application of mutation and crossover genetic operators, optimized long-term NPVs are different. Yet, they converge toward some global maximum value.

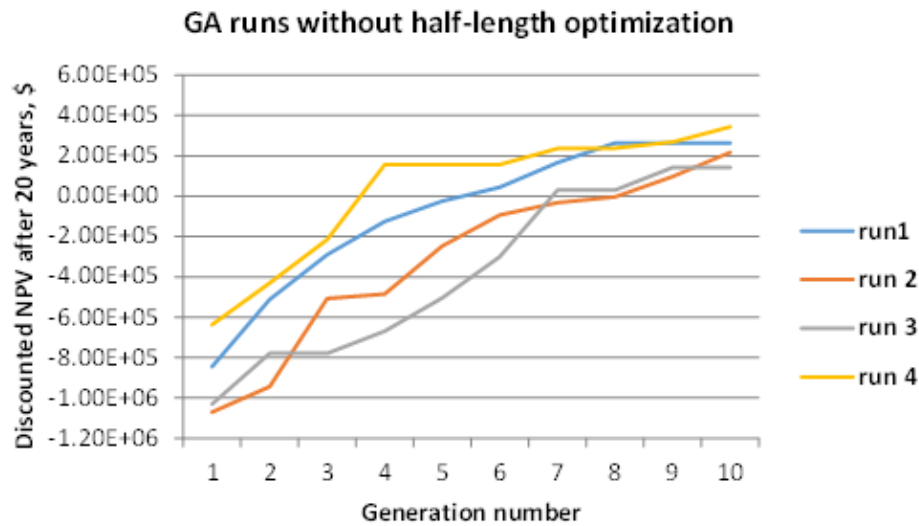


**Figure 3.10. Stochastic optimization of HF stages placement with GA over 10 generations with 30 chromosomes in each generation.**

Schematic **Fig. 3.11** provides visual comparison between spacing and optimal numbers of HFs from the four test cases and a larger test run for the same shale gas model. Here, the reader may observe that the longer GA evolves, the more uniform and wider spacing becomes. For a fixed HF half-length, GA tries to reduce the number of stages and increase spacing between them to avoid interference between the stages. Except for the Run 4, smaller GA runs do not start from “good” initial populations of

chromosomes (their best NPVs in the first generation are below \$-800000) and, thus, take more computational time to evolve to better values of the objective function.

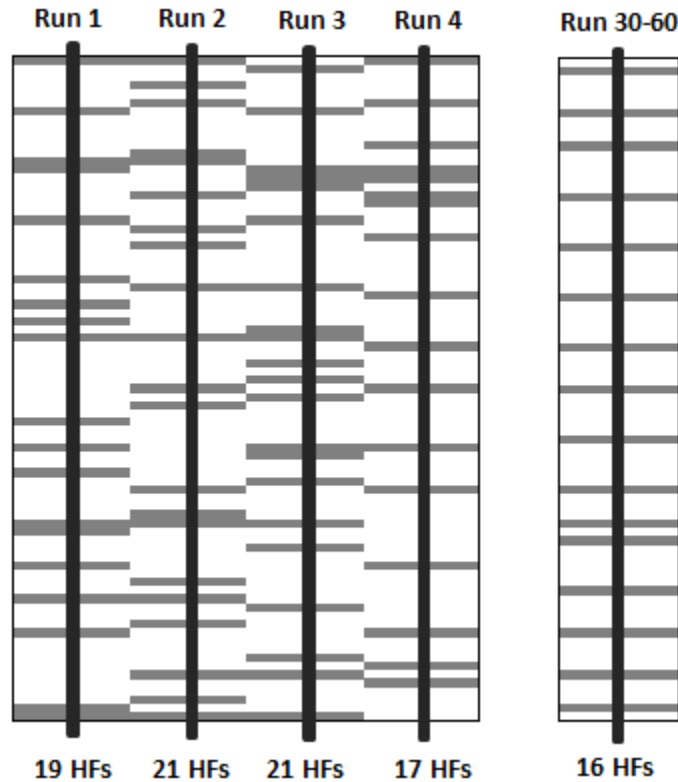


**Figure 3.11. Results of four test runs of GA over 10 generations with 30 chromosomes in each generation juxtaposed with one GA test run over 30 generations with 60 chromosomes. Optimal number of stages and HF locations.**

Scatter plot in **Fig. 3.12** provides relationship between running times and optimized NPVs for all four test runs. The cost of poor initial population is not only lower optimized NPV value, but also higher running time. This is true because Runs 1, 2, and 3 have more HF stages (19, 12, and 21 correspondingly), and, thus, require LGRs in larger number of grid blocks. That drives the computational cost up and overall performance down.

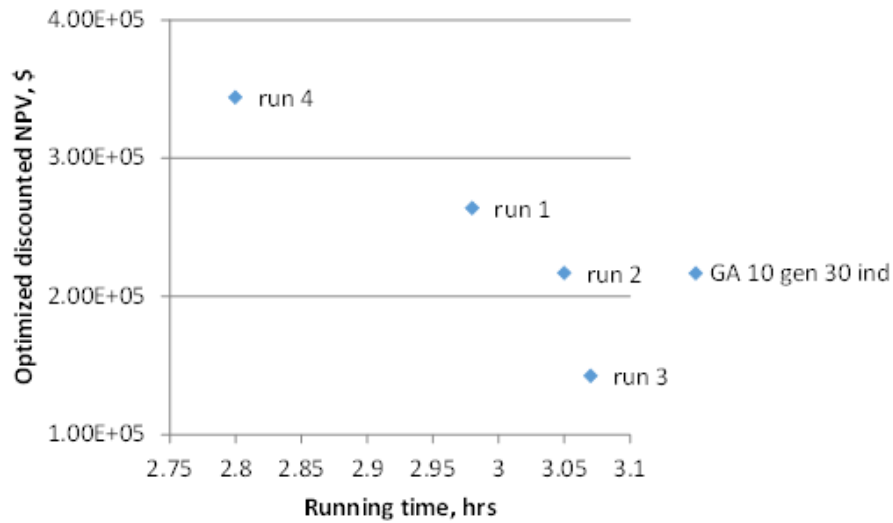


**Figure 3.12. Cross-plot of the highest discounted NPV values for four test runs versus running time (GA over 10 generations with 30 chromosomes in each generation).**

Above we provided one GA test run with the higher number of generations and chromosomes within generation (30 generations and 60 chromosomes) and observed better optimized results. Let us now investigate this run in more detail and see the evidence that longer evolution time can offset the negative effect of poor initial population. **Fig. 3.13** gives snapshots of evolution after the 1<sup>st</sup>, 10<sup>th</sup>, 20<sup>th</sup>, and 30<sup>th</sup> generations. One can see that after the 10<sup>th</sup> generation the situation with HF stage spacing only slightly better than in the four small test runs (the best NPV value at this point is about \$410000 only due to the higher number of chromosomes within each generation). Nevertheless, as we let GA evolve three times longer than in previous short test cases, uniform spacing pattern of HF stages becomes more apparent.

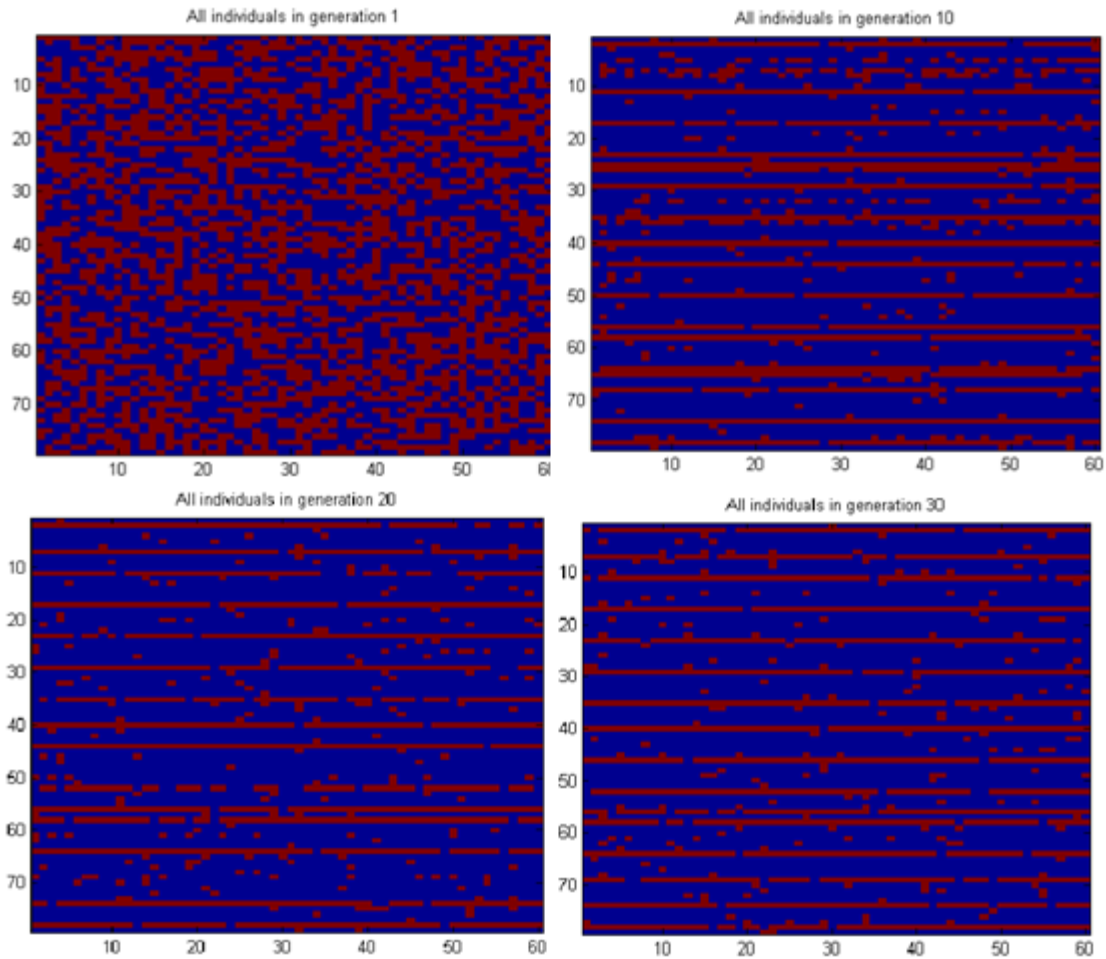


**Figure 3.13. GA for optimization of number and locations of HFs. Evolution of chromosomes through 30 generations exhibits convergence by crossover and diversity by mutation.**

The NPV summary plot in **Fig. 3.14** illustrates that the values monotonically increase with small plateau periods well beyond the 15<sup>th</sup> generation. After the 20<sup>th</sup> generation though, GA stabilizes and only increases once due to successful mutation in some of the chromosomes. From simulator call statistics we observe that elimination of the same chromosomes saved 16 simulator calls. This is a very modest saving of

computational time due to an aggressive mutation strategy that our GA implementation has adopted.

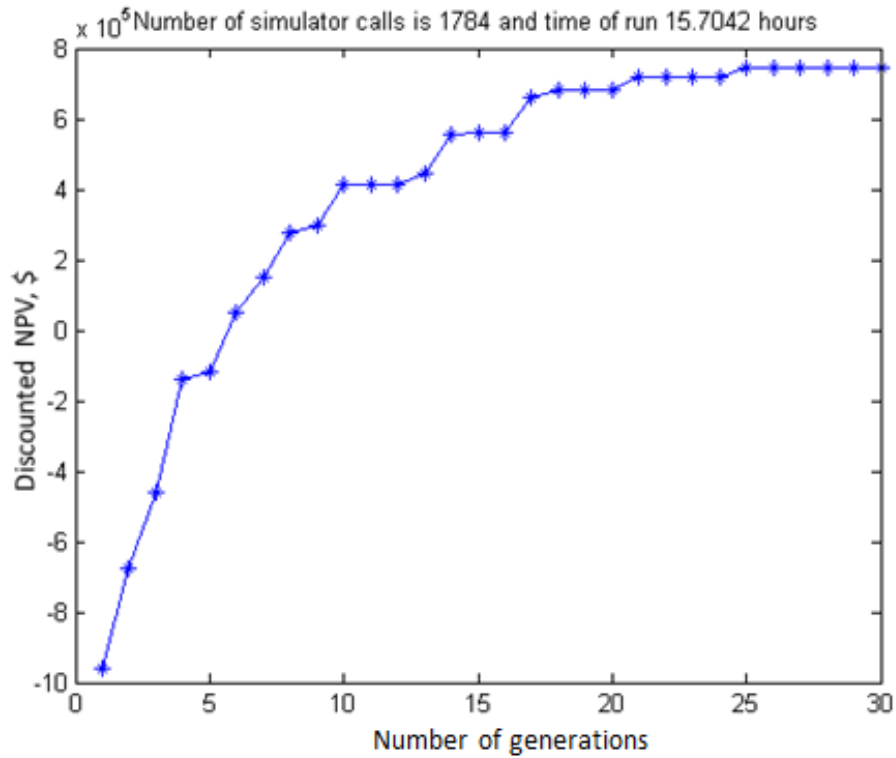


**Figure 3.14. Highest NPV values after 20 years across 30 generations with 60 chromosomes in GA test run.**

Now that we have tested GA for optimization of HF stage number and spacing, let us add another degree of freedom to the optimization problem and optimize HF half-length. Because we are dealing with homogeneous matrix permeability field, all HF stages are assumed to have the same half-length.

### 3.3.2 HF Stage Placement and Half-Length Optimization

In this subsection we investigate coupling between HF stage number and spacing optimization and HF half-length optimization. Let HF half-length change from zero (meaning no HF stage in the gridblock) to maximum physically feasible value for the particular model or reservoir (for example, 33 gridblocks or 660 feet). Then, the constrained optimization problem can be written mathematically as follows:

$$\begin{cases} \max NPV(u) \\ s. t. \tilde{u}_i \leq hl_{max} \\ \tilde{u}_i \geq hl_{min} \\ i = 1, 2, \dots, n. \end{cases} \quad (3.3)$$

In **Eq. 3.3**,  $\tilde{u}_i$  refers to the portion of a chromosome that encodes HF stage half-length,  $hl_{max}$  is maximum feasible half-length,  $hl_{min}$  is minimum feasible half-length. Portion of the chromosome that contains information about half-length is binary like the rest of the genes. This binary number, however, is then converted to decimal in order to construct proper length SRV and LGR in the simulator data file. Half-length is treated no different than the rest of the chromosome for crossover, mutation, and elitism purposes (**Fig. 3.15**). Unlike other genes though, this portion is controlled for maximum decimal value. In other words, if after crossover or mutation we obtain a binary number that converts into a value higher than feasible maximum, it is set to the maximum value. As it is evident from **Eq. 3.1**, the growth of the HF half-length is controlled primarily by economic considerations. The longer HF stages become, the more expensive they become in linear fashion. Linear increase in cost of HF stage length is one of the assumptions that we make in order to have a systematic way to study performance of the simulated system. In reality, nevertheless, linear increase per foot of length might not be

true depending on petrophysical and geomechanical properties of a particular shale formation.

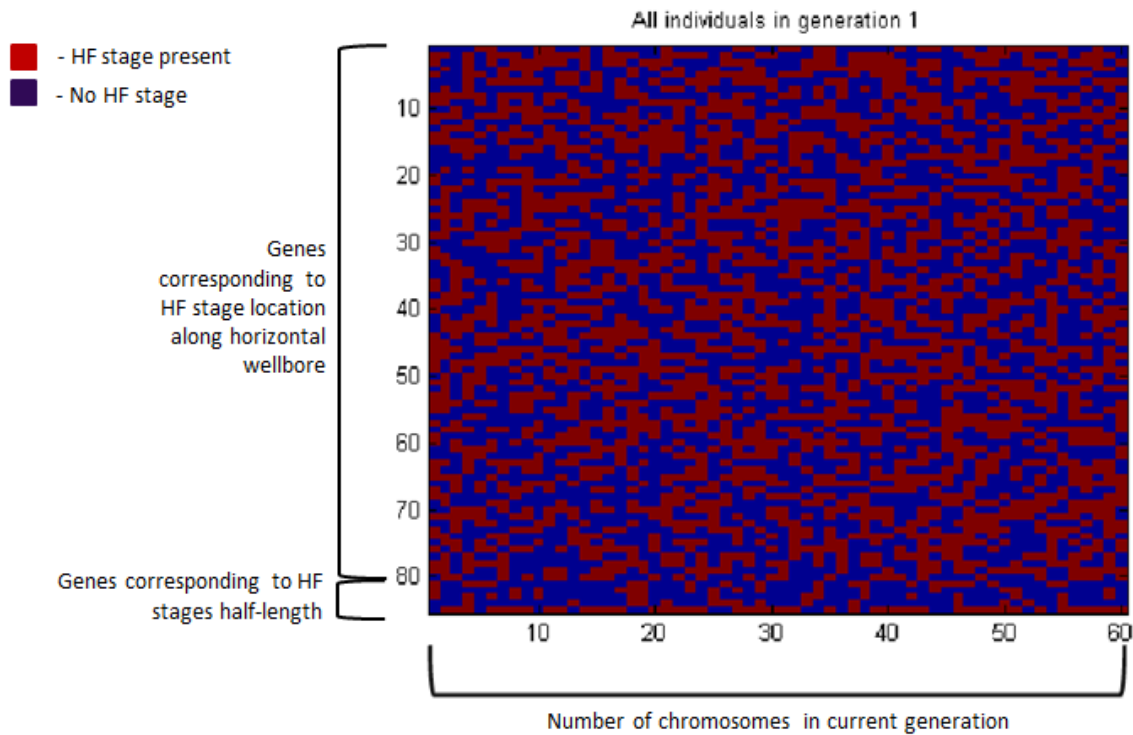


**Figure 3.15. Interpretation of GA's chromosomes and generations for HF stage placement and half-length optimization problem.**

Because simultaneous optimization of number, spacing, and half-length of HF stages is a resource consuming process, we provide some test results of GA optimization with a smaller number of chromosomes within generation and fewer generations. The reason of rapid increase of computational cost is that each additional gridblock added to HF half-length requires LGR and as GA searches through the solution space and tries various half-lengths, the overall simulation time increases rapidly (e.g. for GA with 10

generations and 30 chromosomes the total simulation time is between 5.8 and 6.4 hours, while for GA with 30 generations and 60 chromosomes it goes beyond 30 hours).

Test runs summary plot (**Fig. 3.16**) provides the discounted NPV values for four runs. We observe that all test runs increase monotonically toward the global maximum. All runs reach optimal HF half-length of 33 griblocks (or 660 feet) within the first generation. This can be easily explained by the small binary domain that corresponds to HF half-length. Six binary digits (**Fig. 3.15**) encode HF half-length. This give 64 possible binary strings. In addition to that, not all strings are acceptable because that exceed the maximum allowed half-length. Thus, we expect that the entire domain corresponding to half-length would be search within about two generations (given 30 chromosomes within generation).

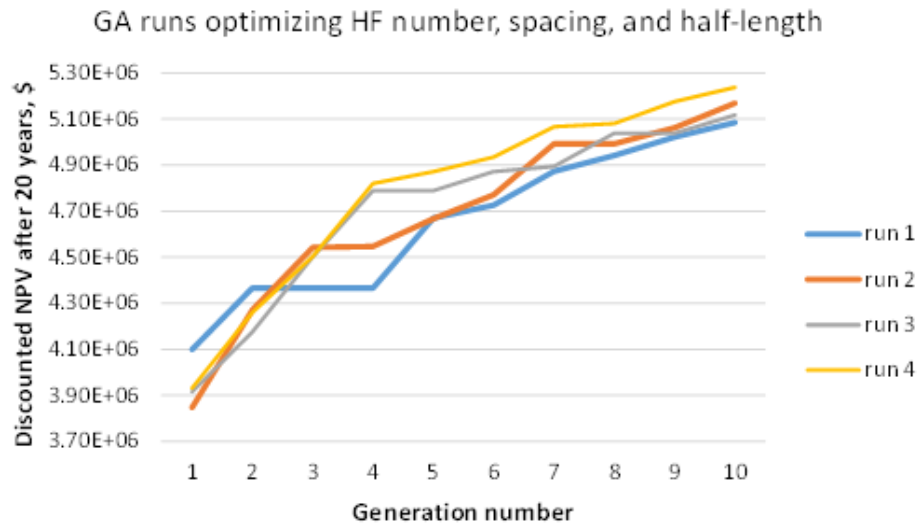


**Figure 3.16. Stochastic optimization of HF stage placement and half-length with GA over 10 generations with 30 chromosomes in each generation.**

Schematic **Fig. 3.17** juxtaposes optimal results (stage locations and spacing) from the test runs mentioned above. This visually effective comparison provides the evidence of stochastic nature of GA in selection of locations and of its efficiency even if the algorithm has been run for a small number of generations and small number of chromosomes. The algorithm is powerful enough to space HFs roughly uniformly after sampling 300 values of the objective function in multi-dimensional space that contains an excess of  $7.7e^{25}$  possible binary strings as the control vector input and comparable number of NPV solutions. From the optimal HF locations in all four runs, we observe that several HF locations are the same. These HF stages would be considered the strongest candidates for stimulation experts.

Scatter plot in **Fig. 3.18** gives a visual measure of computational time versus discounted long-term NPV obtained. Runs that take more simulation time evaluate more production arrangements with longer HF half-length and/or more HF stages. In these cases the model grid has more gridblocks with LGR and, thus, becomes more computationally demanding.

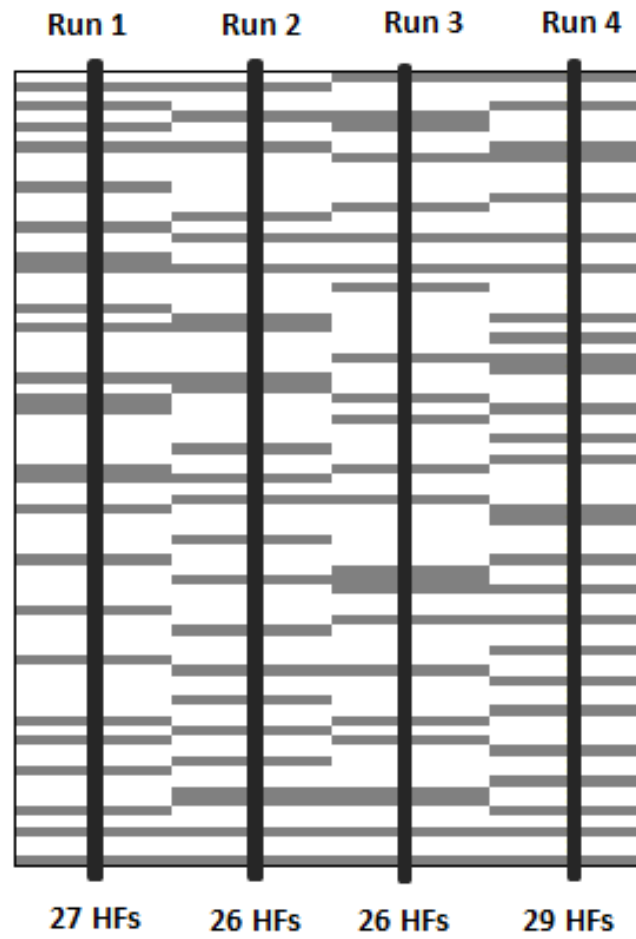
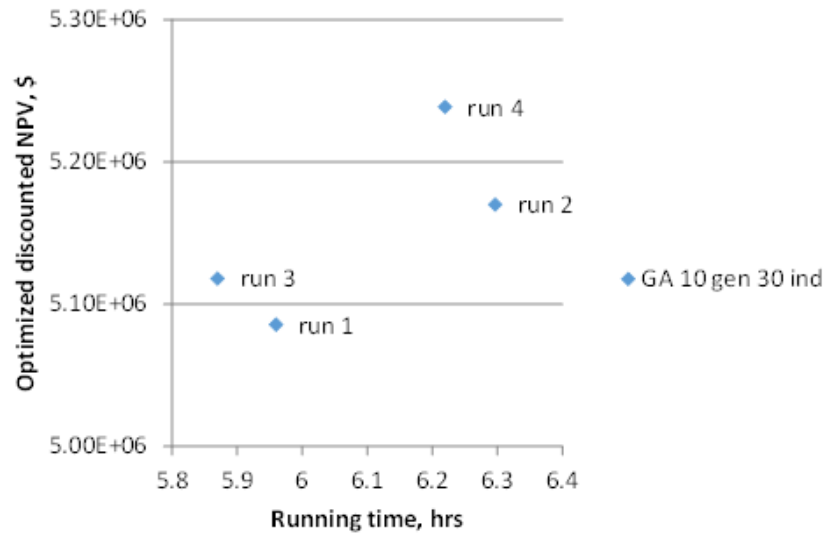
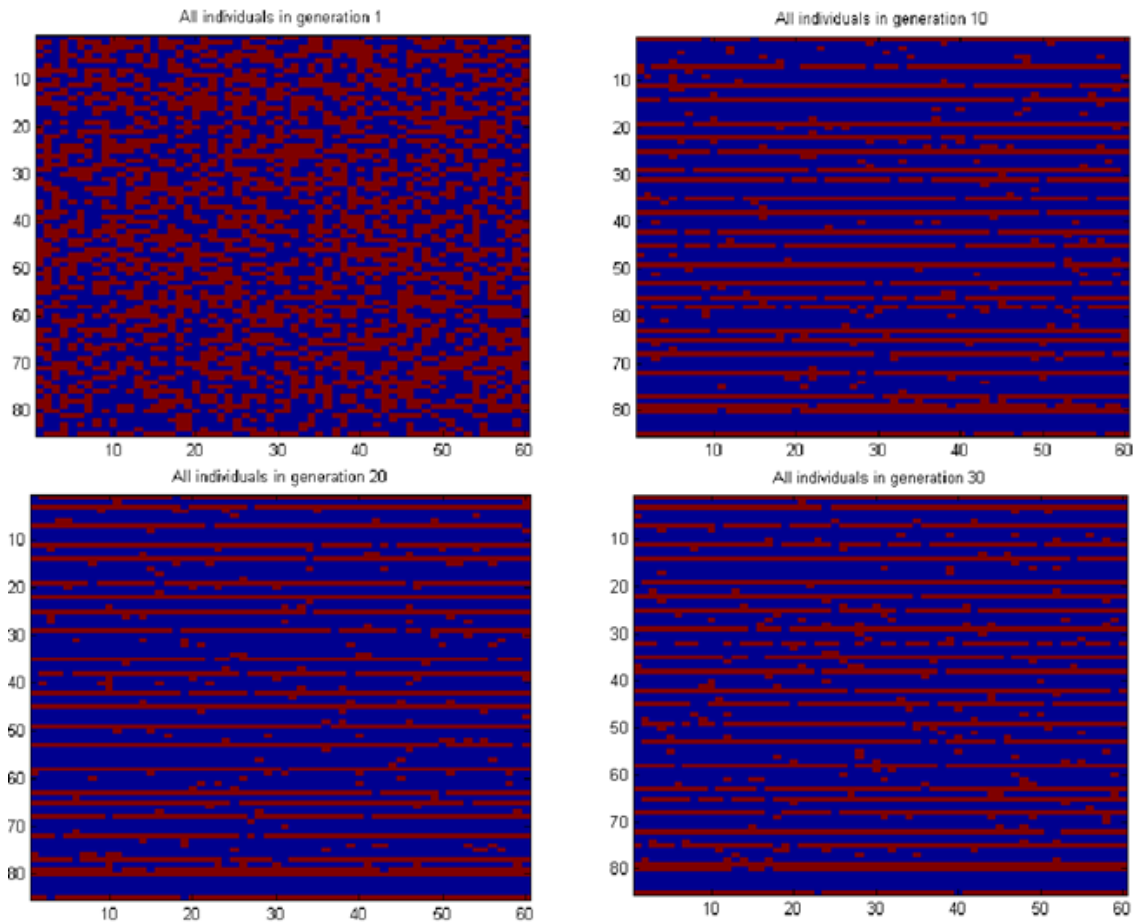


Figure 3.17. Optimal number and HF locations for GA over 10 generations with 30 chromosomes in each generation.



**Figure 3.18. Cross-plot of the highest discounted NPV values for four test runs versus running time (GA over 10 generations with 30 chromosomes in each generation).**

Above we saw that the optimal number of HF stages when minimal spacing is one gridblock is between 26 and 29. Below we provide a larger test run and evolution of the optimal solution (**Fig. 3.19**). GA searches the optimal solution of the number and spacing of HF stages as well as their half-length using 60 chromosomes and 30 generations for the same shale gas model. From four snapshots of the 1<sup>st</sup>, 10<sup>th</sup>, 20<sup>th</sup>, and 30<sup>th</sup> generations, the reader can observe convergence to the global optimum from initial randomness. Preservation of elite chromosomes and crossover ensure monotonical increase of the NPV values (**Fig. 3.20**) while random gene mutation fine-tunes the locations.



**Figure 3.19. Evolution of chromosomes through 30 generations exhibits convergence by crossover and diversity by mutation.**

With same genes elimination procedure, we expect the test run to perform no more than 1800 simulator calls. **Fig. 3.20** shows that GA requested 1770 Eclipse simulator calls which is saving of 30 calls and comparable to a half of one generation. The same plot demonstrates that after about 10 generations the NPVs plateau and stay stable even though GA continues to mutate genes and perturb the control vector.

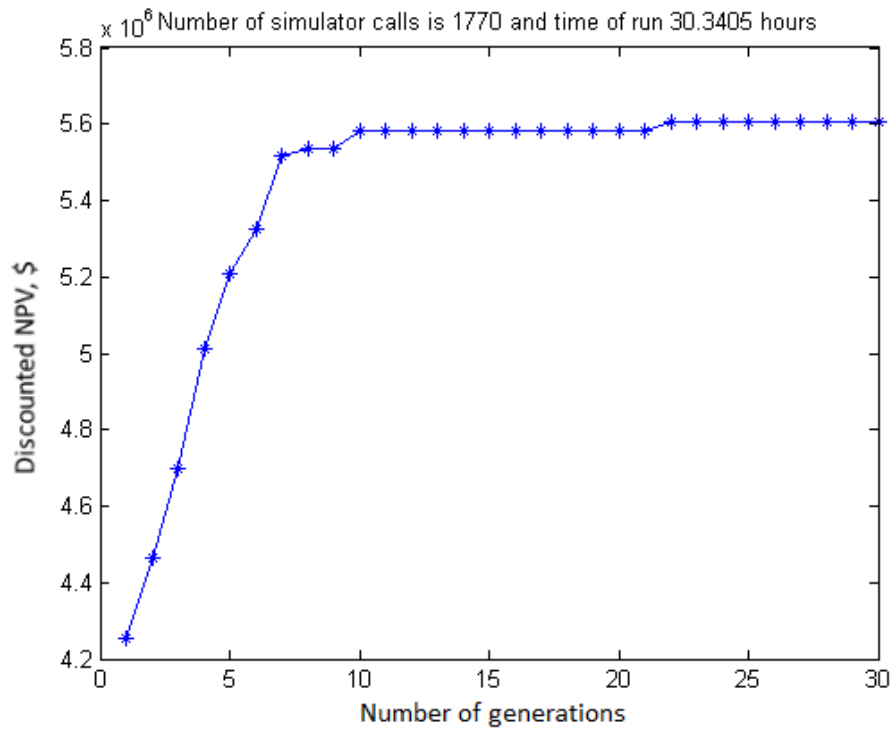


**Figure 3.20. Highest NPV values across 30 generations in GA test run.**

Evolution of best half-lengths across 30 generations shows that GA finds the optimal half-length (the maximum of 33 grid blocks or 660 feet) within the first generation. The subsequent **Fig. 3.21** demonstrates the optimized HF spacing after longer evolution. Here, we have 25 HF stages almost uniformly distributed across the length of the horizontal wellbore. Similarly to the previous subsection, we did not introduce any additional constraint in the form of minimal interval between the HF stages and GA was able to obtain reasonable spacing. This observation emphasizes universality and flexibility of our GA implementation.

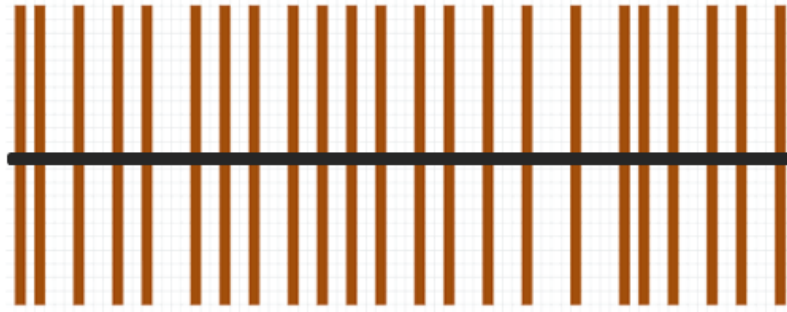


**Figure 3.21. Optimal HF stages placement after 30 generations in GA test run.**

.As we mentioned above, in our optimization framework with GA engine we assume equal half-length for all HF stages. It is important to note that the framework can be easily enhanced to accommodate different half-lengths for each HF stage. This can be accomplished by encoding individual half-lengths in binary sequences corresponding to the HF stages. However, this enhancement comes at great computational price, because for each gene encoding HF stage location we have several additional genes with binary half-length. The dimensionality of such problem will increase dramatically and computational time might require code parallelization and high-performance computational resources.

### 3.4 HF Stage Placement Optimization in Presence of Uncertainty

After we developed and tested the framework for HF stage placement, we answer the question of sensitivity of the optimization results to changes in the most significant explanatory variables. In Chapter II we performed screening of uncertain parameters of the shale gas simulation model and concluded that gas price and rock matrix

permeability had measurable effect on percent change in long-term discounted NPV. Now let us extend the production period to twenty years and apply the optimization framework to an ensemble of five (5) geologic realizations. The only parameter that we vary at this point is matrix permeability. **Table 3.2** lists all values of matrix permeability that we use for five realizations.

**Table 3.2 Rock matrix permeability values for ensemble of geologic realizations.**

Realization	Percent deviation from base case	Matrix permeability
1	0	0.00015 md
2	20%	0.00018 md
3	50%	0.0003 md
4	-20%	0.00012 md
5	-50%	0.000075 md

We provide the summary of the optimized results (HF stage locations) for the ensemble of five realizations in **Fig. 3.22**. Here we use minimum spacing between HF stages of 40 feet. Thus, on the plots below (**Figs. 3.22-3.23**) even though some HF stages are placed next to each other, they are in fact separated by at least 40 feet.

Both plots illustrate that the number of HF stages is not significantly affected by a broad range of uncertainty in matrix permeability (from -50% to +50% from the base value of 0.00015 md). We consistently obtain around 18 HF stages of the same half-length (660 feet). We also observe that the locations of the stages are also fairly

consistent. Though, as expected we see that the tighter matrix leads to the more densely spaced HF's.

**Fig. 3.24** shows the effect of uncertainty in matrix permeability on optimal NPV values. The reader can observe that the band formed by the lines is reasonably narrow. In other word, an error in matrix permeability measurement (even if it comes from the wide range from -50% to +50%) is not likely to affect the economics of the project on the long run.

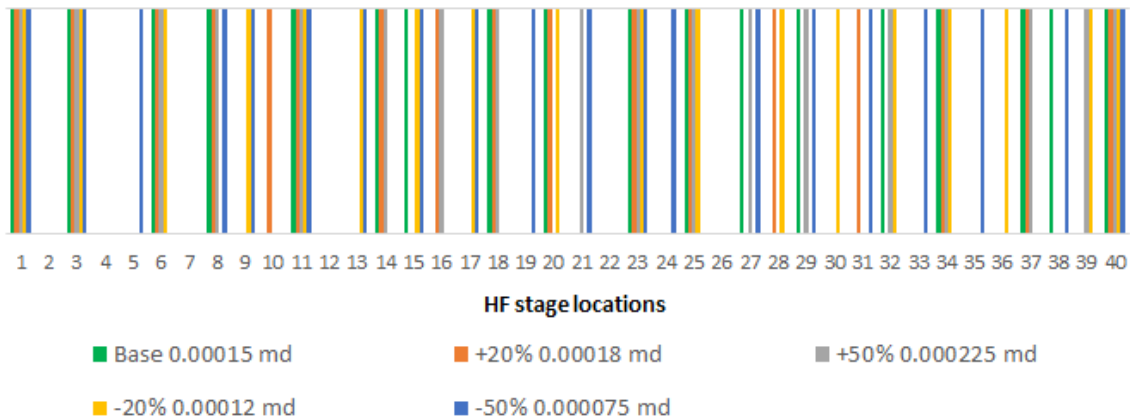


**Figure 3.22. Juxtaposition of optimal HF stage locations for an ensemble of 5 geological realizations (each realization has varying matrix permeability +/-20% and +/- 50% from the base geomodel).**

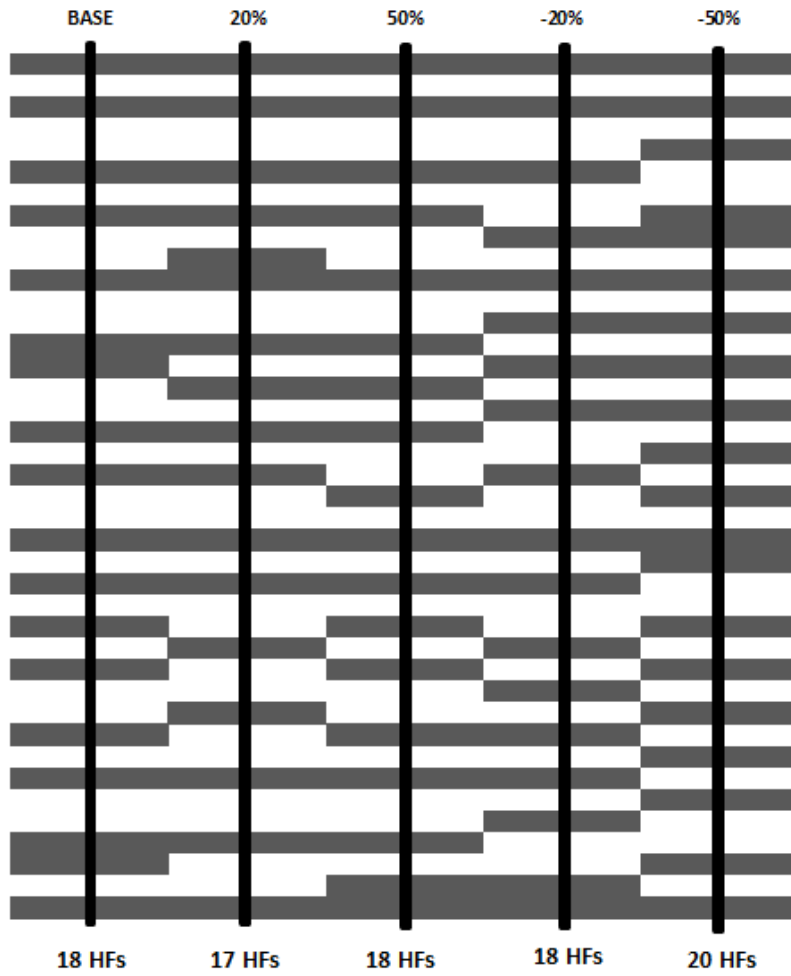


Figure 3.23. Juxtaposition of optimal HF stage locations for an ensemble of 5 geological realizations (well location is unchanged from model to model).

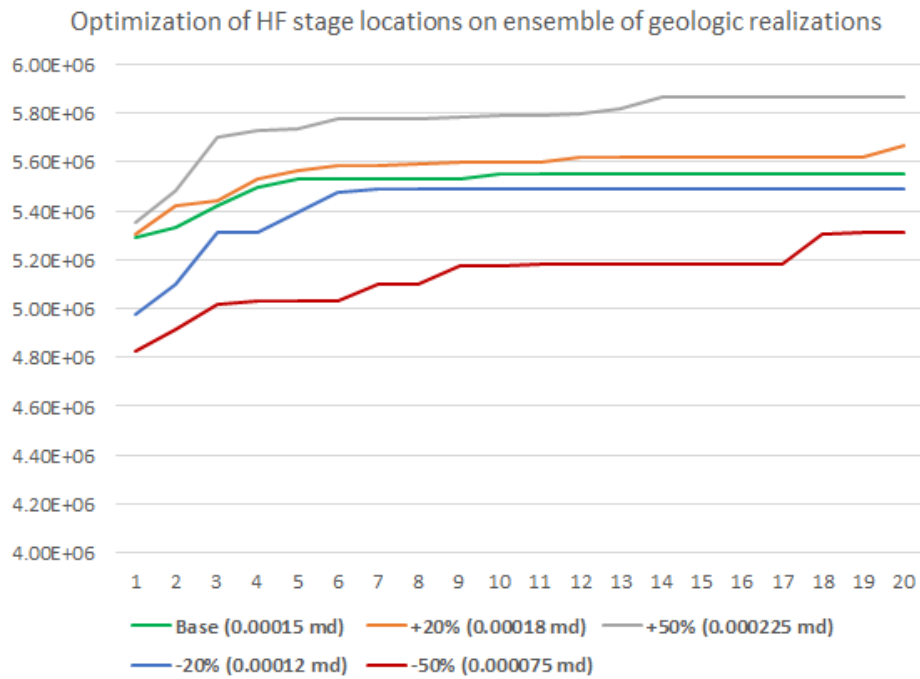


Figure 3.24. Effect of uncertainty in shale matrix permeability on optimal discounted NPV values.

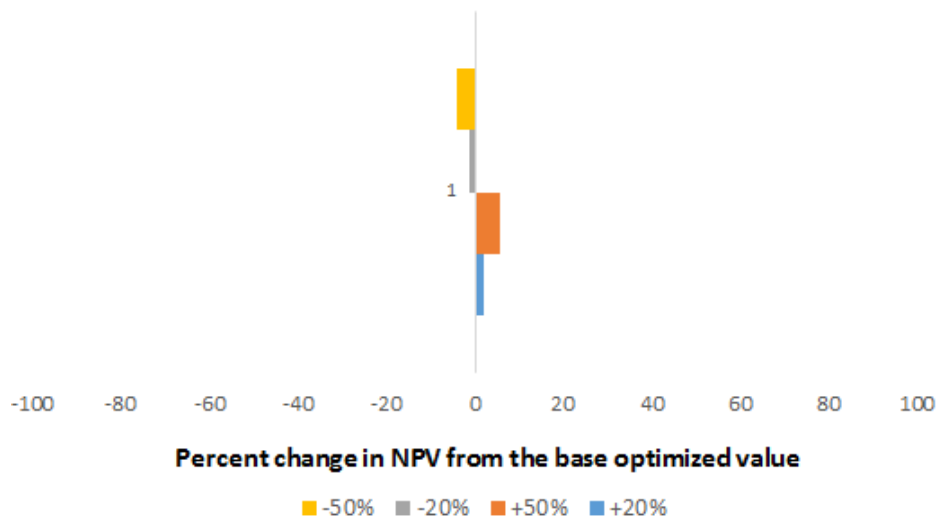


Figure 3.25. Effect of uncertainty in shale matrix permeability: percent change in discounted NPV values from the optimized base value.

**Fig. 3.25** quantifies the small effect of uncertainty in matrix permeability. Uncertainty in permeability between -50% to +50% from the base value translates into the range of NPVs between -5% to 5% from the base optimized NPV value.

Rock matrix permeability is not the only significant parameters that influence the response of the system. Gas price is another uncertain variable that can affect optimization results and project economics. To keep consistent ranges, let us vary gas prices also within -50% to +50% range from the base value of 3.20 \$/mscf (**Table 3.3**).

**Table 3.3 Gas price values for optimization under uncertainty.**

Realization	Percent deviation from base case	Gas price
1	0	3.20 \$/mscf
2	20%	3.84 \$/mscf
3	50%	4.80 \$/mscf
4	-20%	2.56 \$/mscf
5	-50%	1.60 \$/mscf

The optimization results from these five runs reveal magnitude of the impact of gas price uncertainty. Schematic **Fig. 3.26** shows startling difference is the optimal numbers of HF stages and their locations for same models run with different prices, *ceteris paribus*<sup>1</sup>. When the gas price is reduced by 20%, the optimization framework counter-balances the change in price by increased production from more HF stages (20 HF stages in comparison to 17 HF stages in the base case). However, as the price

---

<sup>1</sup> *Ceteris paribus* is Latin for “everything else being equal or kept constant”

continues to fall and is a half of the base value, placing more HF stages consumes too much initial capital and the framework dramatically reduces the number of broadly-spaced stages to fourteen (14).

The NPV line plots in **Fig.3.27** demonstrate the collapse of the project's revenue when the gas price drops to 50%. After twenty (20) years of production, the discounted revenue is only about a half of million dollars. The reader can observe the breadth of the uncertainty band in comparison to one in **Fig. 3.24**.

The percent change chart in **Fig. 3.28** illustrates quantitatively and graphically that 50% reduction or increase in gas price from the base value causes almost 100% change (reduction or increase respectively) from the base optimized NPV value. Thus, the gas price and its change literally “makes or breaks” the economics of a shale gas project.

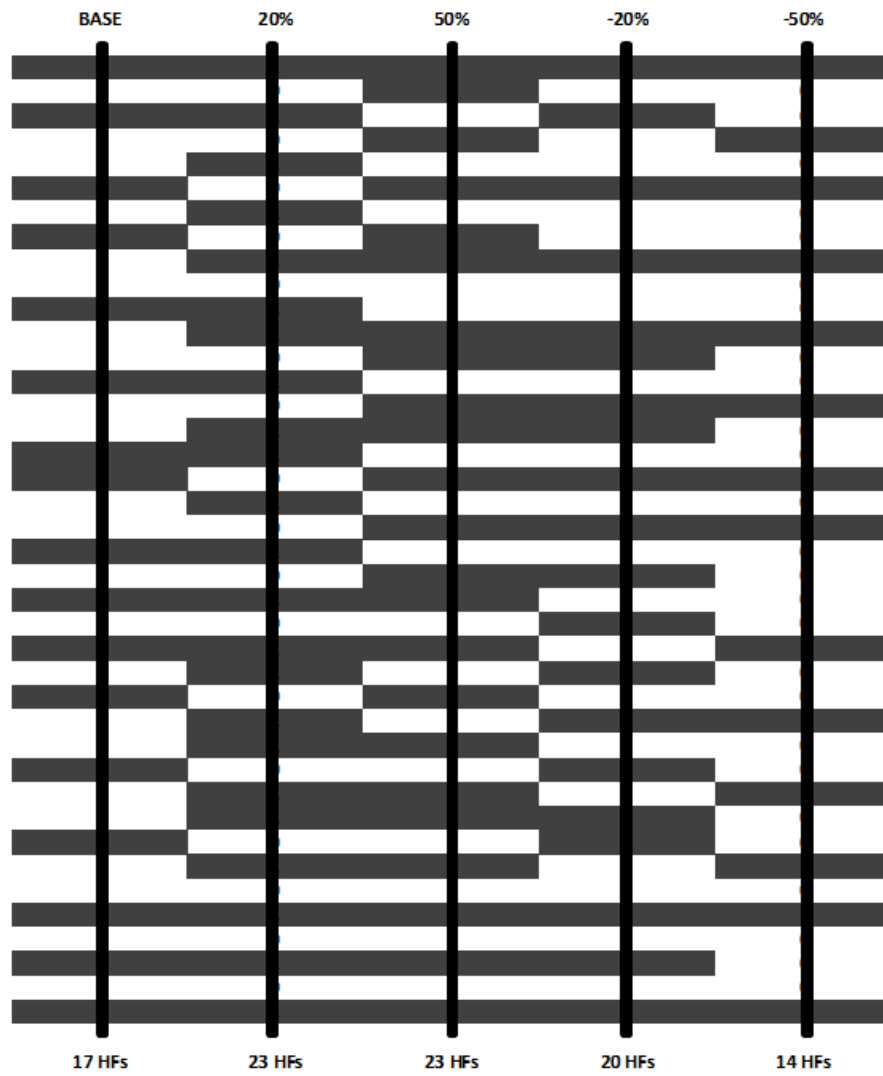


Figure 3.26. Juxtaposition of optimal HF stage locations for uncertain gas price varying from -50% to +50% from the base value (well location is unchanged from model to model).

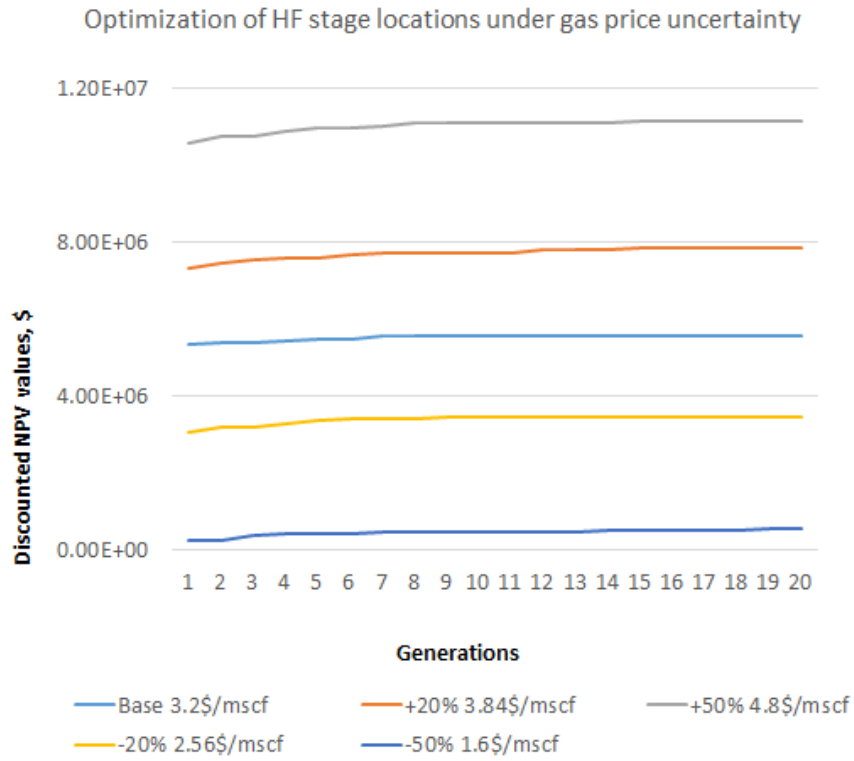


Figure 3.27. Effect of uncertainty in gas price on optimal discounted NPV values.

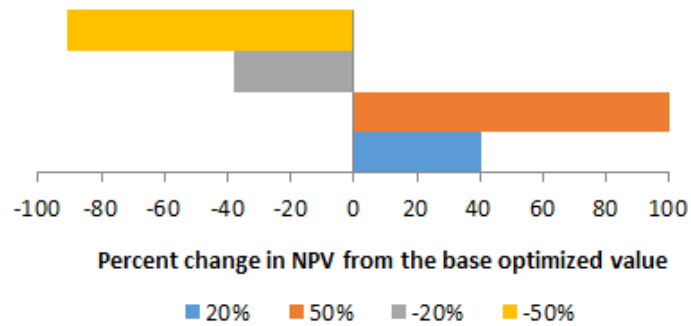


Figure 3.28. Effect of uncertainty in gas price: percent change in discounted NPV values from the optimized base value.

### 3.5 Conclusions

In this chapter, in one large brushstroke we presented a wealth of material that followed up on uncertainty study in Chapter II as well as laid down the groundwork for the upcoming Chapter IV about the integrated optimization framework for simultaneous horizontal wellbore and HF stage placement. Solid understanding and implementation of the GA optimization engine is instrumental in development of the integrated workflow and evolutionary-based MOO in Chapter V.

## CHAPTER IV

### INTEGRATED EVOLUTIONARY-BASED OPTIMIZATION FRAMEWORK FOR HORIZONTAL WELL AND HF STAGE PLACEMENT

#### 4.1 Introduction

In this chapter, we present and test the integrated optimization framework that evaluates optimal number and length of horizontal wellbores as well as number, spacing, and half-length of HF stages along them. This workflow builds up on the GA optimization engine described and tested in the previous chapter. First, we discuss the assumptions which are necessary to satisfy before the integrated framework can be successfully applied. Second, the reader gets insight into conceptual and algorithmic implementation of the integrated optimization scheme. At the end of the chapter, we test and discuss the results of optimization on a large synthetic shale gas model.

#### 4.2 Framework Assumptions

To apply our framework, we assume homogeneous extra-low matrix permeability field. This assumption allows us to partition the shale gas reservoir into several smaller reservoirs each of which can be drained with one horizontal well without significant interference from other wells. Then we apply the optimization engine to the smaller reservoir and obtain the total optimized discounted NPV for the entire play by multiplying the NPV for the smaller reservoir by the number of horizontal wells. In addition to this, we assume symmetry in size, well length, HF stages locations and number in all smaller reservoir partitions.

There are several reasons that make our assumptions valid. First, although any given shale rock fabric does have spatial variance in its geochemical properties, it is uncommon to see high matrix permeability contrasts in shale formations. In addition to this observation, shale matrix permeability is usually orders of magnitude smaller than permeability of SRV. Thus, rock matrix permeability can be modeled with one value and kept fairly homogenous within a continuous shale interval. Second, symmetry in HF stage locations and numbers is also taken from current industry practices such as traditional zipper fracturing (Jacobs, 2014) and simultaneous fracturing (Mutalik and Gibson, 2008). **Fig. 4.1** demonstrates symmetrical placement of HF stages for a shale play developed with three horizontal wells. Last, our framework allows to obtain good estimates of the discounted NPV for the entire field in addition to the number of horizontal producers and HF spacing and intensity within reasonable computational time.

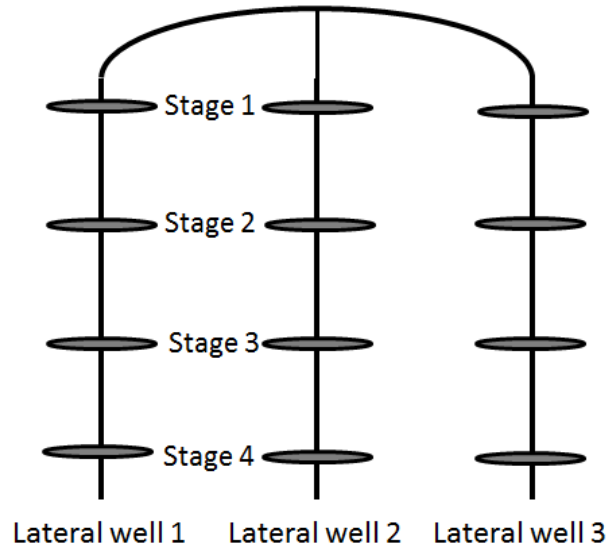


**Figure 4.1. Aerial view of homogeneous matrix permeability field with three horizontal wellbores with symmetrical transverse HF stages.**

Partition of the large reservoir into smaller ones and performing optimization for this smaller problem. In fact, the attempt to use our shale gas model with several wells and multiple HF stages with varying half-length caused rapid increase in the number of grid blocks due to LGR. To avoid the computational problems and to build the optimization framework that calculates optimal number of wells, HF stages, and their half-length, we devised *a conceptually new workflow* that provides answers to all our questions (given that the main assumptions are satisfied) and yet can be performed with available tools and within reasonable computational time.

### 4.3 Novel Framework Structure and Implementation

Conceptually and structurally, the integrated framework is similar to the GA optimization workflow provided in Chapter III (Fig. 4.2). Moreover, GA with strong elitism that previously demonstrated good performance is used without changes in our integrated framework as the optimization engine.

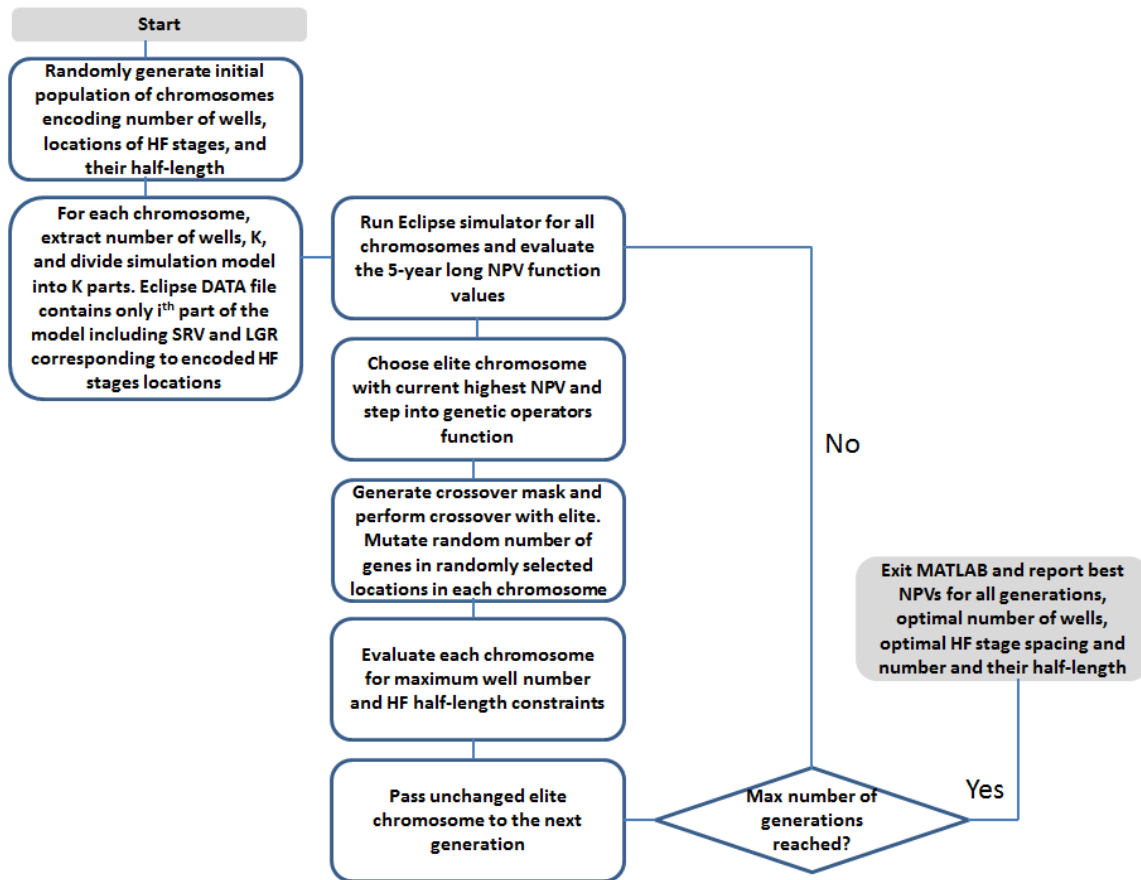
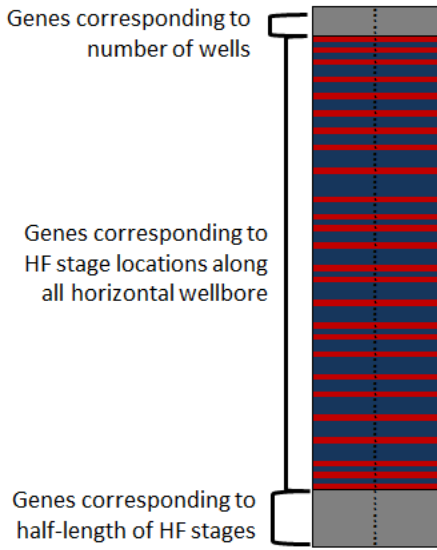


Figure 4.2. Flowchart of the GA-based integrated framework for optimal placement of multiple horizontal wells and HF stages.

The main difference between the flowcharts (and the corresponding MATLAB programs) lies in the definition of the chromosomes and the information that they encode. Like GA chromosomes in Chapter III, the integrated optimization workflow uses fully binary arrays to specify the number of horizontal wells, spacing and the number of HF stages, as well as their half-length (Fig. 4.3). As the reader can see, there are no genes that encode the length of horizontal producers explicitly. Nevertheless, the framework gives answer to how long the wells should be by providing the distance between the first and the last HF stages.



**Figure 4.3. GA chromosome encoding the number and length of horizontal wells as well as the number, spacing, and half-length of HF stages.**

Now let us step inside one iteration (or generation in the GA terminology) of the framework and observe graphically how the optimization algorithm works and what

output the user can obtain. **Fig. 4.4** provides a detailed visual description of the inner working of the integrated workflow that solves constrained optimization problem defined in **Eq. 4.1**.

$$\left\{ \begin{array}{l} \max NPV(u) \\ s. t. \tilde{u}_i \leq hl_{max} \\ \tilde{u}_i \geq hl_{min} \\ \hat{u}_i \leq nl_{max} \\ \hat{u}_i \geq nl_{min} \\ i = 1, 2, \dots, n. \end{array} \right. \quad (4.1)$$

Here,  $\tilde{u}_i$  refers to the portion of a chromosome that encodes the number of horizontal producer wells,  $nl_{max}$  is maximum feasible number of wells,  $nl_{min}$  is minimum feasible number of wells.

The  $M$  chromosomes obtained from the genetic manipulations with the previous generation represent  $M$  number of production plans (or well and HF stage arrangements) for the five-year period. Depending on the number of horizontal wells encoded in a current chromosome (let us say, five), the framework partitions the entire reservoir into smaller sections (also five) and creates a simulation model with a single horizontal well with appropriate maximum and minimum half-lengths for its HF stages and the proper distance to the border of the model that also accounts for SRV. After that this smaller part of the reservoir is assigned proper SRV and LGR to each HF stage and evaluated for five-year discounted NPV (**Eq. 4.2**) using ECLIPSE production output. This discounted NPV value for the smaller reservoir is then multiplied by the number of the partition,  $P$ , (in this case, five).

$$NPV = \sum_{p=1}^P \left( \sum_{k=1}^K \frac{(Q_g^k \cdot r_g - Q_w^k \cdot r_w - 0) \cdot \Delta t^k}{(1+b)^{t^k/365}} - (C_w + N_{HF}(C_{fb} + C_{fl}x_{length}) + L_w C_p) \right). \quad (4.2)$$

Once the entire generation is evaluated, its NPV values are compared and the elite chromosome is selected. Consequently, the genetic operators of crossover and mutation are applied to obtain the  $(n+1)^{st}$  generation. Because the portions of the chromosome that encode HF half-length and the number of wells are smaller than the portion corresponding to HF stage locations and they are constrained more strictly, their domain is searched quickly. Thus, these parts of the chromosomes converge toward their optimal values fairly early in the GA evolution. The reader will observe this fact in the results section of this chapter.

#### 4.4 Integrated Framework Testing

**Figs. 4.5 and 4.6** demonstrate how the number of wells and HF stage half-length change dynamically in order to accommodate the boundaries of the system. The plots show numbers of wells and corresponding HF stage half-lengths within one generation. More horizontal wells necessitate shorter HF stages, while fewer wells require longer stages.

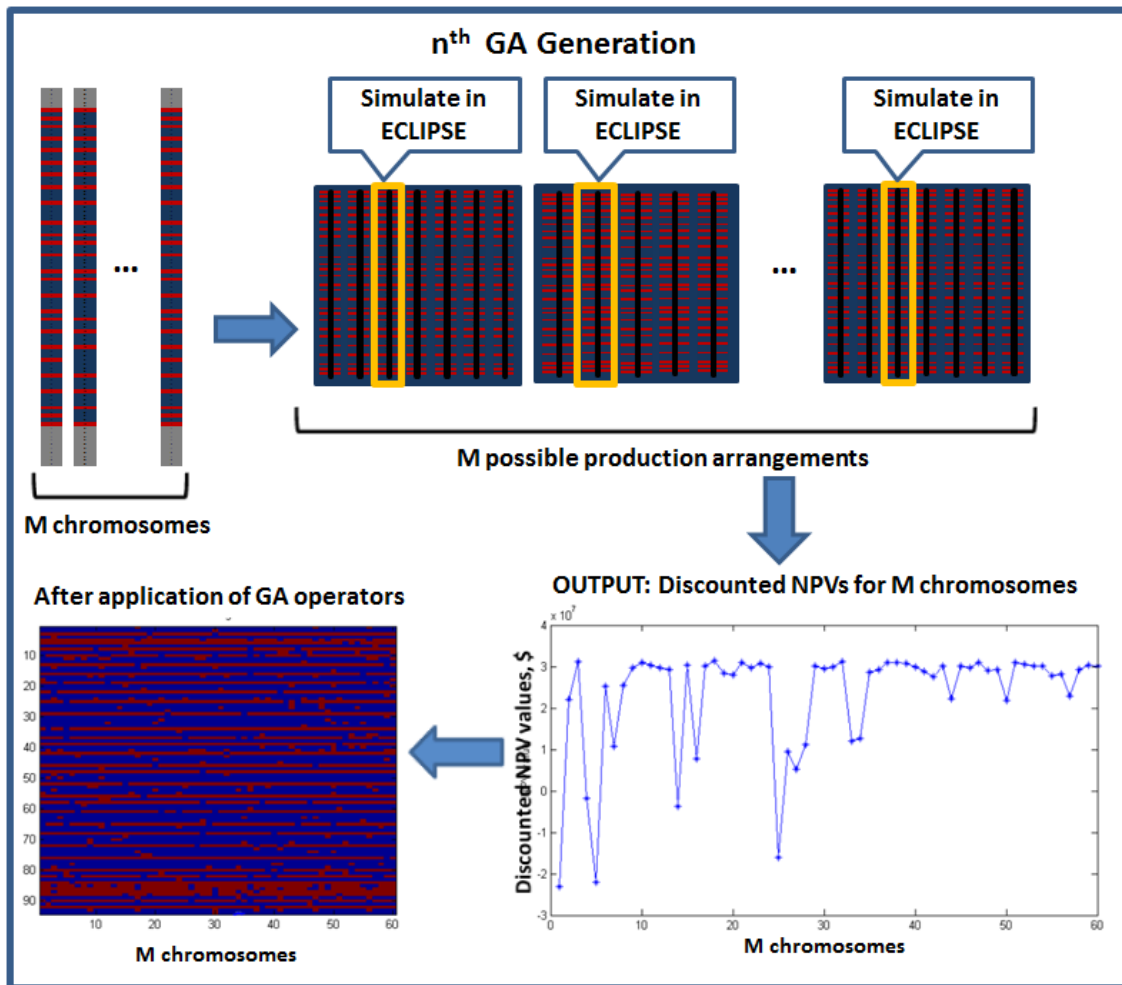
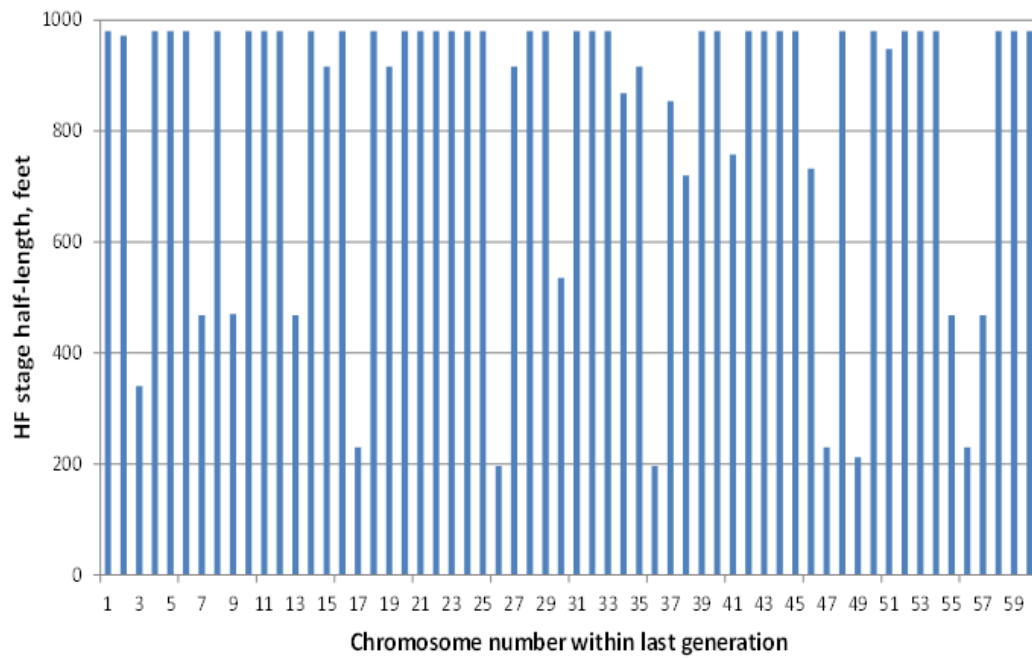
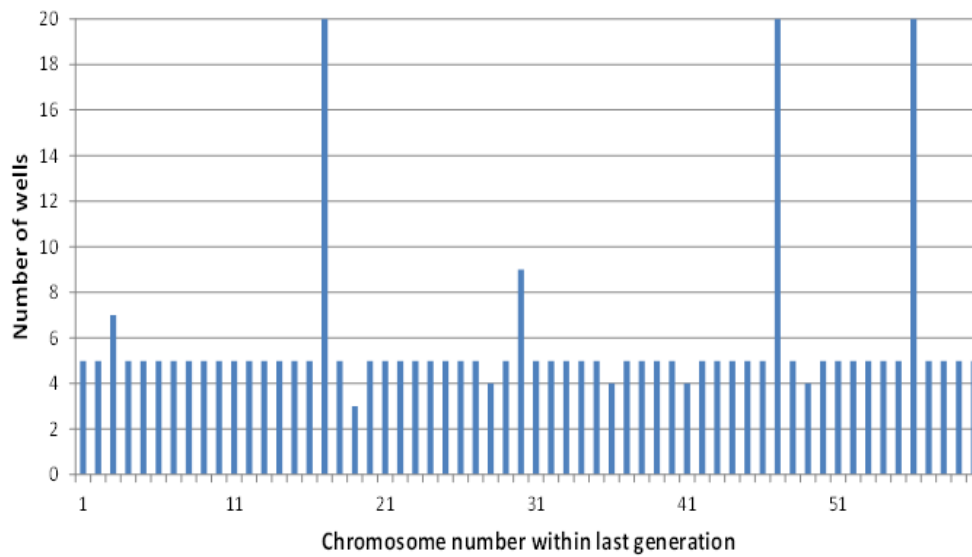


Figure 4.4. Graphical interpretation of one iteration of the integrated optimization framework.



**Figure 4.5. Variability of HF half-lengths within the last generation.**



**Figure 4.6. Variability of well numbers within the last generation.**

In **Fig. 4.7** we present the evolution of HF stage half-length over thirty (30) generations. The framework starts from about 660 feet and evolves to fewer horizontal wells with HF stages of almost 1000 feet.

Similarly to the workflow in the previous chapter, the integrated optimization framework uses the same-chromosome elimination process to save on computational time. The monotonically increasing graph in **Fig. 4.8** provides the evolution of the discounted NPV values toward the global maximum. Here, the code outputs running time of about 31 hours with saving of 38 simulator calls ( $30 \times 60 - 1762 = 38$  calls).

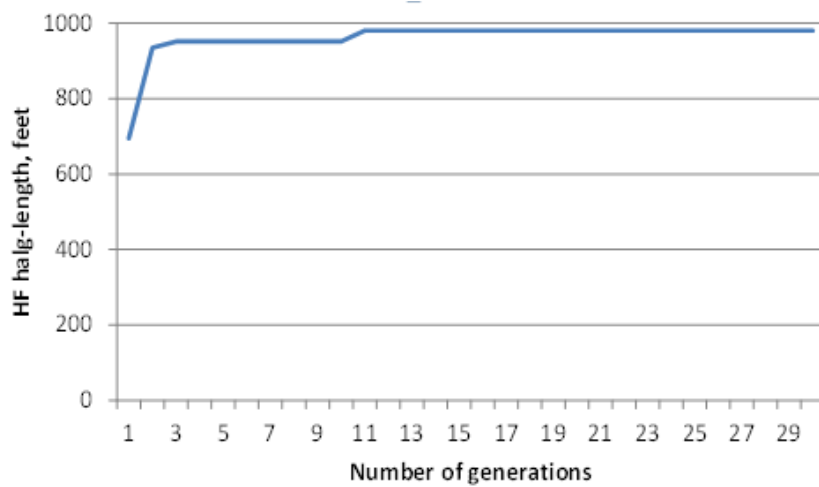


**Figure 4.7. Evolution and convergence of HF half-length over 30 generation.**

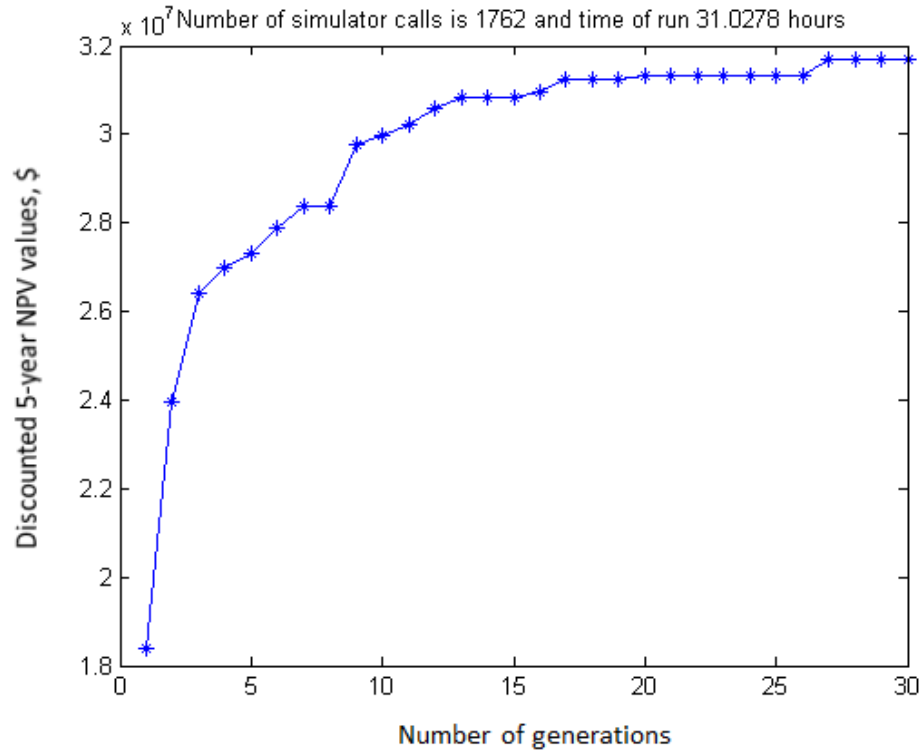


**Figure 4.8. MATLAB output of monotonically increasing 5-year discounted NPVs over 30 generations with 60 chromosomes each.**

#### 4.5 Results and Discussion

The previously mentioned test example showed computational intensity of searching the domain with over 90 dimensions. On standard PC platform (Intel(R) Zeon(R) CPU W3540 @2.93GHz RAM 24.0 GB) it took about one and a half days of uninterrupted simulator calling. Though interesting for comparative purposes, the case with each grid block as a potential place location of HF stage is not realistic. Our powerful GA with strong elitism will eventually find that uniform spacing is optimal for unconstrained problem, but we can specify minimum spacing between stages to cut on unnecessary simulator calls that evaluate production scenarios unacceptable due to the high density of

stages. To demonstrate how we can achieve a reasonable trade-off between minimum HF stage spacing and computational (or running) time, we devise a series of numerical experiments with increasing minimum HF stage spacing (**Table 4.1**). Four test runs encompass intervals from 20 to 80 feet with increment of 20 feet. In addition to discounted NPV values, we also record and compare optimal HF half-length, number of horizontal wells to drain the reservoir, the number of ECLIPSE simulator calls and the overall computational time for each run. The production period is set to five years which can be considered fairly long-term for an unconventional project.

**Table 4.1 Summary of integrated placement runs with varying minimum HF's spacing.**

Minimum HF interval	Running time	Simulator calls	Max NPV	Wells	HF half-length
feet	hours	#	\$	#	feet
20 feet	32.24	1790	31934651.8	5	980.0
40 feet	23.63	1739	31934651.8	5	980.0
60 feet	20.86	1702	32660630.1	6	807.3
80 feet	15.15	1608	29774351.0	8	605.0

**Table 4.2** summarizes reservoir geometric and petrophysical properties, initial conditions at the beginning of the production period and its duration, parameters pertaining to hydraulic fracturing outcomes, and the key economic parameters that are similar to those defined in Chapter III. Here, the model has larger width that enables partitioning the reservoir into smaller portions and assembling the ECLIPSE data file

and production specification for the smaller model. We specify maximum allowable number of wells as twenty (20) and maximum allowable HF half-length as 1000 feet.

**Table 4.2 Reservoir and economic parameters used for the test model.**

<b><i>Parameters</i></b>	<b><i>Values</i></b>	<b><i>Unit</i></b>
Model width	10,000	ft
Model length	2,000	ft
Model thickness	200	ft
Initial reservoir pressure	3000	psi
Reservoir temperature	150	°F
Rock density	161	lbs/ft <sup>3</sup>
Producing bottom hole pressure	500	psi
Production period duration	5	years
Matrix porosity	6	%
Matrix permeability	0.00015	md
Langmuir pressure	650	psi
Langmuir volume	0.096	mscf/ton
Hydraulic fracture height	200	ft
Hydraulic fracture half-length	260 or variable	ft
SRV permeability	0.08	md
Drilling base cost per well (vertical part)	2,000,000	\$
Drilling cost per grid block (horizontal part)	6,000	\$
Daily operating expenses per well	60	\$
Gas price	3.2	\$/mscf
Base cost per HF stage	75,000	\$
Cost per length of HF stage	2,000	\$/ft
Discount rate	12.5	%

**Fig. 4.9** presents the evolution across thirty (30) generations of the discounted NPV values for all four test runs. The reader can observe that minimum spacing of 40 and 60 feet produce higher discounted NPV values. The case with 20 feet minimum spacing (in other words, each grid block can be a potential place for HF stage) achieves results similar to 40 and 60 feet, but it takes more computational time and takes more generations to approach higher NPV values. Large minimum HF spacing (of at least 80 feet) leads to sub-optimal NPV values and requires many wells to drain the reservoir of interest (eight wellbores in comparison to 5 or 6 in other cases).

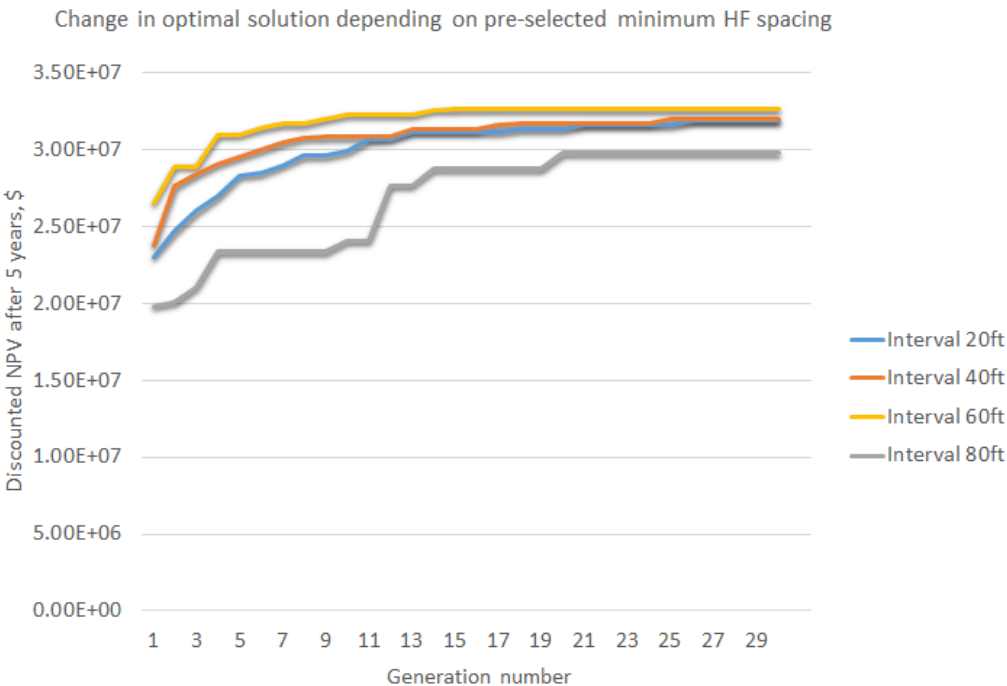


**Figure 4.9. Summary plot of discounted NPVs from four test runs with varying minimal interval between HF stages.**

**Fig. 4.10** shows how a change in minimum HF spacing affects HF stage half-length which is related to the number of horizontal wells that can achieve higher NPV values. The line corresponding to 60 feet minimum spacing (this number is close to the industry widely accepted minimum spacing) achieves optimal half-length almost immediately (Thompson et al., 2011).

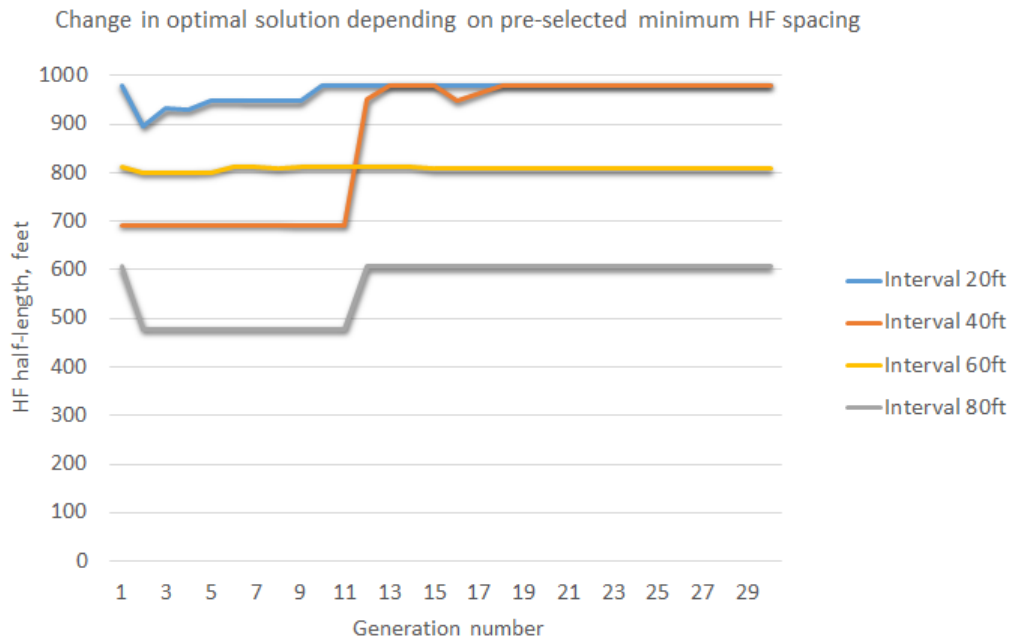


**Figure 4.10. Summary plot of HF half-lengths from four test runs with varying minimal interval between HF stages.**

**Fig. 4.11** is the composite plot that summarizes the effect of minimum stage spacing for the same shale gas model. The graph is loaded with information, but the gist of it is highlighted in red: our integrated framework allows to determine the production scenario that gives the highest discounted NPV values while keeping computational time

and simulator calls at necessary minimum (we only call ECLIPSE when we have a new chromosome, same chromosomes that could occur due to crossover are automatically identified and assigned values based on one evaluation). Minimum HF stage spacing of 60 feet gives us the highest NPV and is an optimum if we consider minimum spacing as an optimization variable.

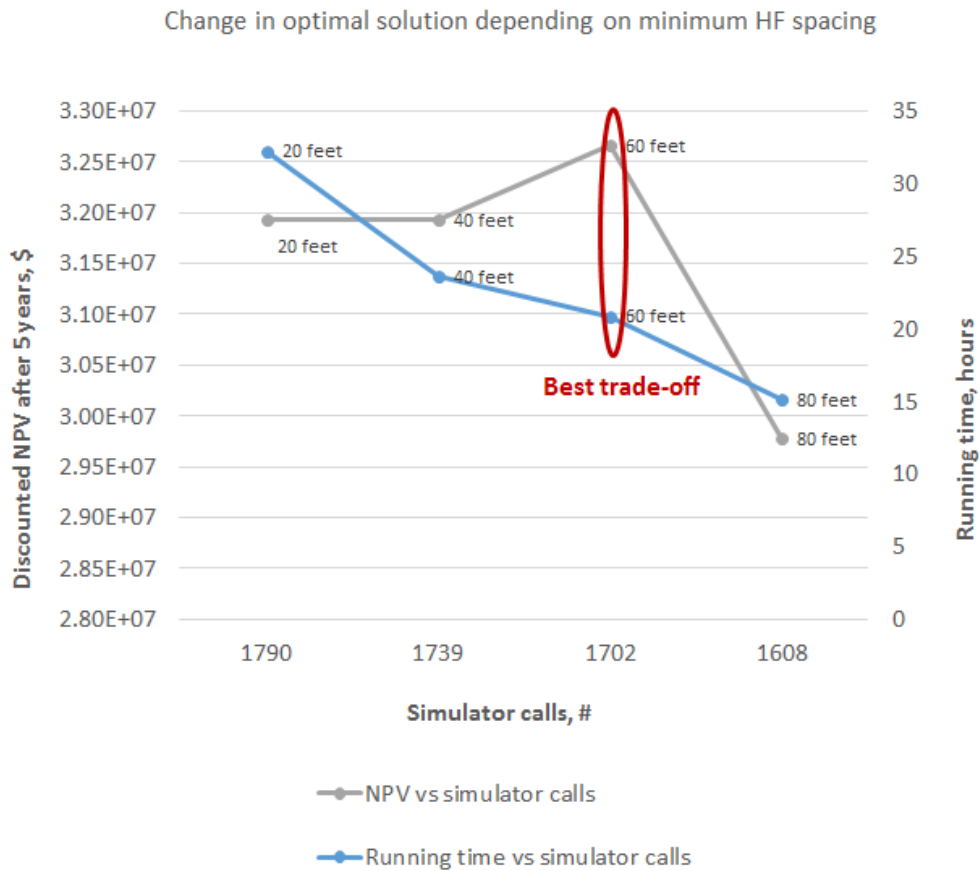


**Figure 4.11. Cross-plot of running time, discounted NPVs, and simulator calls from four test runs with varying minimal interval between HF stages.**

## 4.6 Conclusions

In this chapter, we presented our novel integrated optimization framework that provides answers to a multitude of economic and production questions if the main assumptions are satisfied. First, we devised a computationally efficient workflow that takes advantage of symmetry and reduces optimization of multiple well placement in a large geomodel to a smaller and more manageable problem. Second, our framework honors geometric constraints of the shale model, length and spacing of horizontal producers, spacing and half-length of HF stages. Last, the workflow is fully controlled by the objective function which is customizable depending on the user's needs. In this way, for example, we can provide the answer to the question what minimum HF stage spacing yields the highest NPV values. The reader can also appreciate the amount of technical information that the integrated framework outputs. Not only does it provide the number of horizontal producers with corresponding number of HF stages and their specific locations and half-length, but also spacing between the wells, computational time, and simulator calls. Based on this wealth of information, the engineer can make decision and adjustments to their modeling plan.

Until now, we familiarized the reader with our optimization framework and emphasized that it provided solution to single objective optimization problem. The long-term discounted NPV function defined from the beginning of this dissertation is one of many objectives that the gas operators could be interested in. The upcoming Chapter V takes the discussion to the new level and investigates how our optimization workflow

can be adjusted to solve multi-objective problems in which objectives could be conflicting or not.

## CHAPTER V

### MULTI-OBJECTIVE EVOLUTIONARY OPTIMIZATION FOR HF STAGE

#### PLACEMENT

##### 5.1 Introduction

In recent years, academic scholarship has started to respond to the industrial interest in multi-objective optimization (MOO). MOO allows weighing different production strategies in presence of multiple production and economic goals (or objectives) that can be conflicting or not. MOO addresses this interest and offers a set of algorithms that gives quantitative and qualitative measures of “goodness” of the optimal solutions.

This chapter explores the most recent scholarship on MOO and focuses on one method that is considered one of the fastest and most efficient in construction of the *Pareto front* of the optimal solutions. First, we introduce the key terminology of MOO and the most popular algorithms with their advantages and drawbacks. Then, we elaborate on specifics of the improved non-dominated sorting genetic algorithm (NSGA-II) and its application to our problem of optimal HF stage placement in unconventional gas reservoirs. After laying down this groundwork, we present NSGA-II test runs and results. In conclusion of this chapter, we discuss applicability and efficiency of the algorithm as well as its benefits for future commercial application.

##### 5.2 Approaches to MOO

MOO problems are common in most engineering disciplines including petroleum engineering. Sometimes the objectives can be mutually conflicting. One example is

when we try to maximize performance of a system and minimize operating and capital costs. However, the conflict between the objectives is not required to apply MOO techniques. In fact, objectives might include temporal component that can be valuable to investigate, particularly in case of quickly declining production from shale gas reservoirs. While optimizing the locations, intensity, and half-length of HF stages, we might be interested in impact of our production strategy on short- and long-term revenue or discounted NPV.

As Konak et al. (2005) point out that there are two main approaches to MOO problems. The first one is to create an aggregate objective function that combines expressions of two or more objectives. In this case, we have to address respective weights for each objective and scaling among them (Marler and Arora, 2004). Though powerful on their own right, these methods are sensitive to smallest perturbation in weights and might give drastically different solutions depending on the problem (Das and Dennis, 1997). The second approach avoids the weighting problem altogether and finds the entire set of optimal solutions or a representative subset called the Pareto optimal set. One of the characteristics of points inside the Pareto optimal set is that they are all non-dominated with respect to each other and each solution gains in one objective by sacrificing in another (Sreekanth et al., 2012). **Fig 5.1** illustrates how the Pareto front of optimal solutions is defined for MOO problem with two objectives,  $J_1$  and  $J_2$ . In this maximization problem the solution points in black are completely dominated by the red solution points on the Pareto front. All solutions can be ranked based on their relative

non-dominance. All solution points in *Rank i* are non-dominated by each other, dominated by solutions in *Rank i-1*, and dominate solutions in *Rank i+1*.

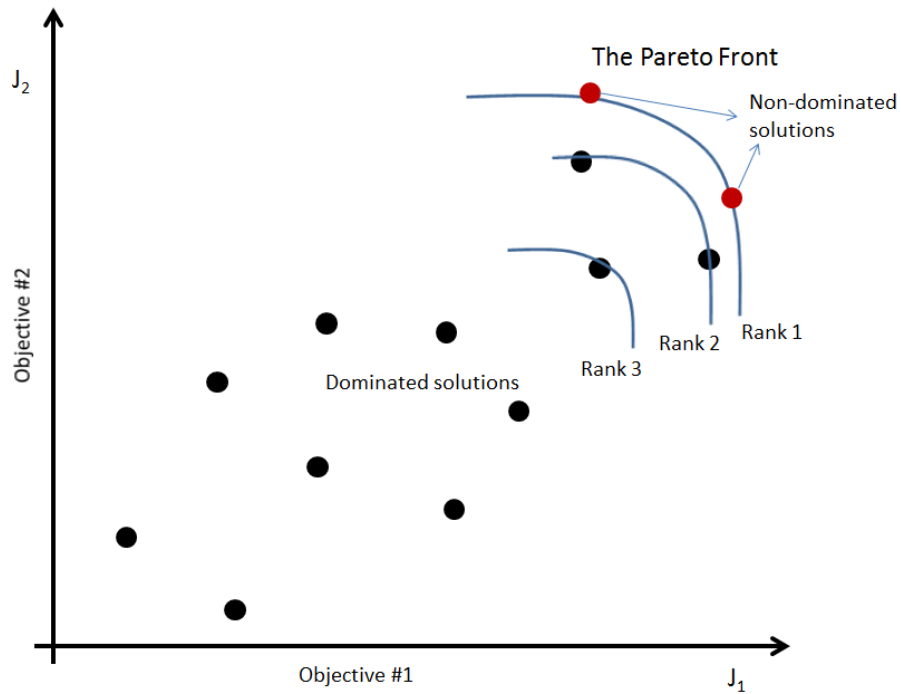


**Figure 5.1. The Pareto Front of non-dominated Pareto optimal solutions for a generic MOO problem.**

Though MOO provides means to assess the solutions with respect to different objectives, it is computationally costly. The first approach (the aggregate function strategy) requires weights sampling and evaluation of the results based on them. The second approach can also be computationally consuming. More specifically, Deb et al. (2002) focus on NSGA, address the problem of its complexity, and bring it from  $O(MN^3)$  to  $O(MN^2)$ , where  $M$  is the number of objectives (in our case two) and  $N$  is the size of

the GA population. The authors speed up performance of the algorithm by bringing into the picture elitism and avoiding the sharing parameter. The essence of the NSGA-II is summarized in the following pseudo-code which will be adopted into our optimization framework and presented in the flowchart in the next section (**Table 5.1**).

**Table 5.1 Pseudo-code of NSGA-II (Deb, 2002).**

fast_nsgall(P)	
for every $p \in P, S_p = \emptyset, n_p = 0$	
for every $q \in P,$	
if $p$ dominates $q, S_p = S_p \cup \{q\},$	% add $q$ to set dominated by $p$
else if $q$ dominates $p, n_p = n_p + 1;$	% increment counter of $p$
if $n_p = 0, p_{rank} = 1, F_1 = F_1 \cup \{p\};$	% $p$ belongs to the first front
$i = 1;$	% start the front counter
while $F_i \neq \emptyset, Q = \emptyset$	% $Q$ is for storing the next front
for every $p \in F_i$	
for every $q \in S_p, n_q = n_q - 1,$	
if $n_q = 0, q_{rank} = i + 1, Q = Q \cup \{q\};$ % $q$ belongs to the next front	
$i = i + 1,$	
$F_i = Q.$	

In this pseudo-code, for each solution we calculate the domination counter  $n_p$ , which represents the number of solutions dominated by the solution  $p$ , and the set  $S_p$  of the solutions dominated by  $p$ . Based on this improved scheme the entire non-dominating

sorting requires  $O(MN^2)$  comparisons instead of  $O(MN^3)$  required by the old NSGA formulation. As for other parameters,  $p_{rank}$  is the rank of the solution and  $F_i$  is the  $i^{\text{th}}$  front. Now that we have rigorously defined NSGA-II and its computational advantages, let us formulate MOO problem with application to HF stage placement along single horizontal wellbore.

### 5.3 Application of NSGA-II to HF Placement Problem

Park et al. (2013) use the idea of NSGA-II for Pareto-based history matching workflow which is designed to minimize misfit in presence of two conflicting objectives (water cut and water saturation changes). Though particularly suitable for conflicting cases, NSGA-II is powerful enough to be applied to non-conflicting objectives as well. In our case, we focus of two objectives that do not necessarily conflict: short- and long-term discounted NPVs. Depending on the company size, the operator might be interested in quantitative assessment of profitability of the project after a short production period and making the decision about lease re-selling, continuing to produce, or re-fracturing. **Fig. 5.2** shows the MOO case in which two objectives (long- and short-term NPVs) are positively correlated. Strong positive correlation is obvious from the positive slope of the fitted linear regression and the high  $R^2$  value.

To demonstrate the full potential of the implemented NSGA-II though, we can devise a synthetic case similar to that in the previous chapter that has conflicting objectives. **Fig. 5.3** brings water production into the picture. Ultimately, we would like to balance between low water production and high gas rate that translates into the high

discounted NPV. Unlike conventional oil reservoir models, our shale gas simulation model does not have much movable water due to extremely tight rock matrix. This circumstance, nonetheless, does not prevent us from the MOO analysis of the results. From the fitted linear regression we observe negative correlation between discounted NPV and water production (note that minus sign in water production is due to conversion from maximization problem to minimization, in other words we are minimizing water production by maximizing its negative value).

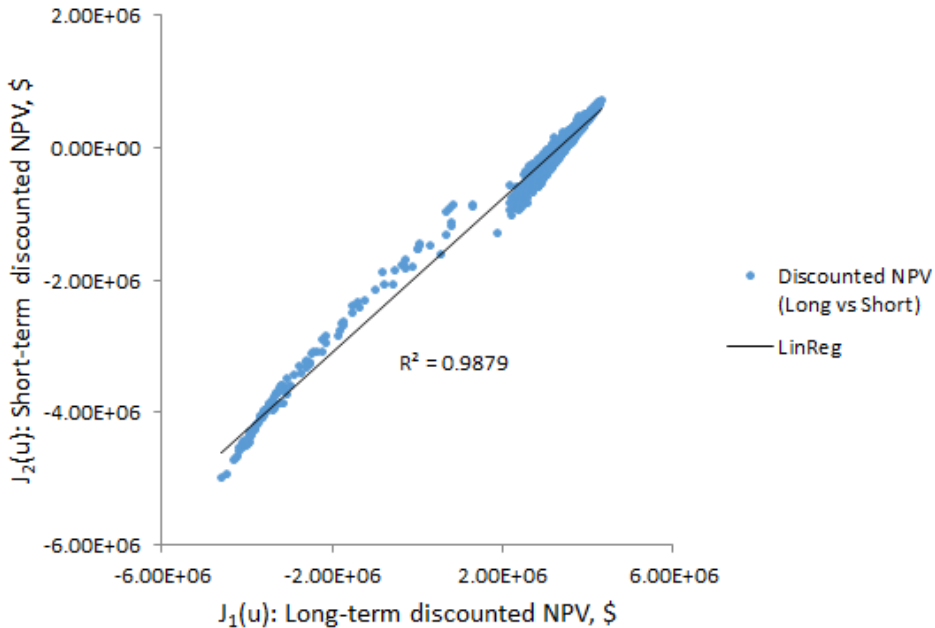


**Figure 5.2. Scatter plot showing short- and long-term discounted NVPs generated by the simulation model.**

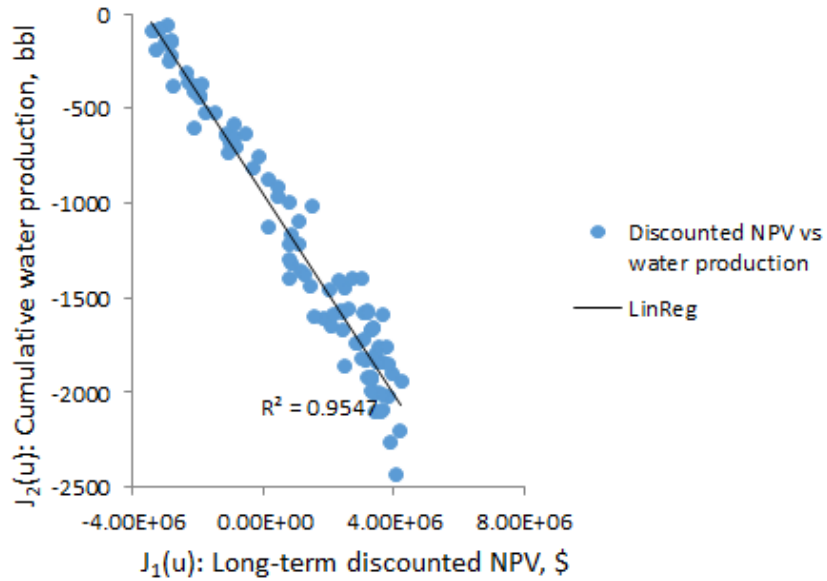


**Figure 5.3. Scatter plot showing long-term discounted NVPs vs water production generated by the simulation model.**

Now that we have discussed the two MOO cases with conflicting and non-conflicting objectives, let us specify the expressions for each objective. For the first case (with data demonstrated on **Fig. 5.2**) with non-conflicting objectives, we use the expression of the discounted NPV from **Eq. 3.1**.  $J_1(u)$  sums and discounts NPV in the long term (5 years) and  $J_2(u)$  does so in the short term (1 year). The for second case with conflicting objectives,  $J_1(u)$  is exactly the same as **Eq. 3.1** summed and discounted for 5 years.  $J_2(u)$ , however, is cumulative water production in barrels.

In each MOO case we are interested in construction of the Pareto front of optimal solutions. NSGA-II offers fast and computational efficient procedure to achieve this result. **Fig. 5.4** demonstrates how NSGA-II manipulates chromosomes made out of the input vectors in order to obtain improving results and yet keeping the number of the

simulator calls at minimum. More specifically, NSGA-II retains chromosomes that correspond to the parents, uses them to generate the children, and then combines both sets for consequent sorting. The sorting is then performed as outlined in **Table 5.1** and all chromosomes are assigned to ranks. The highest rank (or Rank 1) corresponds to the set on non-dominated solutions or the Pareto front. All other ranks are dominated by the Pareto front, but inside them the solutions do not dominate each other. After sorting, NSGA-II retains half of the chromosomes that correspond to the highest ranks and discards the rest. This procedure allows for fast search of the Pareto front members.

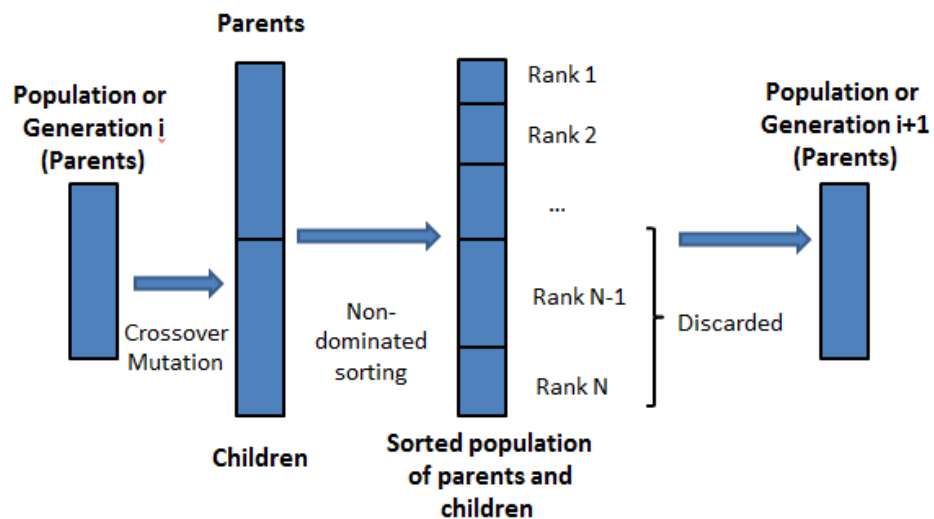


**Figure 5.4. NSGA-II improved scheme for producing new generations without an increase in evaluations of the objective function.**

## 5.4 NSGA-II Testing and Results

This section presents two above-mentioned MOO test cases and the results. **Fig. 5.5** illustrates NSGA-II performance after the first generation for the case of non-conflicting objectives (short- and long-term discounted NPVs). The Pareto front is clearly defined and color coded in MATLAB code. We also outline a couple of subsequent ranks for illustration purposes.

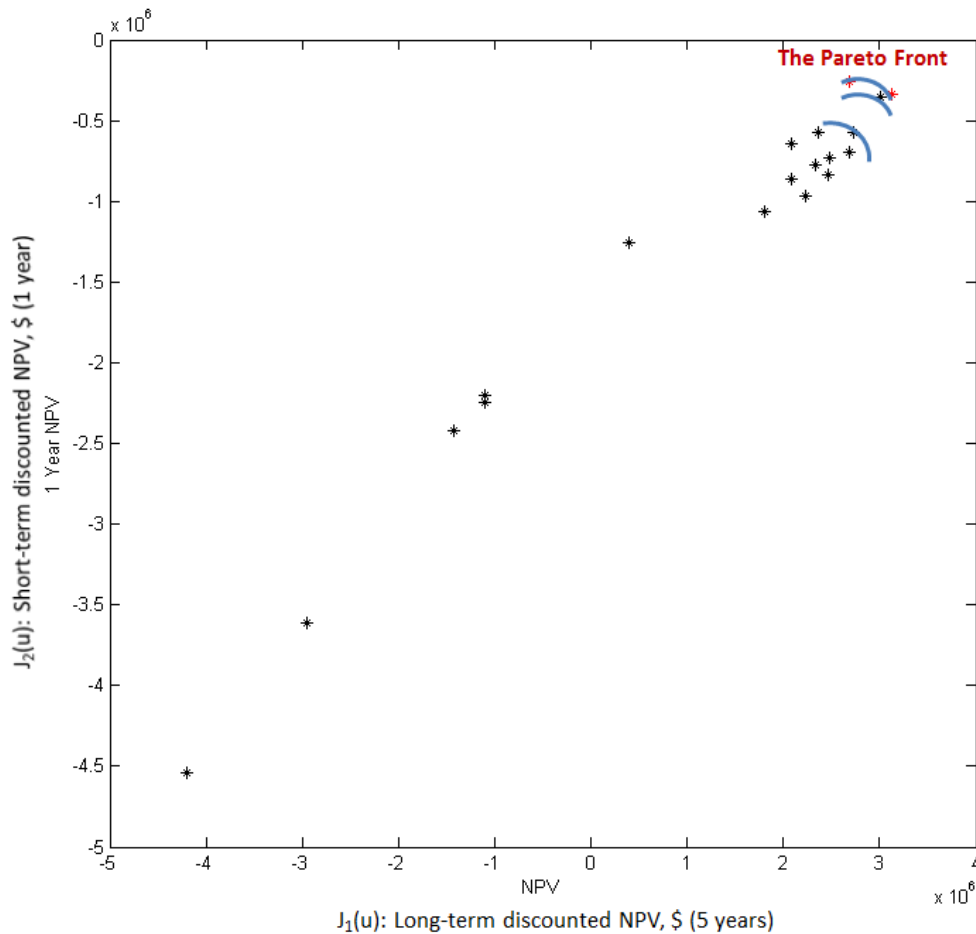


**Figure 5.5. The Pareto front after the first generation of NSGA-II for non-conflicting objectives.**

**Fig. 5.6** shows the final plot after 30 generations and summarizes all 1800 solution points (only non-negative solutions are plotted). Here the Pareto front has only one solution point which dominates solutions in all other ranks. **Fig. 5.7** offers specific chromosomes (or arrangements of HF stages and their half-length) that produce the best solutions in the last generation including the Pareto front solution.

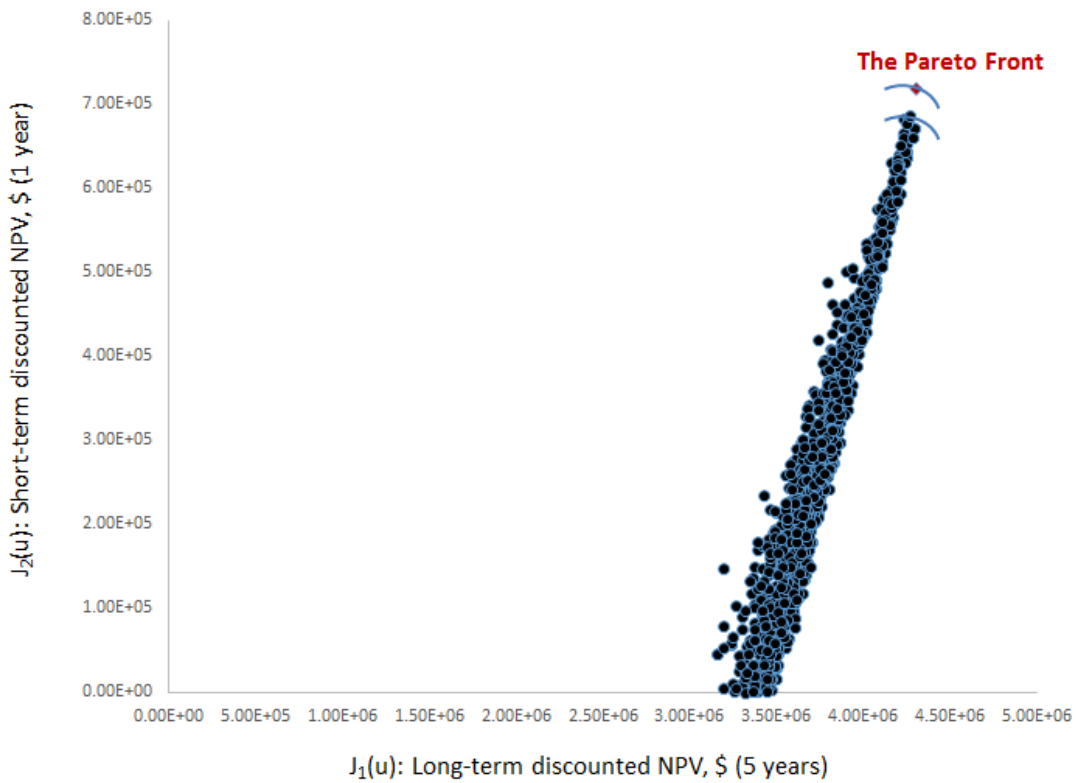


**Figure 5.6.** The Pareto front after 30 generations of NSGA-II for non-conflicting objectives.

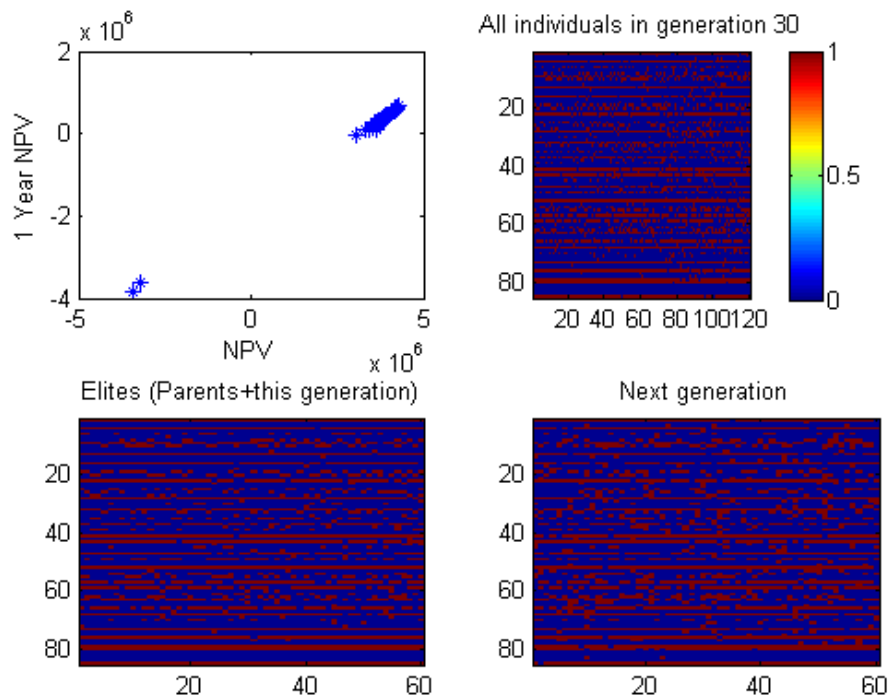


**Figure 5.7. NSGA-II results with optimal locations of HF stages and their half-length after 30 generations of NSGA-II for non-conflicting objectives.**

Now that we discussed the non-conflicting case, let us consider the results of the test run with conflicting objectives (water production and long-term discounted NPV). **Fig. 5.8** shows the cross-plot of solutions for our MOO problem with the Pareto front in red. The Pareto front in this case forms broad range in comparison to the non-conflicting case. This result is expected because there are many solutions that satisfy lower cumulative water production and higher discounted NPV.

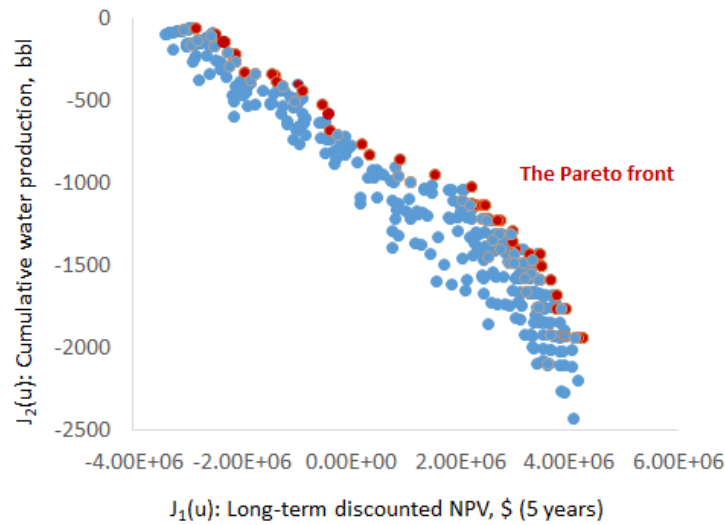


**Figure 5.8. The Pareto front (in red) after 20 generations of NSGA-II for conflicting objectives (long-term NPV and cumulative water production).**

The evolution of the Pareto front can be observed in **Fig. 5.9**. Since this is the last generation, we see that many solution points ended up on the Pareto front (compare **Figs. 5.8 and 5.9**). If we allow NSGA-II to evolve further, we would see refinement of the Pareto front trend, but it would still remain broad encompassing a range of solutions from lower water production and lower NPV to higher cumulative water production and higher NPV. Depending on the operator’s priorities, the engineer could choose any of the solutions (or production plans) from the Pareto front. If high water cut is a considerable objective, then the optimization offers production scenario with fewer HF stages to reduce undesirable expenses associated with water disposal. However, the trade-off in this case would be lower cumulative gas production and, thus, the revenue for the entire project.

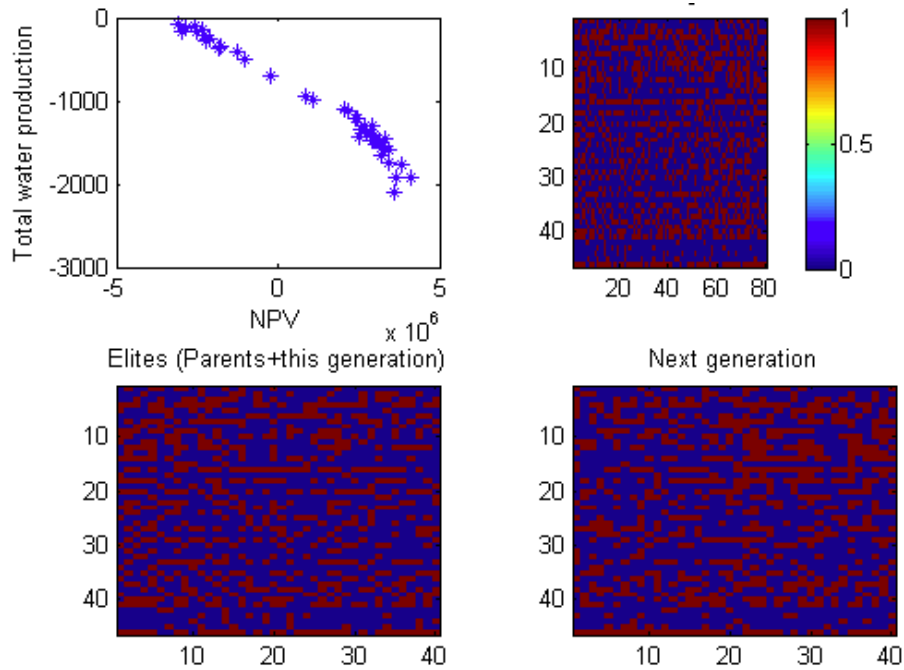


**Figure 5.9. NSGA-II results with optimal locations of HF stages and their half-length after 20 generations of NSGA-II for conflicting objectives.**

### 5.5 Conclusions and Observations

In this chapter we demonstrated with specific examples of conflicting and non-conflicting MOO problems that our framework is flexible enough to be applied in seamless fashion to the problem of HF stage placement in presence of multiple objectives. We showed that these objectives can be of economic (short- and long-term NPV) or production (cumulative water production) nature. The framework handles objectives computationally effectively and produces the Pareto optimal solutions without requiring the user to assign weights to each objective which can be confusing and time consuming.

The user has flexibility of defining their own objectives in separate MATLAB module and applying our workflow to obtain optimal results for them. Also from the MATLAB code standpoint there is no problem of defining more than two objective and turn the problem in truly multi-objective task. However, visualization of the Pareto front could be tricky for three or more objectives. The user would still be able to see cross-plots only of pairs of objectives.

This concludes the description of implementation and testing of our novel optimization framework that is now applicable to multiple objectives. Let us now summarize the achievements and accomplishments of this dissertation and outline the future research venues.

## CHAPTER VI

### CONCLUSIONS AND RECOMMENDATIONS

In this final chapter, we review the main contributions of this dissertation to the current discourse about production and design optimization in unconventional gas assets. Here we summarize specific solutions and implementations that resulted from this research as well as possible future research directions that this dissertation has opened.

#### 6.1 Conclusions

In this dissertation, a novel integrated optimization framework for simultaneous horizontal wellbore and HF stage placement has been developed and tested on a synthetic shale gas simulation model that was built based on the Barnett shale properties. Along the way toward the final implementation of the framework, we investigated, implemented, and analyzed the following:

- i. We described the influence of shale rock fabric composition and horizontal stress anisotropy on shale gas modeling and representation of hydraulic fractures for simulation purposes. Specifically, we considered two scenarios (high and low stress anisotropy), emphasized that anisotropic case required high conductivity central HF and lower permeability SRV, and discussed the impact of choosing one or the other scenario for simulation.
- ii. We performed initial screening of economic and petrophysical parameters with two different tools and found that price of gas and matrix permeability were the most significant explanatory variables in fitted regression.

- iii. We implemented GA with strong elitism and applied it to the problem of optimal HF stage placement with fixed half-length (half-length was not a variable for optimization).
- iv. Once we observed that for homogeneous matrix permeability the results were close to uniform HF stage spacing, we proceeded with HF half-length optimization. In this section we adjusted the objective function to accommodate variable half-length and used primarily economic optimization control (though we did specify maximum feasible HF half-length as a geometric constraint).
- v. Implemented optimization workflow for a single well was coupled with uncertainty assessment. We chose gas price and matrix permeability as the main uncertain parameters and investigated sensitivity of the discounted NPV function response. We found that while matrix permeability did have an impact on the revenue, it was completely overshadowed by the effect of uncertainty in gas price. Gas price change from -50% to +50% from the base value led to discounted NPV values from, what can be interpreted as, complete collapse of the shale gas project to revenue “bonanza.” We also saw that optimization results (number and locations of HF stages) were slightly affected by uncertainty in matrix permeability, while similar change in gas price necessitated drastically different production plans, *ceteris paribus*.
- vi. Next we took advantage of symmetry and homogenous matrix permeability (as well as the ability to incorporate natural fractures into the simulation model as a part of dual permeability system without explicit definition with discrete fracture

network) and built computationally efficient evolutionary-based optimization framework that optimizes number of horizontal producers, number and locations of HF stages as well as their half-length. We observed that continuous and integer variables (such as HF half-length and number of wellbores) can be effectively represented as binary arrays and included into GA chromosomes. After that, chromosomes could be easily manipulated with genetic operators.

- vii. We added to our framework a capability of finding the optimal solution set, the Pareto optimal set, in presence of multiple objectives. Our evolutionary-based framework (coupled with NSGA-II) proved to be effective for problems with non-conflicting objectives (such as long- and short-term revenue) and competing ones (such as long-term revenue and cumulative water production).

Our implementation of the integrated optimization framework has certain advantages over those built or proposed before:

- i. Our workflow has one point control which is the objective function (or multiple functions in case of MOO). Thus, the user can easily re-define the function, its parameters, constraints, or values and the workflow will work flawlessly without any additional changes in code. Because the GA engine is decoupled from the specification of the problem, it will work as long as it is supplied with fully binary arrays.
- ii. The optimization framework is computationally efficient. It evaluates only dissimilar chromosomes due to our same-chromosome elimination process. In some cases computation saving can be considerable. For instance, **Table 4.1**

shows that in one run our algorithm eliminated almost 200 unnecessary simulator calls caused by rapid convergence of chromosomes.

- iii. Our implementation of MOO solves for both conflicting and non-conflicting objectives and requires absolute minimum of simulator calls. It also can easily be extended to three or more objectives, as objectives are defined separately and can be imported on demand.
- iv. Our framework offer fast procedure for selecting optimal number of wells and HF stage spacing and half-length provided that the main assumptions were satisfied.

Now let us finish this overview with the main outputs that our integrated optimization framework provides:

- i. The number of horizontal wellbores with appropriate spacing (minimum distance to the borders of the model can be modified by the user);
- ii. The length of the horizontal section of the well (measured from the first to the last HF stage);
- iii. The optimal half-length of HF stage that is constrained by minimum and maximum feasible half-length as well as the number of the horizontal well;
- iv. Specific locations of HF stages;
- v. The optimal number of HF stages (which is the same for each horizontal well based on symmetry and traditional zipper frac assumptions);
- vi. Evolution of the discounted NPV across the generations;
- vii. Evolution of the optimal HF stage placement;

- viii. Overall computational time and the number of simulator calls;
- ix. The MOO output also includes the Pareto optimal set.

## 6.2 Future Research Directions

This dissertation addressed many aspects of shale gas modeling, optimization of horizontal wellbore and HF placement as well as MOO applied to unconventional gas reservoirs. Many of these topics can be extended further and might include the following directions:

- i. Integration of geomechanical data (such as Young's modulus and Poisson's ratio) into the shale gas geomodel and using integrated optimization framework for these systems with spatially variable properties. This will necessitate major change of assumptions. We would not be able to use symmetry of HF locations from well to well like we did in this dissertation. We would also need to optimize half-length for each HF stage individually which would immediately reflect on computational time. All of this can be achieved with our integrated framework by extending the GA chromosomes, but we would need to obtain commercial (not academic) license of the simulator and gain access to supercomputer (because computational time on current workstation would go to weeks). Jahandideh and Jafarpour (2014) are already making steps in this direction by modeling two wells and simulated geomechanical indices, though they prefer gradient-based optimization methods that could yield sub-optimal results for complex non-convex functions.

- ii. Another direction is addition of spatial flexibility in wellbore placement. It has been brought to our attention shale gas operators are interested in optimizing not only aerial well placement (all parallel to each other in roughly one layer), but also stacking of horizontal wells in several layers. From the simulation standpoint this can be easily achieved by extending GA chromosomes (and, this, computational time) to accommodate three-dimensional well distribution. However, modeling of stacked wells without proper geomechanics might be an absolutely abstract exercise. In this dissertation we assumed that HF stages are fully penetrating from the top to the bottom of the reservoir, and because we are dealing with one homogeneous layer, this assumption is valid. In case of multiple layers, vertical variability of properties might be significant and influences the shape of HFs. Stresses also tend to change due to compositional changes in shale fabric. Thus, stacking of horizontal producers with HF stages along them requires careful petrophysical and geomechanical modeling before optimization can be performed. This is yet another new challenging area of research.
- iii. Further investigation can be done by incorporating HF design into our optimization framework. This only reason why it was not included into this dissertation is coupling and computational challenges. Software products that model individual HFs provide output with geometry of the HF (in our case we modeled it with LGR and SRV in our grid) that could be imported into the model and used for optimization. However, the drawback of this approach is rapid increase of computational time and waste of resources. Optimization algorithms

require many calls of the simulator (in order of thousands) and for each call (that could be just an intermediate solution) and for each well HF software would design 5 - 40 different stages with based on geomechanical properties and proppant material available. This by itself becomes a computationally prohibitive problem. Possible solution could be to optimize the locations of HF stages with fast optimization engine (such as GA) and, once strong candidates for locations are identified, optimize the actual geometry and design of HF stages. In other words, it is possible to make it sequential optimization rather than simultaneous.

- iv. Another important and interesting research venue that this dissertation opens is temporal design optimization. For our integrated framework we assumed that hydraulic fracturing is performed prior to any production and, thus, the production design does not change with time. We can produce for five or twenty years and the number of wells and the number of HF stages would remain the same. Now, what if we could add more wells as we produce from old ones and re-fracture or re-stimulate old wells? These temporal changes might give us yet another degree of freedom in search of optimal production plan. However, this optimization problem cannot be possibly solved without proper and carefully chosen constraints. Additional degrees of freedom increase dimensions in control vector and, thus, computational time. Again, to pursue this direction one might need to change computational platform to supercomputer.

## REFERENCES

- Akaike, H. 1974. A New Look at the Statistical Model Identification. *IEEE Transactions on Automatic Control* **19**(6): 716-723.
- Bittencourt, A. and Horne, R. 1997. Reservoir Development and Design Optimization. Presented at the SPE Annual Technical Conference and Exhibition, San Antonio, Texas, 5-8 October. SPE-38895-MS.  
<http://dx.doi.org.lib-ezproxy.tamu.edu:2048/10.2118/38895-MS>
- Bouzarkouna, Z., Ding, D., and Auger, A. Using Evolution Strategy with Meta-models for Well Placement Optimization. ECMOR XII (12<sup>th</sup> European Conference on the Mathematics of Oil Recovery, Sep 2010, Oxford, United Kingdom. SPE-143292-PA. <http://dx.doi.org/10.2118/143292-PA>
- Bruner, K. and Smosna, R. 2011. A Comparative Study of the Mississippian Barnett Shale, Fort Worth Basin, and Devonian Marcellus Shale, Appalachian Basin. U.S. Department of Energy, National Energy Technology Laboratory, URS Corporation, San Francisco, CA. DOE/NETL/2011/1478.
- Cipolla, C., Lolon, E., Erdle, J. and Tathed, V. 2009. Modeling Well Performance in Shale-Gas Reservoirs. Presented at SPE/EAGE Reservoir Characterization and Simulation Conference, Abu Dhabi, UAE, 19-21 October. SPE-125532-MS. <http://dx.doi.org.lib-ezproxy.tamu.edu:2048/10.2118/125532-MS>
- Das, I. and Dennis, J. 1997. A Closer Look at Drawbacks on Minimizing Weighted Sums of Objectives for Pareto Set Generations in Multi-criteria Optimization

Problems. *Structural and multidisciplinary Optimization* **14** (1): 63-69.  
DOI: 10.1007/BF01197559.

Deb, K., Pratap, A., Agarwal, S., and Meyarivan, T. 2002. A Fast and Elitism Multi-objective Genetic Algorithm: NSGA-II. *IEEE Transactions on Evolutionary Computation* **6** (2): 182-197.

Ding, Y. 2008. Optimization of Well Placement Using Evolutionary Algorithms. Presented at Europec/EAGE Conference and Exhibition, Rome, Italy, 9-12 June. SPE-113525-MS.

<http://dx.doi.org.lib-ezproxy.tamu.edu:2048/10.2118/113525-MS>

ECLIPSE 300, ECLIPSE Technical description Version 2012.2.0.0. ©Schlumberger Ltd.

<http://www.software.slb.com/products/foundation/Pages/eclipse.aspx>

Energy Information Administration, 2013. Shale Gas Production. U.S. Department of Energy, Washington, D.C. Available at:

[http://www.eia.doe.gov/dnav/ng/ng\\_prod\\_shalegas\\_sl\\_a.htm](http://www.eia.doe.gov/dnav/ng/ng_prod_shalegas_sl_a.htm).

Emerick, A., Silva, E., Messer, B., Almeida, L.F., Szwarcman, D., Pacheco, M.A., and Vellasco, M. 2009. Well Placement Optimization Using a Genetic Algorithm with Nonlinear Constraints. Presented at SPE Reservoir Simulation Symposium, The Woodlands, Texas. 2-4 February. SPE-118808-MS.

<http://dx.doi.org.lib-ezproxy.tamu.edu:2048/10.2118/118808-MS>

Forouzanfar, F., Li, G., and Reynolds, A. 2010. A Two-Stage Well Placement Optimization Method Based on Adjoint Gradient. Presented at SPE Annual

Technical Conference and Exhibition, Florence, Italy. 19-22 September.  
SPE-135304-MS.

<http://dx.doi.org.lib-ezproxy.tamu.edu:2048/10.2118/135304-MS>

Gao, S., Yao, J., Sun, Z., Lu, R., Li, L., and Wang, Y. 2012. Optimal Design of Nonuniform Transverse Fractures for Horizontal Wells in Tight Gas Reservoirs. Presented at SPE Unconventional Gas Conference and Exhibition, Muscat, Oman. 28-30 January. SPE-164011-MS.

<http://dx.doi.org.lib-ezproxy.tamu.edu:2048/10.2118/164011-MS>

Guyagular, B., and Horne, R. 2001. Uncertainty Assessment of Well Placement Optimization. Presented at SPE Annual Technical Conference and Exhibition, New Orleans, Louisiana. 30 September-3 October. SPE-71625-MS.

<http://dx.doi.org.lib-ezproxy.tamu.edu:2048/10.2118/71625-MS>

Holditch, S.A.. 2007. Hydraulic Fracturing: Overview, Trends, Issues. *Drilling Contractor* July/August 2007: 26-28.

Holland, J.H. 1975. *Adaptation in Natural and Artificial Systems*. Ann Arbor, Michigan. The University of Michigan Press.

Holt S. 2011. *Numerical Optimization of Hydraulic Fracture Stage Placement in a Gas Shale Reservoir*. MS Thesis, Delft University of Technology, Netherlands (May 2011).

Jacobs, T. 2014. The Shale Evolution: Zipper Fracture Takes Hold. *Journal of Petroleum Technology* **66** (10). pp. 60-67.

Jahandideh, A. and Jafarpour, B. 2014. Optimization of Hydraulic Fracturing Design under Spatially Variable Shale Fracability. Presented at SPE Western North American and Rocky Mountain Joint Meeting, Denver, Colorado. 17-18 April. SPE-169521-MS.

<http://dx.doi.org.lib-ezproxy.tamu.edu:2048/10.2118/169521-MS>

King, G. 2010. Thirty Years of Gas Shale Fracturing: What Have We Learned? *Journal of Petroleum Technology* **62** (11): 88-90.

<http://dx.doi.org.lib-ezproxy.tamu.edu:2048/10.2118/1110-0088-JPT>

Konak, A., Coit, D., and Smith, A. 2006. Multi-Objective Optimization Using Genetic Algorithms: A Tutorial. *Reliability Engineering and System Safety* **91** (2006): 992-1007.

Lyons, J. and Nasrabadi, H. 2013. Well Placement Optimization under Time-Dependent Uncertainty using an Ensemble Kalman Filter and a Genetic Algorithm. *Journal of Petroleum Science and Engineering* **109** (2013): 70–79.

Ma, X. 2013. *Integrated Hydraulic Fracture Placement and Design Optimization in Unconventional Gas Reservoirs*. PhD Dissertation. Texas A&M University, College Station, TX, USA (December 2013).

Ma, X., Plaksina, T., and Gildin, E. 2013. Optimization of Placement of Hydraulic Fracture Stages in Horizontal Wells Drilled in Shale Gas Reservoirs. Presented at Unconventional Resources Technology Conference, Denver, Colorado, USA. 12-14 August. SPE-1580378-MS.

<http://dx.doi.org.lib-ezproxy.tamu.edu:2048/10.1190/URTEC2013-151>

Ma, X., Plaksina, T., and Gildin, E. 2013. Integrated Horizontal Well Placement and Hydraulic Fracture Stages Design Optimization in Unconventional Gas Reservoirs. Presented at SPE Unconventional Resources Conference Canada, Calgary, Alberta, Canada. 5-7 November SPE-167246-MS.

<http://dx.doi.org.lib-ezproxy.tamu.edu:2048/10.2118/167246-MS>

Marler, R. and Arora, J. 2004. Survey of Multi-Objective Optimization Methods for Engineering. *Structural and Multidisciplinary Optimization* **26** (6): 369-395.

MATLAB and Statistics Toolbox Release 2012b, The MathWorks, Inc., Natick, Massachusetts, United States.

Mayerhofer, M., Lolon, E., Warpinski, N., Cipolla, C., Walser, D., and Rightmire, C. 2010. What is Stimulated Reservoir Volume? *SPE Production & Operations*. February 2010: 89-98.

Montes, G., Bartolome, P., and Udias, A.L. 2001. The Use of Genetic Algorithms in Well Placement Optimization. Presented at SPE Latin American and Caribbean Petroleum Engineering Conference, Buenos Aires, Argentina. 25-28 March. SPE-69439-MS.

<http://dx.doi.org.lib-ezproxy.tamu.edu:2048/10.2118/69439-MS>

Morales, A., Nasrabadi, H., and Zhu, D. 2010. A Modified Genetic Algorithm for Horizontal Well Placement Optimization in Gas Condensate Reservoirs. Presented at SPE Annual Technical Conference and Exhibition, Florence, Italy. 19-22 September. SPE-135182-MS.

<http://dx.doi.org.lib-ezproxy.tamu.edu:2048/10.2118/135182-MS>

Mutalik, A. and Gibson, B. 2008. Case History of Sequential and Simultaneous Fracturing of the Barnett Shale in Parker County. Presented at SPE Annual Technical Conference and Exhibition, Denver, Colorado, USA. 21-24 September. SPE-116124-MS.

<http://dx.doi.org.lib-ezproxy.tamu.edu:2048/10.2118/116124-MS>

Nakajima, L. and Schiozer, D. 2003. Horizontal Well Placement Optimization Using Quality Map Definition. Presented at Canadian International Petroleum Conference, Calgary, Alberta. 10-12 June PETSOC-2003-053-P.

<http://dx.doi.org.lib-ezproxy.tamu.edu:2048/10.2118/2003-053>

*NIST/SEMATECH e-Handbook of Statistical Methods*. NIST is an agency of the [U.S.](#)

[Department of Commerce](#). <http://www.itl.nist.gov/div898/handbook/>, 2012.

Nocedal, J. and Wright, S. 1999. *Numerical Optimization*. New York, USA. Springer Series in Operations Research.

Park, H., Datta-Gupta, A., and King, M. 2013. Handling Conflicting Multiple Objective Using Pareto-based Evolutionary Algorithms During History Matching of Reservoir Performance. Presented at SPE Reservoir Simulation Symposium, The Woodlands, Texas, USA. 18-20 February SPE-163623-MS.

<http://dx.doi.org.lib-ezproxy.tamu.edu:2048/10.2118/163623-MS>

R Core Team. 2013. R: A Language and Environment for Statistical Computing. R Foundation for Statistical Computing, Vienna, Austria. ISBN 3-900051-07-0.

[URL http://www.R-project.org/](http://www.R-project.org/).

Savitski, A., Lin, M., Riahi, A., Damjanac, B. and Nagel, N. 2013. Explicit Modeling of Hydraulic Fracture Propagation in Fractured Shales. Presented at International Petroleum Technology Conference, Beijing, China. 26-28 March. IPTC-17073-MS.

<http://dx.doi.org.lib-ezproxy.tamu.edu:2048/10.2523/17073-MS>

Schweitzer, R. and Bilgesu, H.I. 2009. The Role of Economics on Well and Fracture Design Completions of Marcellus Shale Wells. Presented at SPE Eastern Regional Meeting, Charleston, West Virginia, USA. 23-25 September. SPE-125975-MS.

<http://dx.doi.org.lib-ezproxy.tamu.edu:2048/10.2118/125975-MS>

Skeekanth, J., Datta, B., and Mohapatra, P. 2012. Optimal Short-Term Reservoir Operation with Integrated Long-term Goals. *Water Resources Management* **26**: 2833-2850.

Thompson, J., Fan, L., Grant, D., Martin, R., Kanneganti, K., and Lindsay, G. 2011. An Overview of Horizontal Well Completions in the Haynesville Shale. *Journal of Canadian Petroleum Technology* (June 2011): 22-35.

Vishkai, M., Hareland, G., and Gates, I. 2014. Influence of Stress Anisotropy on Hydraulic Fracturing. Presented at 48th U.S. Rock Mechanics/Geomechanics Symposium, Minneapolis, Minnesota. 1-4 June ARMA-2014-7360.

Waters, G., Lewis, R., and Bentley, D. 2011. The Effect of Mechanical Properties Anisotropy in the Generation of Hydraulic Fractures in Organic Shales.

Presented at SPE Annual Technical Conference and Exhibition, Denver, Colorado, USA. 30 October - 2 November, SPE-146776-MS.

<http://dx.doi.org.lib-ezproxy.tamu.edu:2048/10.2118/146776-MS>

Yeten, B. 2003. *Optimum Deployment of Nonconventional Wells*. PhD Dissertation, Stanford University, Stanford, California (June 2003).

Yu, W. and Sepehrmoori, K. 2013. Optimization of Multiple Hydraulically Fractured Horizontal Wells in Unconventional Gas Reservoirs. Presented at SPE Production and Operations Symposium, Oklahoma City, Oklahoma, USA. 23-26 March. SPE-164509-MS.

<http://dx.doi.org.lib-ezproxy.tamu.edu:2048/10.2118/164509-MS>

APPENDIX A

Table A.1 Two-level full factorial DoE for anisotropic horizontal stress model.

FULL FACTORIAL EXPERIMENTAL DESIGN FOR ANISOTROPIC MODEL

CASE/VALUE	PARAMETERS				
	HF perm	SRV perm	Matrix perm	Gas price	HF cost
low	1000 md	0.0001 md	0.00001 md	\$3/MCF	\$100,000
high	100000 md	0.001 md	0.001 md	\$6/MCF	\$300,000
1	low	low	low	low	low
2	low	low	low	low	high
3	low	low	low	high	low
4	low	low	low	high	high
5	low	low	high	low	low
6	low	low	high	low	high
7	low	low	high	high	low
8	low	low	high	high	high
9	low	high	low	low	low
10	low	high	low	low	high
11	low	high	low	high	low
12	low	high	low	high	high
13	low	high	high	low	low
14	low	high	high	low	high
15	low	high	high	high	low
16	low	high	high	high	high
17	high	high	high	low	low
18	high	high	high	low	high
19	high	high	high	high	low
20	high	high	high	high	high
21	high	high	low	low	low
22	high	high	low	low	high
23	high	high	low	high	low
24	high	high	low	high	high
25	high	low	high	low	low
26	high	low	high	low	high
27	high	low	high	high	low
28	high	low	high	high	high
29	high	low	low	low	low
30	high	low	low	low	high
31	high	low	low	high	low
32	high	low	low	high	high

**Table A.2 Two-level full factorial DoE for isotropic horizontal stress model.**

**FULL FACTORIAL EXPERIMENTAL DESIGN FOR ISOTROPIC MODEL**

CASE/VALUE	PARAMETERS			
	SRV perm	Matrix perm	Gas price	HF cost
low	50 md	0.00001 md	\$3/MCF	\$100,000
high	200 md	0.001 md	\$6/MCF	\$300,000
1	low	low	low	low
2	low	low	low	high
3	low	low	high	low
4	low	low	high	high
5	low	high	low	low
6	low	high	low	high
7	low	high	high	low
8	low	high	high	high
9	low	low	low	low
10	low	low	low	high
11	low	low	high	low
12	low	low	high	high
13	low	high	low	low
14	low	high	low	high
15	low	high	high	low
16	low	high	high	high

## APPENDIX B

### PARAMETER SCREENING FOR UNCERTAINTY ASSESSMENT

#### Statistical Analysis of Anisotropic DoE Results

Below we provide the detailed R (2013) code that was used for parameter screening as a part of UA. The suite of simulation results (short-term discounted NPV,  $y1npv$ , and long-term discounted NPV,  $npv$ ) with corresponding values of matrix permeability ( $km$ ), HF permeability ( $khf$ ), SRV permeability ( $ksrv$ ), price of gas ( $pg$ ), and cost of hydraulic fracturing ( $hcost$ ) are loaded into the statistical environment and analyzed for significance with stepwise regression and Akaike information criterion (Akaike, 1974).

Each step of the statistical analysis is commented below:

```
> ani <- read.csv("doe_results.csv")
> ani
```

```
% Load and summarize the dataset
```

	npv	y1npv	khf	ksrv	km	pg	hcost
1	-1035692.9	-2341634.62	1000	1e-04	1e-05	3	100000
2	-3435692.9	-4741634.62	1000	1e-04	1e-05	3	300000
3	1359755.0	-1391377.51	1000	1e-04	1e-05	6	100000
4	-1040245.0	-3791377.51	1000	1e-04	1e-05	6	300000
5	2848962.1	206089.43	1000	1e-04	1e-03	3	100000
6	448962.1	-2193910.57	1000	1e-04	1e-03	3	300000
7	9129266.8	3704190.29	1000	1e-04	1e-03	6	100000
8	6729266.8	1304190.29	1000	1e-04	1e-03	6	300000
9	172727.5	-1625913.95	1000	1e-03	1e-05	3	100000
10	-2227272.5	-4025913.95	1000	1e-03	1e-05	3	300000
11	3776691.3	40125.27	1000	1e-03	1e-05	6	100000
12	1376691.3	-2359874.73	1000	1e-03	1e-05	6	300000
13	3113823.9	534671.44	1000	1e-03	1e-03	3	100000
14	713823.9	-1865328.56	1000	1e-03	1e-03	3	300000
15	9658994.9	4361360.25	1000	1e-03	1e-03	6	100000
16	7258994.9	1961360.25	1000	1e-03	1e-03	6	300000
17	3159252.2	605035.09	100000	1e-03	1e-03	3	100000
18	759252.2	-1794964.91	100000	1e-03	1e-03	3	300000
19	9749993.1	4502226.99	100000	1e-03	1e-03	6	100000
20	7349993.1	2102226.99	100000	1e-03	1e-03	6	300000
21	192603.5	-1596785.99	100000	1e-03	1e-05	3	100000
22	-2207396.5	-3996785.99	100000	1e-03	1e-05	3	300000
23	3816472.0	98408.07	100000	1e-03	1e-05	6	100000
24	1416472.0	-2301591.93	100000	1e-03	1e-05	6	300000
25	2894927.1	286057.96	100000	1e-04	1e-03	3	100000

```

26 494927.1 -2113942.04 100000 1e-04 1e-03 3 300000
27 9221350.4 3864280.94 100000 1e-04 1e-03 6 100000
28 6821350.4 1464280.94 100000 1e-04 1e-03 6 300000
29 -1023886.4 -2323035.36 100000 1e-04 1e-05 3 100000
30 -3423886.4 -4723035.36 100000 1e-04 1e-05 3 300000
31 1383382.8 -1354164.10 100000 1e-04 1e-05 6 100000
32 -1016617.2 -3754164.10 100000 1e-04 1e-05 6 300000

```

```

> fit1 <- lm(y1npv ~ khf*ksrv*km+pg*hcost, data=ani)
> fit1

```

```

% Fit and summarize linear model with interactions between petrophysical properties
and economic parameters

```

```

Call:
lm(formula = y1npv ~ khf * ksrv * km + pg * hcost, data = ani)

```

```

Coefficients:
(Intercept)          khf          ksrv          km          pg
-4.590e+06  2.544e-01  1.199e+09  3.924e+09  8.367e+05  -
1.200e+01
khf:ksrv      khf:km      ksrv:km      pg:hcost  khf:ksrv:km
1.807e+02  9.742e+02 -6.514e+11 -3.125e-11 -3.425e+05

```

```

> require(MASS)
Loading required package: MASS
> step<-stepAIC(fit1, direction="both")

```

```

% Perform stepwise regression, go through models and select model with the highest

```

```

AIC value

```

```

Start: AIC=874.7
y1npv ~ khf * ksrv * km + pg * hcost

```

```

      Df Sum of Sq      RSS      AIC
- pg:hcost  1  0.0000e+00 1.1959e+13 872.7
- khf:ksrv:km  1 456425619 1.1960e+13 872.7
<none>                1.1959e+13 874.7

```

```

Step: AIC=872.7
y1npv ~ khf + ksrv + km + pg + hcost + khf:ksrv + khf:km + ksrv:km +
khf:ksrv:km

```

```

      Df Sum of Sq      RSS      AIC
- khf:ksrv:km  1 4.5643e+08 1.1960e+13 870.70
<none>                1.1959e+13 872.70
+ pg:hcost  1 0.0000e+00 1.1959e+13 874.70
- hcost  1 4.6080e+13 5.8039e+13 921.25
- pg  1 5.0404e+13 6.2363e+13 923.54

```

```

Step: AIC=870.7

```

ylnpv ~ khf + ksrv + km + pg + hcost + khf:ksrv + khf:km + ksrv:km

	Df	Sum of Sq	RSS	AIC
- khf:ksrv	1	9.5863e+05	1.1960e+13	868.70
- khf:km	1	1.1863e+10	1.1972e+13	868.73
- ksrv:km	1	7.1006e+11	1.2670e+13	870.54
<none>			1.1960e+13	870.70
+ khf:ksrv:km	1	4.5643e+08	1.1959e+13	872.70
+ pg:hcost	1	0.0000e+00	1.1960e+13	872.70
- hcost	1	4.6080e+13	5.8040e+13	919.25
- pg	1	5.0404e+13	6.2364e+13	921.54

Step: AIC=868.7

ylnpv ~ khf + ksrv + km + pg + hcost + khf:km + ksrv:km

	Df	Sum of Sq	RSS	AIC
- khf:km	1	1.1863e+10	1.1972e+13	866.73
- ksrv:km	1	7.1006e+11	1.2670e+13	868.54
<none>			1.1960e+13	868.70
+ khf:ksrv	1	9.5863e+05	1.1960e+13	870.70
+ pg:hcost	1	0.0000e+00	1.1960e+13	870.70
- hcost	1	4.6080e+13	5.8040e+13	917.25
- pg	1	5.0404e+13	6.2364e+13	919.54

Step: AIC=866.73

ylnpv ~ khf + ksrv + km + pg + hcost + ksrv:km

	Df	Sum of Sq	RSS	AIC
- khf	1	4.4181e+10	1.2016e+13	864.85
- ksrv:km	1	7.1006e+11	1.2682e+13	866.57
<none>			1.1972e+13	866.73
+ khf:km	1	1.1863e+10	1.1960e+13	868.70
+ khf:ksrv	1	9.5863e+05	1.1972e+13	868.73
+ pg:hcost	1	0.0000e+00	1.1972e+13	868.73
- hcost	1	4.6080e+13	5.8052e+13	915.25
- pg	1	5.0404e+13	6.2375e+13	917.55

Step: AIC=864.85

ylnpv ~ ksrv + km + pg + hcost + ksrv:km

	Df	Sum of Sq	RSS	AIC
- ksrv:km	1	7.1006e+11	1.2726e+13	864.69
<none>			1.2016e+13	864.85
+ khf	1	4.4181e+10	1.1972e+13	866.73
+ pg:hcost	1	0.0000e+00	1.2016e+13	866.85
- hcost	1	4.6080e+13	5.8096e+13	913.28
- pg	1	5.0404e+13	6.2420e+13	915.57

Step: AIC=864.69

ylnpv ~ ksrv + km + pg + hcost

	Df	Sum of Sq	RSS	AIC
<none>			1.2726e+13	864.69
+ ksrv:km	1	7.1006e+11	1.2016e+13	864.85
+ khf	1	4.4181e+10	1.2682e+13	866.57
+ pg:hcost	1	0.0000e+00	1.2726e+13	866.69
- ksrv	1	4.9121e+12	1.7638e+13	873.13
- hcost	1	4.6080e+13	5.8806e+13	911.66
- pg	1	5.0404e+13	6.3130e+13	913.94
- km	1	1.0195e+14	1.1467e+14	933.04

> step\$anova

```
% Perform anova test
```

```
Stepwise Model Path  
Analysis of Deviance Table
```

```
Initial Model:  
y1npv ~ khf * ksrv * km + pg * hcost
```

```
Final Model:  
y1npv ~ ksrv + km + pg + hcost
```

	Step	Df	Deviance	Resid. Df	Resid. Dev	AIC
1				21	1.195947e+13	874.6979
2	- pg:hcost	1	1.953125e-03	22	1.195947e+13	872.6979
3	- khf:ksrv:km	1	4.564256e+08	23	1.195993e+13	870.6991
4	- khf:ksrv	1	9.586326e+05	24	1.195993e+13	868.6991
5	- khf:km	1	1.186309e+10	25	1.197179e+13	866.7308
6	- khf	1	4.418072e+10	26	1.201597e+13	864.8487
7	- ksrv:km	1	7.100565e+11	27	1.272603e+13	864.6859

```
> newfit1 <- lm(y1npv ~ ksrv+km+pg+hcconst, data=ani)  
> anova(newfit1)
```

```
Analysis of Variance Table
```

```
Response: y1npv
```

	Df	Sum Sq	Mean Sq	F value	Pr(>F)	
ksrv	1	4.9121e+12	4.9121e+12	10.422	0.00326	**
km	1	1.0195e+14	1.0195e+14	216.294	2.073e-14	***
pg	1	5.0404e+13	5.0404e+13	106.938	6.880e-11	***
hcconst	1	4.6080e+13	4.6080e+13	97.765	1.808e-10	***
Residuals	27	1.2726e+13	4.7133e+11			

```
---  
Signif. codes: 0 '***' 0.001 '**' 0.01 '*' 0.05 '.' 0.1 ' ' 1
```

```
> fit2 <- lm(npv ~ khf*ksrv*km+pg*hcconst, data=ani)  
> fit2
```

```
Call:
```

```
lm(formula = npv ~ khf * ksrv * km + pg * hcconst, data = ani)
```

```
Coefficients:
```

(Intercept)	khf	ksrv	km	pg	
-5.982e+06	1.600e-01	2.030e+09	6.044e+09	1.574e+06	-
1.200e+01					
khf:ksrv	khf:km	ksrv:km	pg:hcconst	khf:ksrv:km	
1.374e+02	5.381e+02	-1.588e+12	2.083e-11	-1.465e+05	

```
> step<-stepAIC(fit2, direction="both")
```

```
Start: AIC=898.35
```

```
npv ~ khf * ksrv * km + pg * hcconst
```

	Df	Sum of Sq	RSS	AIC
- pg:hcost	1	0	2.5045e+13	896.35
- khf:ksrv:km	1	83492127	2.5045e+13	896.35
<none>			2.5045e+13	898.35

Step: AIC=896.35  
 npv ~ khf + ksrv + km + pg + hcost + khf:ksrv + khf:km + ksrv:km +  
 khf:ksrv:km

	Df	Sum of Sq	RSS	AIC
- khf:ksrv:km	1	8.3492e+07	2.5045e+13	894.35
<none>			2.5045e+13	896.35
+ pg:hcconst	1	0.0000e+00	2.5045e+13	898.35
- hconst	1	4.6080e+13	7.1125e+13	927.75
- pg	1	1.7835e+14	2.0340e+14	961.37

Step: AIC=894.35  
 npv ~ khf + ksrv + km + pg + hcost + khf:ksrv + khf:km + ksrv:km

	Df	Sum of Sq	RSS	AIC
- khf:ksrv	1	6.3848e+07	2.5046e+13	892.35
- khf:km	1	4.0223e+09	2.5049e+13	892.36
<none>			2.5045e+13	894.35
+ khf:ksrv:km	1	8.3492e+07	2.5045e+13	896.35
+ pg:hcconst	1	0.0000e+00	2.5045e+13	896.35
- ksrv:km	1	4.0433e+12	2.9089e+13	897.14
- hconst	1	4.6080e+13	7.1125e+13	925.75
- pg	1	1.7835e+14	2.0340e+14	959.37

Step: AIC=892.35  
 npv ~ khf + ksrv + km + pg + hcost + khf:km + ksrv:km

	Df	Sum of Sq	RSS	AIC
- khf:km	1	4.0223e+09	2.5050e+13	890.36
<none>			2.5046e+13	892.35
+ khf:ksrv	1	6.3848e+07	2.5045e+13	894.35
+ pg:hcconst	1	0.0000e+00	2.5046e+13	894.35
- ksrv:km	1	4.0433e+12	2.9089e+13	895.14
- hconst	1	4.6080e+13	7.1126e+13	923.75
- pg	1	1.7835e+14	2.0340e+14	957.37

Step: AIC=890.36  
 npv ~ khf + ksrv + km + pg + hcost + ksrv:km

	Df	Sum of Sq	RSS	AIC
- khf	1	1.7072e+10	2.5067e+13	888.38
<none>			2.5050e+13	890.36
+ khf:km	1	4.0223e+09	2.5046e+13	892.35
+ khf:ksrv	1	6.3848e+07	2.5049e+13	892.36
+ pg:hcconst	1	0.0000e+00	2.5050e+13	892.36
- ksrv:km	1	4.0433e+12	2.9093e+13	893.14
- hconst	1	4.6080e+13	7.1130e+13	921.75
- pg	1	1.7835e+14	2.0340e+14	955.37

Step: AIC=888.38  
 npv ~ ksrv + km + pg + hcost + ksrv:km

	Df	Sum of Sq	RSS	AIC
<none>			2.5067e+13	888.38
+ khf	1	1.7072e+10	2.5050e+13	890.36
+ pg:hcconst	1	0.0000e+00	2.5067e+13	890.38
- ksrv:km	1	4.0433e+12	2.9110e+13	891.16
- hconst	1	4.6080e+13	7.1147e+13	919.76
- pg	1	1.7835e+14	2.0342e+14	953.38

> step\$anova  
 Stepwise Model Path

Analysis of Deviance Table

Initial Model:

npv ~ khf \* ksrv \* km + pg \* hcost

Final Model:

npv ~ ksrv + km + pg + hcost + ksrv:km

	Step	Df	Deviance	Resid. Df	Resid. Dev	AIC
1				21	2.504535e+13	898.3512
2	- pg:hcost	1	7.812500e-03	22	2.504535e+13	896.3512
3	- khf:ksrv:km	1	8.349213e+07	23	2.504544e+13	894.3513
4	- khf:ksrv	1	6.384772e+07	24	2.504550e+13	892.3513
5	- khf:km	1	4.022333e+09	25	2.504952e+13	890.3565
6	- khf	1	1.707240e+10	26	2.506660e+13	888.3783

```
> newfit2 <- lm(npv ~ ksrv+km+pg+hcost, data=ani)
```

```
> anova(newfit2)
```

Analysis of Variance Table

Response: npv

	Df	Sum Sq	Mean Sq	F value	Pr(>F)	
ksrv	1	9.8180e+12	9.8180e+12	9.1064	0.005502	**
km	1	2.1151e+14	2.1151e+14	196.1761	6.681e-14	***
pg	1	1.7835e+14	1.7835e+14	165.4248	4.995e-13	***
hcost	1	4.6080e+13	4.6080e+13	42.7401	5.199e-07	***
Residuals	27	2.9110e+13	1.0781e+12			

Signif. codes: 0 '\*\*\*' 0.001 '\*\*' 0.01 '\*' 0.05 '.' 0.1 ' ' 1

```
> summary(newfit1)
```

Call:

```
lm(formula = y1npv ~ ksrv + km + pg + hcost, data = ani)
```

Residuals:

Min	1Q	Median	3Q	Max
-942821	-501230	109958	586573	743052

Coefficients:

	Estimate	Std. Error	t value	Pr(> t )	
(Intercept)	-4.392e+06	4.935e+05	-8.899	1.63e-09	***
ksrv	8.707e+08	2.697e+08	3.228	0.00326	**
km	3.606e+09	2.452e+08	14.707	2.07e-14	***
pg	8.367e+05	8.091e+04	10.341	6.88e-11	***
hcost	-1.200e+01	1.214e+00	-9.888	1.81e-10	***

Signif. codes: 0 '\*\*\*' 0.001 '\*\*' 0.01 '\*' 0.05 '.' 0.1 ' ' 1

Residual standard error: 686500 on 27 degrees of freedom

Multiple R-squared: 0.9411, Adjusted R-squared: 0.9324

F-statistic: 107.9 on 4 and 27 DF, p-value: 3.414e-16

```
> summary(newfit2)
```

Call:

```
lm(formula = npv ~ ksrv + km + pg + hcost, data = ani)
```

Residuals:

Min	1Q	Median	3Q	Max
-----	----	--------	----	-----

-1527420 -657759 171839 832788 1192361

Coefficients:

	Estimate	Std. Error	t value	Pr(> t )	
(Intercept)	-5.531e+06	7.464e+05	-7.411	5.69e-08	***
ksrv	1.231e+09	4.079e+08	3.018	0.0055	**
km	5.194e+09	3.708e+08	14.006	6.68e-14	***
pg	1.574e+06	1.224e+05	12.862	5.00e-13	***
hcost	-1.200e+01	1.836e+00	-6.538	5.20e-07	***

---  
Signif. codes: 0 '\*\*\*' 0.001 '\*\*' 0.01 '\*' 0.05 '.' 0.1 ' ' 1

Residual standard error: 1038000 on 27 degrees of freedom  
Multiple R-squared: 0.9387, Adjusted R-squared: 0.9296  
F-statistic: 103.4 on 4 and 27 DF, p-value: 5.844e-16

### Statistical Analysis of Isotropic DoE Results

```
> iso <- read.csv("iso.csv")
> iso
  ksrv km pg hcost npv npv1
1 50 1e-05 3 100000 689791.6 -1113713.1
2 50 1e-05 3 300000 -1710208.4 -3513713.1
3 50 1e-05 6 100000 4810283.2 1064124.7
4 50 1e-05 6 300000 2410283.2 -1335875.3
5 50 1e-03 3 100000 3858054.1 1500437.2
6 50 1e-03 3 300000 1458054.1 -899562.8
7 50 1e-03 6 100000 11146799.6 6292429.0
8 50 1e-03 6 300000 8746799.6 3892429.0
9 200 1e-05 3 100000 704675.2 -1085210.0
10 200 1e-05 3 300000 -1695324.8 -3485210.0
11 200 1e-05 6 100000 4840051.0 1121132.6
12 200 1e-05 6 300000 2440051.0 -1278867.4
13 200 1e-03 3 100000 3886776.5 1572599.8
14 200 1e-03 3 300000 1486776.5 -827400.2
15 200 1e-03 6 100000 11204245.0 6436755.3
16 200 1e-03 6 300000 8804245.0 4036755.3

> fit3 <- lm(npv1 ~ ksrv*km+pg*hcost, data=iso)
> fit3
```

Call:

```
lm(formula = npv1 ~ ksrv * km + pg * hcost, data = iso)
```

Coefficients:

	ksrv	km	pg	hcost
(Intercept)				
ksrv:km	pg:hcost			
-4.144e+06	2.806e+02	3.939e+09	1.170e+06	-1.200e+01
4.410e+05	-1.250e-10			

```
> step<-stepAIC(fit3, direction="both")
```

Start: AIC=442.76

```
npv1 ~ ksrv * km + pg * hcost
```

	Df	Sum of Sq	RSS	AIC
- pg:hcost	1	0	6.9514e+12	440.76
- ksrv:km	1	4288798509	6.9557e+12	440.77
<none>			6.9514e+12	442.76

Step: AIC=440.76  
 npv1 ~ ksrv + km + pg + hcost + ksrv:km

	Df	Sum of Sq	RSS	AIC
- ksrv:km	1	4.2888e+09	6.9557e+12	438.77
<none>			6.9514e+12	440.76
+ pg:hcst	1	0.0000e+00	6.9514e+12	442.76
- hcost	1	2.3040e+13	2.9991e+13	462.15
- pg	1	4.9283e+13	5.6234e+13	472.21

Step: AIC=438.77  
 npv1 ~ ksrv + km + pg + hcost

	Df	Sum of Sq	RSS	AIC
- ksrv	1	2.2801e+10	6.9785e+12	436.82
<none>			6.9557e+12	438.77
+ ksrv:km	1	4.2888e+09	6.9514e+12	440.76
+ pg:hcst	1	0.0000e+00	6.9557e+12	440.77
- hcost	1	2.3040e+13	2.9996e+13	460.15
- pg	1	4.9283e+13	5.6238e+13	470.21
- km	1	6.2536e+13	6.9491e+13	473.59

Step: AIC=436.82  
 npv1 ~ km + pg + hcost

	Df	Sum of Sq	RSS	AIC
<none>			6.9785e+12	436.82
+ ksrv	1	2.2801e+10	6.9557e+12	438.77
+ pg:hcst	1	0.0000e+00	6.9785e+12	438.82
- hcost	1	2.3040e+13	3.0019e+13	458.16
- pg	1	4.9283e+13	5.6261e+13	468.22
- km	1	6.2536e+13	6.9514e+13	471.60

> step\$anova

Stepwise Model Path  
 Analysis of Deviance Table

Initial Model:  
 npv1 ~ ksrv \* km + pg \* hcost

Final Model:  
 npv1 ~ km + pg + hcost

	Step	Df	Deviance	Resid. Df	Resid. Dev	AIC
1				9	6.951419e+12	442.7581
2	- pg:hcst	1	1.953125e-03	10	6.951419e+12	440.7581
3	- ksrv:km	1	4.288799e+09	11	6.955708e+12	438.7679
4	- ksrv	1	2.280096e+10	12	6.978509e+12	436.8203

> newfit3 <- ltm(npv1 ~ km+pg+hcst, data=iso)

> summary(newfit3)

Call:  
 ltm(formula = npv1 ~ km + pg + hcost, data = iso)

Residuals:  
 Min 1Q Median 3Q Max  
 -695077 -644744 -18041 651870 731159

Coefficients:  
 Estimate Std. Error t value Pr(>|t|)

```

(Intercept) -4.108e+06  7.394e+05  -5.557 0.000124 ***
km           3.994e+09  3.851e+08  10.370 2.42e-07 ***
pg           1.170e+06  1.271e+05   9.206 8.69e-07 ***
hcost       -1.200e+01  1.906e+00  -6.294 3.98e-05 ***
---

```

Signif. codes: 0 '\*\*\*' 0.001 '\*\*' 0.01 '\*' 0.05 '.' 0.1 ' ' 1

Residual standard error: 762600 on 12 degrees of freedom  
Multiple R-squared: 0.9508, Adjusted R-squared: 0.9385  
F-statistic: 77.3 on 3 and 12 DF, p-value: 4.071e-08

```

> fit4 <- lm(npv ~ ksrv*km+pg*hcost, data=iso)
> fit4

```

```

Call:
lm(formula = npv ~ ksrv * km + pg * hcost, data = iso)

```

```

Coefficients:
(Intercept)          ksrv              km              pg              hcost
ksrv:km      pg:hcost
-4.679e+06    1.474e+02    4.793e+09    1.905e+06   -1.200e+01
1.398e+05    -7.917e-10

```

```

> step<-stepAIC(fit4, direction="both")

```

```

Start: AIC=448.71
npv ~ ksrv * km + pg * hcost

```

```

      Df Sum of Sq      RSS      AIC
- pg:hcost  1          0 1.0082e+13 446.71
- ksrv:km   1 430904263 1.0083e+13 446.71
<none>                    1.0082e+13 448.71

```

```

Step: AIC=446.71
npv ~ ksrv + km + pg + hcost + ksrv:km

```

```

      Df Sum of Sq      RSS      AIC
- ksrv:km  1 4.3090e+08 1.0083e+13 444.71
<none>                    1.0082e+13 446.71
+ pg:hcost  1 0.0000e+00 1.0082e+13 448.71
- hcost    1 2.3040e+13 3.3122e+13 463.74
- pg       1 1.3067e+14 1.4075e+14 486.89

```

```

Step: AIC=444.71
npv ~ ksrv + km + pg + hcost

```

```

      Df Sum of Sq      RSS      AIC
- ksrv   1 4.2784e+09 1.0087e+13 442.71
<none>                    1.0083e+13 444.71
+ ksrv:km  1 4.3090e+08 1.0082e+13 446.71
+ pg:hcost  1 0.0000e+00 1.0083e+13 446.71
- hcost    1 2.3040e+13 3.3123e+13 461.74
- km       1 9.0736e+13 1.0082e+14 479.55
- pg       1 1.3067e+14 1.4075e+14 484.89

```

```

Step: AIC=442.71
npv ~ km + pg + hcost

```

```

      Df Sum of Sq      RSS      AIC
<none>                    1.0087e+13 442.71
+ ksrv   1 4.2784e+09 1.0083e+13 444.71
+ pg:hcost  1 0.0000e+00 1.0087e+13 444.71

```

```

- hcost      1 2.3040e+13 3.3127e+13 459.74
- km         1 9.0736e+13 1.0082e+14 477.55
- pg         1 1.3067e+14 1.4076e+14 482.89

```

```
> step$anova
```

```

Stepwise Model Path
Analysis of Deviance Table

```

```
Initial Model:
```

```
npv ~ ksrv * km + pg * hcost
```

```
Final Model:
```

```
npv ~ km + pg + hcost
```

	Step	Df	Deviance	Resid. Df	Resid. Dev	AIC
1				9	1.008225e+13	448.7073
2	- pg:hcost	1	0	10	1.008225e+13	446.7073
3	- ksrv:km	1	430904263	11	1.008268e+13	444.7080
4	- ksrv	1	4278420007	12	1.008696e+13	442.7148

```
> newfit4 <- lm(npv ~ km+pg+hcost, data=iso)
```

```
> summary(newfit4)
```

```
Call:
```

```
lm(formula = npv ~ km + pg + hcost, data = iso)
```

```
Residuals:
```

Min	1Q	Median	3Q	Max
-808677	-786613	-6919	790072	822516

```
Coefficients:
```

	Estimate	Std. Error	t value	Pr(> t )
(Intercept)	-4.660e+06	8.889e+05	-5.242	0.000207 ***
km	4.811e+09	4.630e+08	10.390	2.37e-07 ***
pg	1.905e+06	1.528e+05	12.468	3.15e-08 ***
hcost	-1.200e+01	2.292e+00	-5.235	0.000209 ***

```
---
Signif. codes:  0 '***' 0.001 '**' 0.01 '*' 0.05 '.' 0.1 ' ' 1
```

```

Residual standard error: 916800 on 12 degrees of freedom
Multiple R-squared:  0.9604,    Adjusted R-squared:  0.9505
F-statistic: 96.93 on 3 and 12 DF,  p-value: 1.117e-08

```